Quantum Launch System

Design of an economically viable, sustainable launch system to put multiple nanosatellites into Low Earth Orbit

T.J. Becx	4062965	L.E. van der Linden	4217934
A. Gianolio	4162749	G. Phua	4055349
B. Helder	4152751	Y. Shewan	4109686
T.G.E. van 't Klooster	4163397	G.J.A Theodoulou	1507923
S.T. Koehler	4235436	P.I. Wiegman	4009061
		M.C. Koivisto	4152565

Final Report

Design Synthesis Exercise

TU Delft Delft University of Technology

Aerospace Engineering

January 2016

QUANTUM LAUNCH SYSTEM

DESIGN OF AN ECONOMICALLY VIABLE, SUSTAINABLE LAUNCH SYSTEM TO PUT MULTIPLE NANOSATELLITES INTO LOW EARTH ORBIT

by

T.J. Becx, A. Gianolio, B. Helder, T.G.E. van 't Klooster, S.T. Koehler, M.C. Koivisto, L.E. van der Linden, G. Phua, Y. Shewan, G.J.A. Theodoulou, P.I. Wiegman

as part of the

Design Synthesis Exercise (DSE)

in BSc. Aerospace Engineering

at Delft University of Technology

Tutor:	Ir. M. C. Naeije	TU Delft/AS
Coaches:	Ir. J. F. G. Schneiders	TU Delft/Aero
	Ir. J. Carvajal Godinez	TU Delft/SSE
Client:	Prof. Dr. E. K. A. Gill	TU Delft/SSE

TU Delft Delft University of Technology

VERSION CONTROL

Table 1: Version Table

Version	Date	Changes
1.0	15-12-2015	Creation of draft version
1.1	04-01-2016	Changed: Structure of report
		Added: Started writing all chapters
1.2	19-01-2016	Changed: Layout style of report
		Added: Design process and post-DSE activities sections
1.3	20-01-2016	Final draft version
2.0	26-01-2016	Final report available upon request

PREFACE

This is the Final Report of group 3, 'Quantum Space', for the Fall 2015 Design Synthesis Exercise (DSE) of the Bachelor programme of Aerospace Engineering at Delft University of Technology. The Design Synthesis Exercise is the final part of the bachelor phase of our studies and is performed full-time during a period of 10 weeks.

We would like to express our gratitude to our supervisor Marc Naeije and our coaches Jan Schneiders and Johan Carvajal Godinez for their tutoring. Next to that, we would like to thank Frederique van 't Klooster for appointing and hosting the Final Review at the Concurrent Design Facility at ESA ESTEC. Special thanks also go to all the guests who were present at this Review. Furthermore, thanks goes to Professor Eberhard Gill for his input as client and guidance in establishing requirements. Finally, we would like to thank the Delft University of Technology, particularly the faculty of Aerospace Engineering, for letting us use their facilities.

DSE Group 03, Faculty of Aerospace Engineering, Delft University of Technology, The Netherlands
January 26, 2016

SUMMARY

There is a trend in the miniaturisation of satellites. Clusters of small satellites in Low Earth Orbit (LEO) are used more and more often to conduct scientific research or demonstrate novel technologies. These satellites are mostly nanosatellites, defined as having a mass between 1 and 10kg. However, there is no dedicated launcher available for these missions. The only option for these satellites is to piggy-back on another mission. However, this offers very limited flexibility and can cost as much as $50,000 per kg of payload. The Delft University of Technology has asked for an affordable and sustainable way to launch these nanosatellites that provides more flexibility than piggy-backing. The most important top-level constraints are a payload mass of 60kg, a first launch in 2021 and a competitive price-per-kg compared to piggybacking.

Quantum Launch Systems rises to this need by aiming for the market gap at 350km altitude with flexible launching schedules. There are several challenges that need to be addressed to reach this goal: the cost of developing a launcher, the recurring production cost and operation cost, as well as the lower technological readiness of sustainable solutions in space industry. This report discusses the design of a partially reusable rocket to reach these goals. The way to achieve the design was an iterative design process together with a systems engineering approach. Many iterations were made and to optimise the design with respect to lift-off mass.

The Quantum Launcher is a three stage launcher with six engines and a reusable first stage. Its lift-off mass is just over 9200kg, and is designed with affordability and sustainability as first considerations. To that end, it uses fully 3D-printed, LOX/LCH4 (Liquid Oxygen/Liquid Methane) propelled engines, of which it contains four in the first stage and one in the second and third stages. This propellant combination has very low soot emissions, minimising refurbishment costs and ensuring the first stage engines can be reused up to ten times. By using similar engines in each stage, the development costs are kept low, as the acquired expertise for one engine can be maintained for other engine and less facilities for production and testing are needed.

Sustainability was incorporated as a driving factor in the design rather than an afterthought. The LOX/LCH4 propellant has less emissions, is less toxic, and is more environmentally friendly than other propellant combinations with similar performance. The recovery of the first stage, that accounts for more than 65% of the structure, also reduces the required materials for subsequent launches, which reduces our overall footprint on the environment. In addition, the use of a 507m^2 controllable parafoil parachute reduces the emissions by requiring less propellant for the recovery and makes the first stage able to land with 20 m accuracy. The target orbit of 350km altitude also solves the biggest issue in the ever-increasing satellite market: space debris. This orbit is self-cleaning: all payloads are guaranteed to decay within 25 years, but will most probably decay in less than a year because of the low orbit.

The resulting Quantum Launch System is able to deliver a 60kg payload into a circular orbit of 350km altitude. For altitudes with lower inclination, the possibility of using less propellant or carrying more payload mass is available. Cost analysis has shown that the launcher can do this at a price of $42,850 per kg, or a total of approximately $2.6 million per launch, assuming the first stage can be used ten times. Cost savings have been achieved in two ways: with the re-use of the first stage, and by the implementation of modern production strategies such as additive manufacturing.

NOMENCLATURE

Abbreviation	Description
ADCS	Attitude Determination and Control System
C&DH	Command & Data Handling
CG	Centre of Gravity
CFRP	Carbon Fiber Reinforced Polymer
COTS	Commercial-Off-The-Shelf
DoD	Depth of Discharge
DSE	Design Synthesis Exercise
EPS	Electrical Power System
FBS	Function Breakdown Structure
FDS	Flight Destruction System
FFD	Function Flow Diagram
FTS	Flight Termination System
FR	Final Report
GNC	Guidance and Navigation Control
IMU	Inertial Measurement Unit
LCH4	Liquid Methane
LEO	Low Earth Orbit
LOX	Liquid Methane
MAI	Manufacturing, Assembly & Integration
MER	Mass Estimation Relation
MGTOW	Maximum Gross Take-Off Weight
QLS	Quantum Launch System
RP-1	Rocket Propellant One
RPA	Rocket Propulsion Analysis
RAMS	Reliability, Availability, Maintainability and Safety
SAT	Staging Analysis Tool
SNR	Signal-to-Noise Ratio
SOFI	Spray On Foam Insulation
TST	Trajectory Simulation Tool
TTS	Thrust Termination System
TVC	Thrust Vector Control
V&V	Verification and Validation
VRS	Vehicle Recovery System

List of Symbols

Symbol	Description	Unit
A	Area	[m^2]
a	Vehicle acceleration	[m/s^2]
A_e	Nozzle exit area	[m^2]
A_i	Nozzle inlet area	[m^2]
A_R	Receiver antenna area	[m^2]
A_T	Transmitter area	[m^2]
A_t	Nozzle throat area	[m^2]
c^*	Characteristic velocity	[m/s]
C_D	Drag Coefficient	[−]
C_{engine}	Cost of single engine	[$]
C_M	Mission cost	[$]
C_{m_α}	Moment Coefficient w.r.t angle of attack	[−]
$C_{m_{\dot{\alpha}}}$	Moment Coefficient w.r. $\dot{\alpha}$	[−]
C_{m_q}	Moment Coefficient w.r.t. pitch rate	[−]
C_{ops}	Operational costs	[$]
C_{Rec}	Recovery cost	[$]
C_r	Capacity	[Wh]
C_{stage}	Cost of single stage	[$]
D_c	Chamber diameter	[m]
E	E-modulus	[GPa]
E	Energy density	[Wh/kg]
f	Frequency	[Hz]
f_4	Cost reduction factor	[−]
f_8	Productivity factor	[−]
f_{10}	Automatic production reduction factor	[−]
f_{11}	Commercial cost reduction factor	[−]
f_c	Vehicle integration factor	[−]
F_T	Thrust Force	[N]
f_v	Vehicle type factor	[−]
G_R	Receiver gain	[dB]
G_T	Transmitter gain	[dB]
g_0	Sea-level gravity	[m/s^2]
h	Height	[m]
I	Moment of Inertia/Second Moment of Inertia	[m^4]
I_{sp}	Specific Impulse	[s]
I_{xx}	Mass moment of Inertia around x-axis	[kg m^2]
I_{yy}	Mass moment of Inertia around y-axis	[kg m^2]
j	Safety factor	[−]
K_g	Geometry factor	[−]
k	Boltzmann constant	[J/K]
L	Length	[m]
L	Launch rate	[$year^{-1}$]
L_a	Atmospheric loss	[dB]
L_c	Chamber length	[m]
L_i	Transmitter loss factor	[−]
L_n	Bell nozzle length	[m]
L_R	Receiver loss factor	[−]
L_s	Free space loss	[dB]
L_T	Transmitter loss	[dB]
L^*	Characteristic Length	[m]

M	Mach number	[-]
M_{bat}	Battery mass	[kg]
M_c	Combustion chamber mass	[kg]
M_n	Nozzle mass	[kg]
M_{Tank}	Tank mass	[kg]
M_w	Molecular weight	[kg]
Myr	Manyear	[$]
$\dot{m}$	Mass flow	[kg/s]
N	Number of launches	[−]
N	Load factor	[−]
P	Pressure	[Pa]
p	Learning factor	[Pa]
P_a	Ambient pressure	[Pa]
P_b	Battery power	[W]
P_c	Chamber pressure	[Pa]
P_e	Exit pressure	[Pa]
P_t	Tank pressure	[Pa]
P_T	Transmitter power	[W]
Q_N	Complexity factor	[−]
R	Data rate	[Mbit/s]
R_e	Exit radius	[m]
R_t	Throat radius	[m]
r	Radius	[m]
S	Frontal surface area	[m^2]
T	Thrust	[N]
T_c	Combustion temperature	[K]
T_s	System noise temperature	[K]
t	Thickness	[m]
t_{burn}	Burn time	[s]
V_{prop}	Propellant volume	[m^3]
V_c	Combustion chamber volume	[m^3]
V_e	Exhaust velocity	[m/s]
x_{cp}	Center of pressure location	[m]
x_{cg}	Center of gravity location	[m]
α	Angle of attack	[°]
α	Half angle	[°]
$\dot{\alpha}$	AoA rate	[rad/s]
ΔP_t	Turbopump pressure increase	[Pa]
ΔV	Velocity increment	[m/s]
ϵ	Expansion ratio	[−]
Γ	Vandenkerckhove function	[−]
γ	Specific heat ratio	[−]
η	Antenna efficiency	[−]
η_m	Electric motor efficiency	[−]
η_p	Turbo pump efficiency	[−]
θ	Parabola angle	[°]
λ	Wavelength	[m]
μ	Hinge angle	[°]
σ_{euler}	Euler buckling stress	[Pa]
σ_{shell}	Shell buckling stress	[Pa]
σ_{vm}	Von Mises stress	[Pa]
σ_θ	Hoop stress	[Pa]
ρ	Density	[kg/m^3]

CONTENTS

1

INTRODUCTION

There is a trend in the miniaturisation of satellites. The number of small satellites launched has already reached 100 per year, and is expected to grow by 23.8% per year until 2020. Many companies and universities are developing satellites of up to 6kg for many different purposes. Currently, these have to be launched into space piggy backing with other, larger, missions. This has primarily been done to save costs. The biggest disadvantage in this way of launching is that the satellite missions have limited flexibility for their orbits and launch dates. However, as of yet, no dedicated launch system for small payload exists. Quantum Space was asked to develop a solution to this problem. This project explores the possibility for a dedicated, economically viable, launch system.

This report is preceded by a project plan, a baseline report and a mid-term report. In these previous efforts, the project was set up, initial top-level constraints were translated into system requirements and a market analysis was performed. Then, initial concepts were developed and a trade-off was performed.

The purpose of this report is to present a detailed design of the chosen concept, the ground launch. The different subsystems are designed and the possibilities to reduce costs in terms of development, production and operation are examined. The way to achieve the design was an iterative design process together with a systems engineering approach. Many iterations were made and to optimise the design with respect to lift-off mass. Furthermore, the next steps in the project are set up.

The structure of the report is as follows, firstly a brief overview of the project is given in Chapter 2. After that, the different subsystems of the rocket are designed in more detail in Chapter 3. In Chapter 4 the design is analysed and verified. Chapter 5 details the performance analysis of the launcher and chapter 6 details the project sustainability strategy. Next, in Chapter 7, the development of the project is discussed. After that a business plan is given in Chapter 8, which contains a market analysis and the post-DSE (Design Synthesis Exercise) activities. Finally, in Chapter 9, further recommendations are given.

2

Project Overview

In recent times satellites have become smaller because of technological developments. However, dedicated launchers for these smaller satellites do not exist at this moment. Small satellites are piggybacked on other missions, to save costs. The disadvantage for the customer of the small satellite is that he or she is dependent on the chosen inclination and altitude of the launch mission. Some commercial companies are developing smaller rockets for smaller payloads. They aim at a payload of 250 kg and more. However, studies show that the market for satellites up to 10 kg will grow 23.8% every year until 2020. This project is started to develop a launcher which is capable of launching satellites up to 60 kg into LEO. The reader is referred to Section 8.1 for a more detailed market analysis.

At the start of the project, as many concepts as possible were considered. In an early stage of this project they were traded off against each other in terms of costs, complexity and feasibility. Three different concepts survived this trade off, which were a fighter jet air launch rocket, a railgun assisted launch system and a ground launch rocket. These are shown in Figure 2.1, 2.2 and 2.3 respectively.

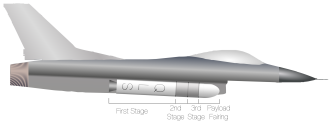

Figure 2.1: Fighter jet air launch

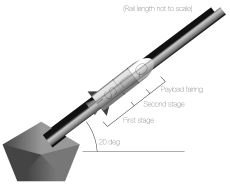

Figure 2.2: Railgun

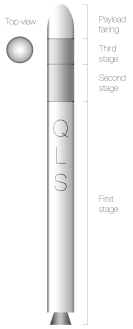

Figure 2.3: Ground launch

In the next phase of the project, these three different concepts were designed in some more detail, to find out which was the best solution. From this design phase it was concluded that the railgun was not possible due to high g-loads during launch, and an air launch was not possible due to the size of the rocket. Finally the ground launch is chosen, since its proven technology and simplicity. The rocket should be reusable in some manner, to reduce the costs to launch for a competitive price of less than $ 50,000 per kg payload.

In this report the ground launch concept is further designed, both the technical aspects, starting in Chapter 3, and the non-technical aspects, starting in Chapter 7. The mission requirements are shown in the compliance matrix in Section 4.4.

3

DETAILED DESIGN

In this chapter the technical design of the rocket is discussed: the sizing and designing methodology of the various subsystems is given, followed by important design parameters that were generated from design iterations. The flight dynamics, including astrodynamics, are calculated and presented in Section 3.1, after that the rocket engine has been designed in Section 3.2. Once the propellant is known and the engines are sized, the main rocket structure, including fuel and oxidiser tanks, can be determined, which is done in Section 3.3. Then aerodynamic characteristics are presented in Section 3.4 followed by the design of the attitude determination and control system (ADCS) in Section 3.5. The electrical power system (EPS) is then sized in Section 3.6 and the power budget is estimated. The communication system is then discussed in Section 3.7, followed by the recovery subsystem in Section 3.8. The last subsystem that is then presented is the flight termination system (FTS) in Section 3.9. The payload integration is then discussed in Section 3.10. Then, since all the subystems are analysed, it will be discussed how one depends on the other during the iterations in Section 3.11. A complete layout of the rocket is then given in Section 3.12 and the mass budget is estimated in this section as well.

3.1. FLIGHT DYNAMICS

This section describes the methods and tools used to describe the flight trajectory of the launch vehicle. First the parameters of interest are discussed in Section 3.1.1. Next the Staging Analysis Tool (SAT) will be described in Section 3.1.2 and the Trajectory Simulation Tool (TST) is described in Section 3.1.3.

3.1.1. PARAMETERS OF INTEREST

In order to design the launch system it is required to relate the design to key flight performance parameters. These parameters affect the design to such an extent that they require more accurate predictions than can be provided analytically. Tools have been developed to estimate and evaluate the following parameters:

- ΔV provided
- ΔV losses
- Loads encountered
- Engine performance and throttling requirements
- Flight profile
- Boost-back capability

Each of these parameters depend primarily on the design, but also vary greatly with a change in trajectory. A shallower ascent will encounter more drag, affecting both the structural loads as well as drag losses, but it will also reduce gravity losses. A first stage providing a relatively large portion of ΔV will bring it further down-range and increase the velocity tangential to the surface, requiring substantially more propellant for a boost-back burn, and it will also require more throttling as the engine performance will have a larger variation throughout the atmosphere. The developed tools are used to quantify these effects in order to tune the design.

3.1.2. STAGING ANALYSIS TOOL

The Staging Analysis Tool was designed to quickly size the launcher based on high level design characteristics. It uses the payload mass, the total ΔV required, the ratio of ΔV provided by each stage and the structural efficiencies to calculate the masses for each stage. The ΔV is further expanded by adding a fraction for contingency propellant, as well as a factor for propellant needed for the boost-back manoeuvre. The key benefit of this tool is its speed, allowing for quick estimation of the impact of individual design parameters. It is also used in the design iteration, where the structural efficiency obtained after subsystem sizing is used to evaluate the design and to estimate a new starting point for the following design iteration.

ASSUMPTIONS AND LIMITATIONS

The SAT is based on Tsiolkovsky's equation, which is well established. The input values however are always an assumption based on literature or previous iterations.

- The specific impulse, for which it is assumed that a time-average specific impulse can be used, for the stage ΔV is taken from the TST described below.
- The total required ΔV is taken from the TST.
- The contingency propellant is taken to be 2% from reference data[1].
- The Structural Efficiency is the most important value coming from previous iterations.

There are no limitations imposed by the implementation, but from the theory. When the structural efficiency is too high, there is insufficient mass fraction for propellant, and the requested ΔV for that stage cannot be reached.

3.1.3. TRAJECTORY SIMULATION TOOL

The Trajectory Simulation Tool was developed to model the flight of the launcher in detail. Its main inputs are the design parameters for the launcher, including masses of the stages, propellant masses and g-load limitations. Next to this several engine characteristics are input for each of the stages, allowing accurate thrust calculations at each altitude. Engine data is provided in several throttle settings per stage, allowing selection of lower thrust profiles to ensure compliance with g-limits. The tool interpolates the atmosphere from data from the MSIS-E-90 model, which is used to calculate local pressure, density and speed of sound throughout the flight. Finally for drag the diameter of the launcher is input, along with the drag coefficient for a wide range of Mach numbers.

The TST uses a pure gravity turn ascent, after a 50 meter vertical climb, initiated by a small kick angle. After this the launcher continues at full thrust until it exceeds the g-limit, at which point it will switch to the next engine thrust setting automatically. Once the primary propellant of the stage is consumed the launcher coasts for a predetermined amount of seconds and subsequently drops the lower stage and ignites the following stage engine(s). This process continues until orbit is reached. The key input parameters in this simulation are the kick angle and the coast time per stage. The kick angle strongly influences how soon the trajectory is curved by gravity, especially for low thrust-to-weight lift-off. The coast time, and specifically that between the second and third stages, allows the trajectory to be curved further before the subsequent burn. Without this the kick-angle would be uniquely defined by the desired orbit altitude.

Alternatively the TST can be set to follow the first stage upon separation, such that the boost-back manoeuvre can be simulated. In this case the launcher waits an additional time before firing the engines in a predefined thrust setting, and with the launcher pointed in the direction opposite to the velocity tangential to the surface. This counters the tangential velocity and gives the rocket a smaller tangential velocity back towards the launch site. The radial velocity is not modified, such that the launcher continues to climb until culmination. After the boost-back burn the launcher follows a ballistic trajectory until the parachutes are deployed.

The main outputs for the TST are the instantaneous position vector, velocity vector, mass and mass flow, throughout the entire flight. From these values derived quantities can be output, such as altitude, down-range distance and pitch angle. The TST can also output all data it uses to calculate the accelerations at each instant, which includes atmospheric properties, Mach number, drag, engine thrust and g-loads. The TST also calculates and outputs losses due to both drag and gravity. A successful launch trajectory, seen by the second pass intersecting the injection point, is shown in Figure 3.1. The other outputs from the TST are shown and discussed in more detail in Chapter 5.

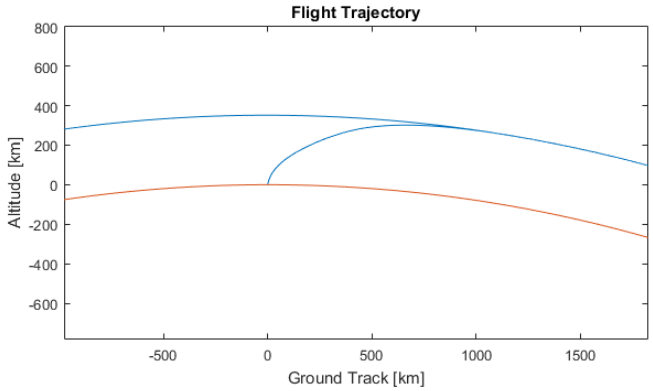

Figure 3.1: An example trajectory for a succesfull launch, showing the trajectory in blue and the Earth surface in red.

ASSUMPTIONS AND LIMITATIONS

The simulation can calculate instantaneous accelerations and uses these in a Runga-Kutta (RK4) method to solve the second order differential equation for velocity and position. It assumes the following values:

- The gravity is calculated assuming a spherical, homogeneous Earth, i.e. the gravity field around Earth varies only with altitude and not longitude or latitude.
- The simulation is two-dimensional, where the orbit axis extends into the page/screen
- Control losses are not yet implemented, as control system was still being designed
- The angle of attack is forced to be 0, effectively rotating the launcher parallel to its velocity
- Disturbance forces such as wind are not yet implemented
- The drag coefficient is not varied when the rocket stages.
- Engines start instantaneously, meaning they go from 0 thrust to design thrust without delay.
- The ratio of specific heats for air is assumed constant, which is only valid up to roughly 100 kilometres. this affects the speed of sound, which because of this less accurate above 100 kilometres.
- The first stage of the launcher is assumed to be able to withstand reentry from its culmination altitude, not requiring additional burns.

The tool itself has no hard limitations, but source data for the atmosphere is only provided up to 1000 kilometres, after which the atmosphere will be modelled equal to the final value. As with any propagation model the accuracy decreases with larger time-steps or with the total time of the simulation. Numerical error and computer memory would not allow for this script to be used accurately for more than a few orbits. It is unsuited for orbit life estimations.

3.2. PROPULSION SUBSYSTEM

This section elaborates on the mass and geometry sizing of the propulsion system. First, the propellant is selected in Section 3.2.1. Subsequently, the nozzle is selected and sized for all rocket stages in Section 3.2.2. Afterwards, the feed system and the turbo pumps are explained and displayed in Sections 3.2.3 and 3.2.4 respectively. Next to that, the performance and propulsion characteristics based on the selected propellants is determined in Section 3.2.5. Finally, all the propulsion system geometries and masses are evaluated in Section 3.2.6.

3.2.1. PROPELLANT SELECTION

Since the first stage is going to be recovered, liquid propellants will be used. In this way, the boost back manoeuvre can be initiated and controlled, in order to direct the first stage to the landing area. Secondly, the least amount of refurbishment effort is needed to prepare the stage for a new launch.

A trade off has been performed on the type of fuel. The following fuels have been considered: liquid hydrogen (LH2), liquid methane (LCH4), and refined kerosene (RP-1). The oxidiser will for all fuels be liquid oxygen (LOX). LCH4 has been selected as liquid propellant, since it performs best in the following criteria:

Combustion Characteristics - LCH4 does not coke (polymerise) at the operating temperatures of the rocket engine, since the coking point is about twice as high [2]. This causes the amount of soot and other residues in the rocket engine to drastically decrease, compared to if RP-1 were to be used. Eventually, this has a benefit on the reusability of the rocket engine and hence the whole stage. Both LCH4 and LH2 are also 'green' propellants, having a lower environmental impact than RP-1. Additionally, LH2 also does not leave soot, as the only combustion product is water.

Bulk Density - With 830 kg/m^3 for LCH4 vs 1030 kg/m^3 for RP-1, LCH4 has a lower bulk density. It is the density of the combined fuel and oxidiser load in their appropriate O/F ratios. Since LCH4 is ignited with 3.5 parts of LOX, whereas RP-1 with 2.1. This causes the rocket to be carrying more oxygen and less fuel by weight. The density of LOX is 1140 kg/m^3. The bulk density of LH2 is worse: 290 kg/m^3 [3] [4].

Cooling Requirements - The LOX has to be cooled to a temperature of 90K.The boiling point of methane is about 110K, hydrogen at 20K and RP-1 does not have to be cooled. Since cooling systems add mass cooling is not preferred. But since LCH4 needs the same system as LOX, which has to be developed anyway, this makes it more acceptable. Furthermore, expensive helium has to be used for LH2 as pressurisation gas, since nitrogen freezes at the temperatures of LH2. The cooling requirements of LH2 in combination with the bulk density of LH2 is the reason to eliminate

LH2 of the propellant trade off. For cooling of the engine, the cooling capability of LCH4 is three times higher than that of RP-1 [2] [5].

Propellant Costs - Despite the fact that propellant costs only make up a small part of the total launch costs, about 1% [1], the acquisition cost of LCH4 is about three times smaller than for RP-1. Next to that, the long-term availability is considerably higher [6]. Aside, from a futuristic point of view, LCH4 can be easily produced on extraterrestrial bodies, e.g. Mars. Imported water or hydrogen together with CO_2 can be converted into CH_4, methane.

A summary of the trade off can be seen in Table 3.1, from which LCH4 is selected. This conclusion is confirmed by [2], where it is mentioned that RP-1 and LCH4 perform equally with respect to bulk density and I_{sp}. Since reusability is required, LCH4 is the best fuel.

Table 3.1: Propellant Characteristics

Characteristic/Fuel	LH2	RP-1	LCH4
Reusability	Leaves no soot	Leaves soot	Minimal soot
Bulk Density	Very low	High	Medium
Cooling requirements	Very low temperature	Not needed	Equal to LOX
Performance	Highest I_{sp}	Good I_{sp}	I_{sp} 10s higher than RP-1

3.2.2. NOZZLE SELECTION AND SIZING

The nozzle is the component of the rocket that produces thrust. This will be accomplished by converting the thermal energy of the ignited propellants in the combustion chamber into kinetic energy directed along the axis of the nozzle [7] [1]. Different types of nozzles exist. In order to accelerate the flow beyond $M = 1$, a convergent-divergent Laval type nozzle is needed. The main ones used are the conical nozzles, the bell nozzles and the aerospike plug nozzles. These geometries can be seen in Figure 3.2.

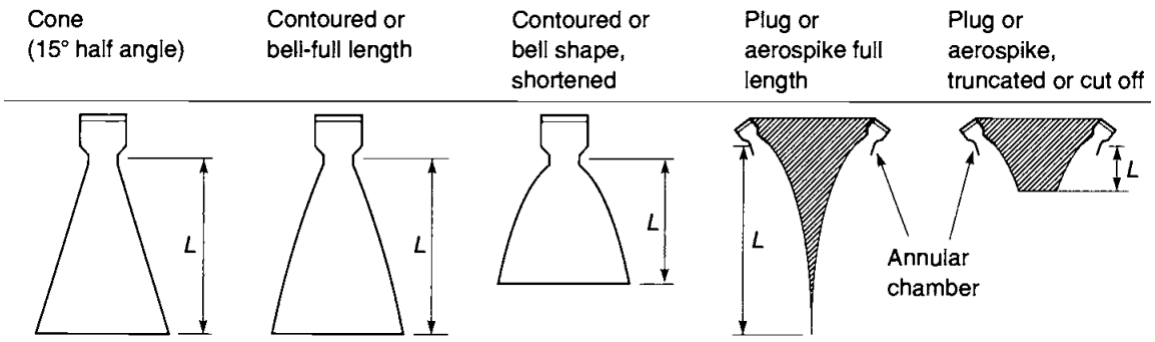

Figure 3.2: Different Nozzle Configurations [7]

Conical Nozzles
The conical nozzle is the simplest one of the three, with a conical divergent part. It has a conical divergent part, which follows the cone half-angle α. There is an optimum conical nozzle shape and length, which is a compromise on length hence mass and performance, dependent on the space mission and flight path. The half angle α, between the vertical axis and one nozzle wall, usually varies between 12 and 18 degrees [7] [1].

Bell Shaped Nozzles
The bell nozzle obtained its name due to its resemblance to bell shape geometry. It has a high expansion section right after the throat, with angles ranging from 20 to 60 degrees [3] [1]. Afterwards, the nozzle contour gradually reverses up to the exit area. Ideal bell nozzles exist for optimum expansion ratios and truncated nozzles exist for cut-off bell nozzles. The bell nozzles related to the optimum expansion ratios, which can go up to in the order of $\epsilon =$ several thousands for the 2nd and 3rd stage of the rocket. In order to prevent very large nozzles and corresponding nozzle masses, the bell nozzle is truncated at one point, in order to obtain an appropriate nozzle exit diameter for the corresponding rocket stage [7].

Figure 3.3 [1] shows the different nozzle expansion types of the flow. From left to right, (a) to (b), the nozzle is over expanded, fully expanded at adapted nozzle conditions and under expanded. Adapted nozzle conditions involve that the exit pressure of the flow is equal to the ambient pressure of the rocket, providing the maximum operating nozzle efficiency.

[1] http://www.aerospaceweb.org/design/aerospike/compensation.shtml, visited on: 4-01-2016

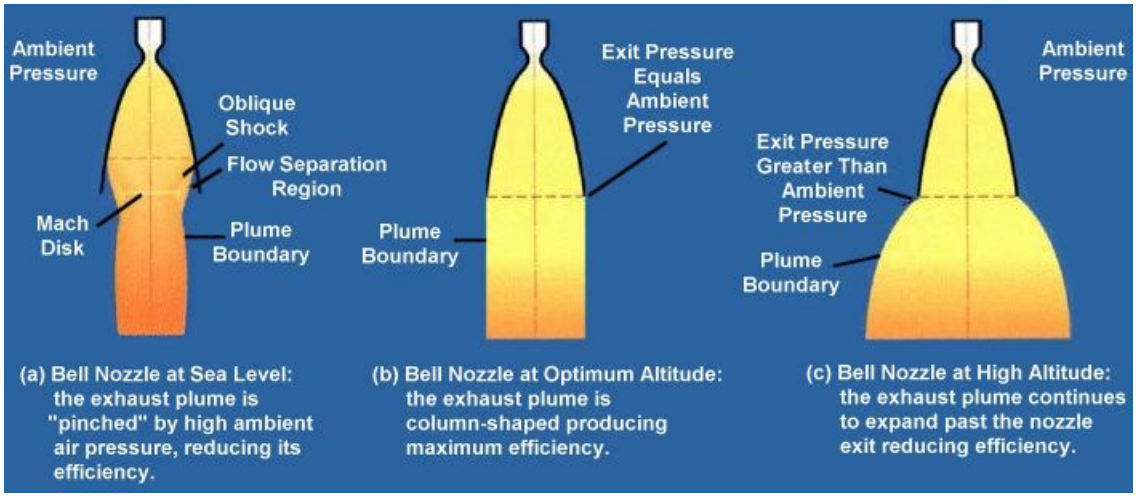

Figure 3.3: Bell Nozzle Expansion Types

Aerospike Plug Nozzles

Aerospike nozzles have as an main advantage that they allow for altitude compensation, because they have a geometry such that the jet is open on one side [1]. They are sometimes also referred to as plug nozzles, because they incorporate a centre body plug inside the nozzle, which blocks the flow from what would be the centre portion of a conical or bell nozzle. This causes the exhaust to be forced inwards, while increasing the pressure on the centre body plug and hence the thrust. If the aerospike engine is operated at high altitudes, the exhaust flow is constrained by expansion and compression waves that cause the thrust on the centre plug to be maintained. The result is a high efficiency column shaped exhaust. This is illustrated in Figure 3.4.

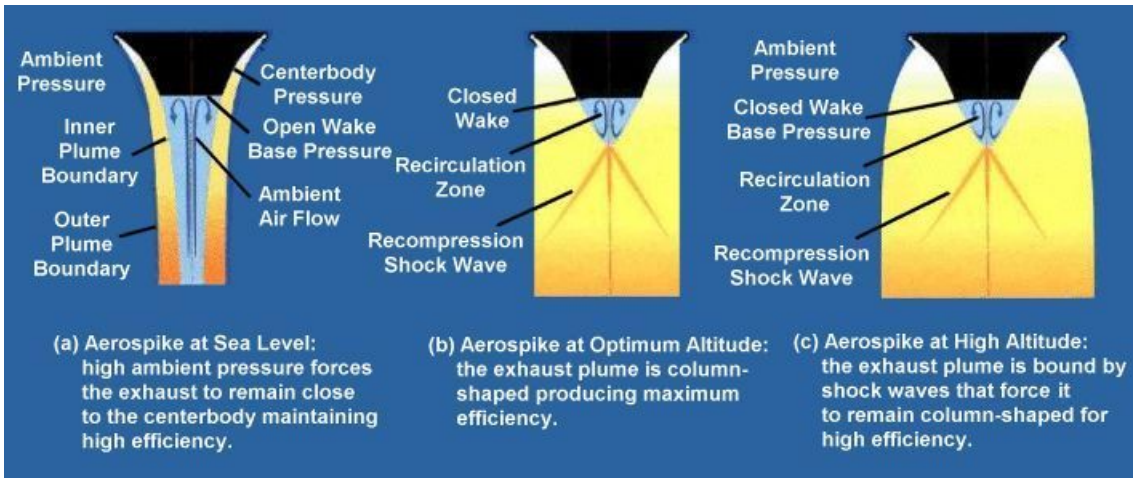

Figure 3.4: Exhaust Flow Aerospike Engine

Selected Nozzle Type and Geometry - Bell Nozzle

Plug nozzles are the least employed ones of all the previous discussed nozzle types. This is due to their enormous complexity. Next to that, interest in plug nozzles is mostly for the use on aerospace planes, where altitude compensation is requested [1]. In the case of rocket stage separation, bell nozzles can be designed for optimum performance.

Since the wall contour of the bell nozzle is designed to minimise losses, the expansion of the exhausts is more efficient than in a simple straight cone of similar area expansion ratio and length. Theory reveals, that bell nozzles that have 80% the length of 15° half angle conical nozzles, are able to obtain the same efficiency, maintaining the same expansion ratio [1].
The geometry of the bell shaped nozzle is determined by the throat radius R_t, the exit radius R_e, the initial parabola angle θ_n and the final parabola angle θ_e. These parameters are illustrated in Figure 3.5. These shapes are optimised by Rao [8] and have been applied to many existing nozzle designs [1] [9]. The length L_n of the bell nozzle is determined as a 80% value as if it was a 15° half angle conical nozzle, with the same expansion ratio and radii.

Looking at the relation for the expansion ratio and nozzle angles in Figure 3.6, the bell nozzle angles can be deter-

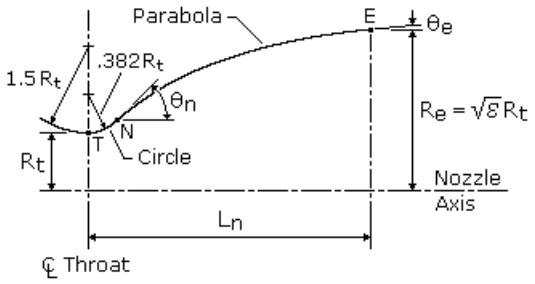

Figure 3.5: Bell Nozzle Geometry [7]

mined using the selected nozzle expansion ratio per stage and the 80% nozzle length value. All the nozzle geometry values can be found in Table 3.3.

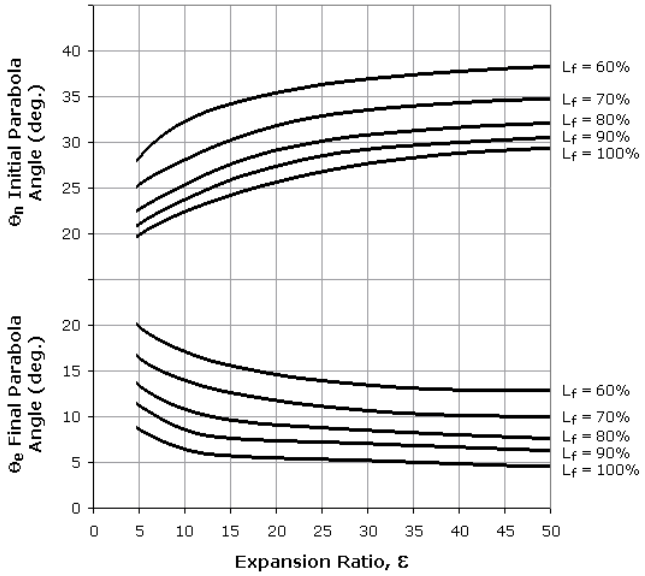

Figure 3.6: Expansion Ratio vs. Bell Nozzle Angles [7]

During the design process it turned out that for the second but mainly for the third stage, the mass of the nozzle would be extremely high if it would be made completely out of steel. Therefore, a more advanced design has been selected. All three nozzles can be seen in Figure 3.7. The first stage nozzle and chamber, seen on the left, will be completely regenerative cooled with the LCH4. The manifold that injects the fuel into the end of the nozzle can be seen in the figure. Then for the second and third stage engine, a carbon fibre reinforced ablative cooled extension skirt is added after an expansion ratio of 40. By adding ablative material to the inside face of the carbon fibre nozzle, a passive cooling system is created as the ablative takes up energy in the form of heat in order to decompose when the engine is firing.

This has several advantages. Firstly, the experience gained on the development and production of the regenerative cooled chamber and nozzle from the first stage engine can be used. While the ablative cooled nozzle cannot be reused, this does not matter since the second and third stage burn up. Finally a large mass reduction in the nozzle mass is achieved by using the ablative nozzle.

3.2.3. FEED SYSTEM

In this section the layout out of the feed system is discussed. A general sketch can be seen in Figure 3.8. Only for the first and second stage a turbo pump is used, hence the dotted lines. Furthermore, for the first stage there are four nozzles in total.
The LOX has a higher density than the LCH4 and is therefore placed above the LCH4. This is to place the centre of gravity as high as possible for better stability characteristics of the whole launcher.

In order to get the propellant into the turbo pump the tanks have to pressurised. This will be done by high pressure nitrogen gas that is stored in a separate tank, as can be seen in Figure 3.8. Every pressure vessel should be able to be filled and drained, this can be done by the same valve. Furthermore all pressure vessels have a safety valve that

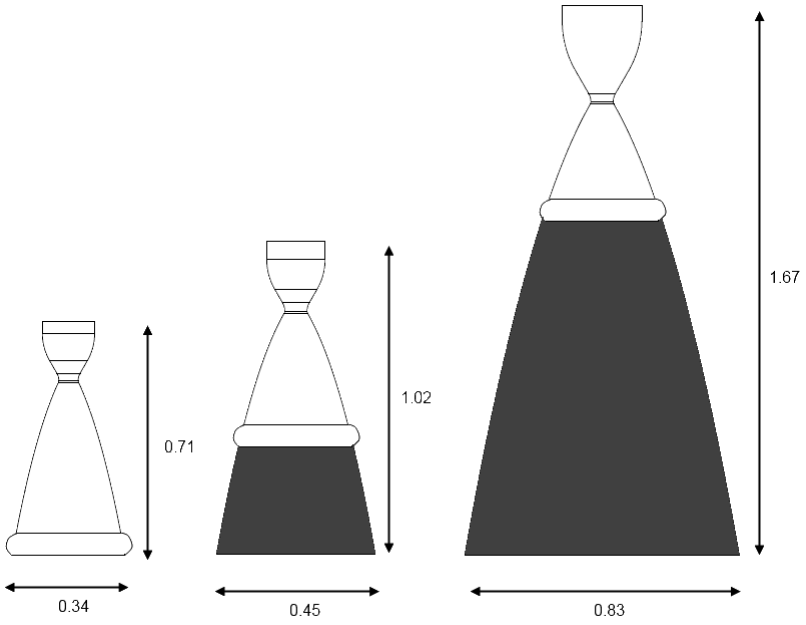

Figure 3.7: Nozzle Geometry Stage 1, 2 and 3 (with black ablative extension skirts)

opens automatically if a critical pressure is reached. The cryogenic tanks also have a separate vent valve, to vent during hold down on the pad.

3.2.4. TURBO PUMP SIZING

Pump fed engines can be used up to thrust levels of 50 kN whereas above that level turbo pumps are required [10]. Turbo pumps are expensive to develop and manufacture (around 25% of engine production cost [10]) and have been the reason for several delays in rocket engine development. In this section the turbo pump design is discussed. However, because of the complexity of turbo pumps, the actual design of the pump out of the scope of this project. But the inputs and outputs of the pump can be given, as well as a mass estimation.

It was decided to use a turbo pump driven by an electric motor powered by a battery pack, instead of the usual gas generator driven turbine. This might increase mass of the turbo pump, but definitely reduces complexity and thus cost. The required power that has to be provided by the power source, in this case the batteries is given by Equation (3.1) [1]. In this equation, $\dot{m}$ equals the mass flow in kg/s of either the fuel or oxidiser, ΔP_t is the increase in pressure in Pa, ρ is the density of the propellant in kg/m^3, η_p is the efficiency of the turbo pump and η_m is the efficiency of the electric motor. The used values can be seen in Table 3.2.

The required power the battery mass can be determined using the Equation (3.2), where E equals the energy density. The burn time follows from trajectory simulations and energy density as can be seen in Table 3.2.

$$P_b = \frac{\dot{m} \cdot \Delta P_t}{\rho} \cdot \frac{1}{\eta_p \cdot \eta_m} \tag{3.1}$$

$$M_{bat} = \frac{t_{burn} \cdot P_b}{E \cdot 3600} \tag{3.2}$$

Table 3.2: Values for the parameters used in Equation (3.1) and (3.2)

Parameter	Value	Comment
P_t	68 bar	$1.2 \cdot P_c$ - Tank Pressure
η_p	0.75	Based on reference pumps
η_m	0.92	Based on efficiency of brushless DC motor
Energy density	265 Wh/kg	Based on high performance LiPo batteries

Afterwards, based on reference data, the mass of the electric motor is estimated on 15kg [2] and the pump itself on 10kg.

A sketch of the turbo pump assembly can be seen in Figure 3.9. It consists of three parts. At the top the pump is located, then directly under it the electric motor. The battery is located under the motor and dependent on the total

[2] http://www.electricmotorsport.com/me1115-brushless-motor-24-96v-5000rpm-12-kw-cont-30-kw-pk.html, visited on: 9-01-2016

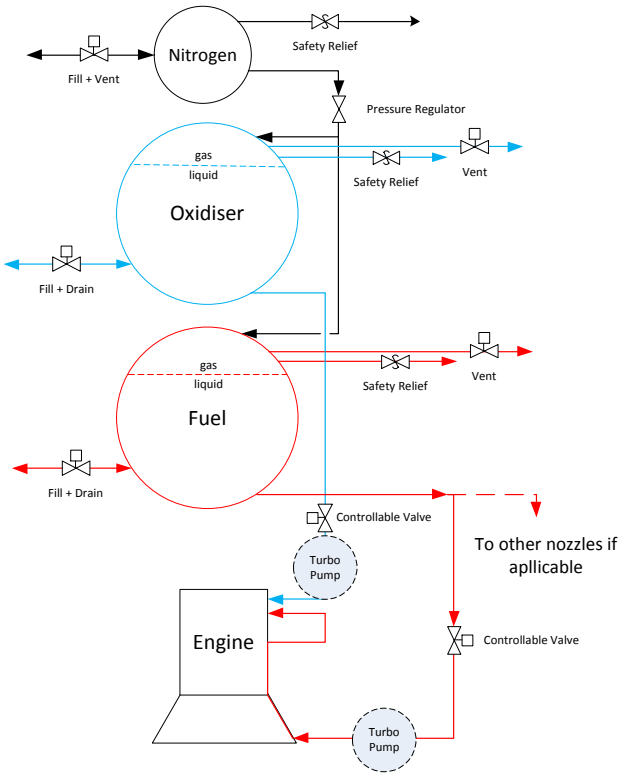

Figure 3.8: A general sketch of the feedsystem for all stages

energy needed the length is scaled, while the diameter stays the same. This means that for every stage and fuel or oxidiser flow the same pump and motor can be used, and that only the battery changes. The final masses are given in Table 3.3.

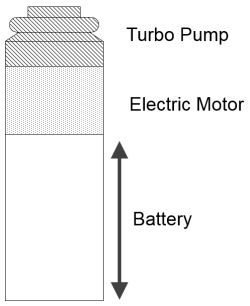

Figure 3.9: A sketch of the turbo pump assembly

3.2.5. PROPULSION PERFORMANCE CALCULATIONS

A combination of the software tool Rocket Propulsion Analysis (RPA [11]) and self-developed code was used for designing the propulsion system. Inputs for RPA are the used propellants, chamber pressure (P_c) and expansion ratio (ϵ). The later used outputs that RPA gives are: exit pressure (P_e), exhaust velocity (V_e), combustion temperature (T_c), ratio of specific heat (γ), molecular weight (M_w), characteristic velocity c^* and I_{sp}. Furthermore RPA determines the estimated delivered performance, so including nozzle and reaction efficiencies.

With the required thrust per stage, given by Equation (3.3), and the outputs from RPA, the required mass flows can be calculated using Equation (3.4):

$$F_T = am[N] \tag{3.3}$$

Where F_T is the required thrust for the stage (following from Trajectory Simulation), and a is the pre-set acceleration of the stage and m is the mass of the stage.

$$\dot{m} = \frac{F_T}{I_{sp}} \frac{1}{amountofengines} [kg/s] \tag{3.4}$$

Then the throat area is given by (3.5) [12]:

$$\dot{m} = \frac{\Gamma \cdot P_c \cdot A_t}{\sqrt{\frac{R_A}{M_w}} \cdot T_c} \tag{3.5}$$

RPA is capable of calculating mass flows and throat areas on its own, but this was not used because implementation in the self-developed code was not convenient. However, this gave a way of verifying the code (see Chapter 4).

Then with all required engine parameters known the thrust at a certain altitude can be calculated with Equation (3.6):

$$F_T = \dot{m} \cdot V_e + (P_e - P_a) A_e \tag{3.6}$$

EXPANSION RATIO

An iterative loop was used to determine the expansion ratio of the second and third stage nozzles, which can be seen in Figure 3.10. The iteration was started with the optimum expansion ratio, determined by the ambient pressure. This resulted in very long, wide and heavy nozzles, which conflicted with the maximum dimensions of the rocket. Then a new expansion ratio is calculated driven by the maximum exit diameter and given as input to RPA. This, however, gives a lower I_{sp}, so the A_t should be bigger. After a few iterations the calculations converges to the solution.

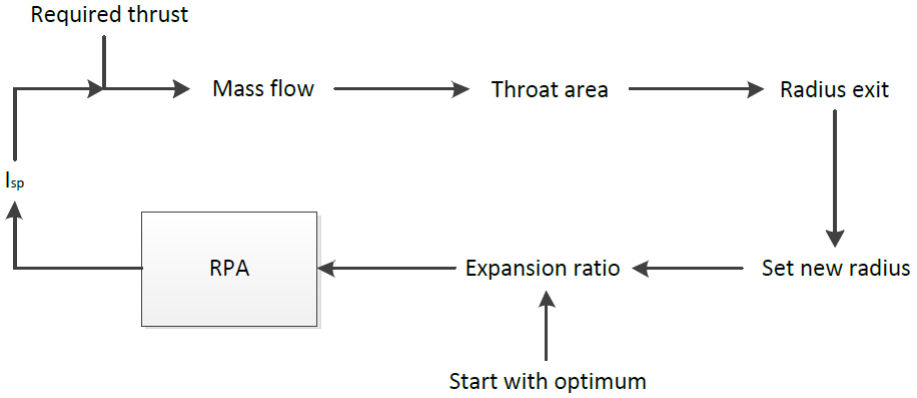

Figure 3.10: Flow chart on how to determine expansion ratio

The nozzle of the first staged was optimised for the average ambient pressure of the stage while travelling through the atmosphere. This value follows from the trajectory simulation. The expansion ratios of the nozzle per stage can be seen in Table 3.3.

THROTTLING

The rocket requires throttling of the engines to keep the accelerations acceptable. RPA is used to calculate the exhaust velocity at several throttling values, i.e. different chamber pressures for the same engine. The used throttling values vary between 0.6 and 1.0. Then this exhaust velocity can be used in Equation (3.6). RPA can also calculate the thrust, but it was not convenient to implement this in the written code. However this gave a way to verify the thrust calculations made (see Chapter 4).

It was assumed that γ, T_c and O/F ratio were constant for the different chamber pressures, which is a simplification and this is discussed in Chapter 4. Mass flow can be calculated with Equation (3.5) and exit pressure with (3.7). But because of these assumptions mass flow and P_e varies now linearly with throttle ratio, which makes the calculations significantly easier. These values can then also placed in Equation (3.6) to calculate the thrust.

$$\frac{A_e}{A_t} = \frac{\Gamma}{\sqrt{\frac{2\gamma}{\gamma-1} \cdot \left(\frac{p_e}{p_c}\right)^{\frac{2}{\gamma}} \left(1 - \left(\frac{p_e}{p_c}\right)^{\frac{\gamma-1}{\gamma}}\right)}} \tag{3.7}$$

3.2.6. ENGINE MASS SIZING

The combustion chambers need to have the appropriate volume that is required for proper combustion. An important parameter in the combustion chamber design, is the characteristic length, L^*, as determined by Equation (3.8). This parameter is a measure for the chamber volume divided by the nozzle sonic throat area [13].

$$L^* = \frac{V_C}{A_t} \tag{3.8}$$

The value of L^* relies on past experience with similar propellants and engine sizes. Next to that, it depends on the mixture ratio, chamber pressure and injector and chamber geometry. It is evaluated from actual usage of combustion chambers in experiments. It does not widely vary for the propellants that are in use today and the value used for LCH4 and LOX is $L^* = 0.88$ [3] [1] [7].
L^* is given as input to RPA and then RPA gives the chamber geometries. The masses are determined with Mass Estimation Relations (MER) from [1]. The reason for the use of MERs is required since many iterations had to be done to find the overall optimum launcher performance.
Equation (3.9) is used in order to determine the combustion chamber mass. K_g is a geometry factor, which is defined by Equation (3.10). The thickness of a cylindrical chamber is determined with Equation (3.11). In order to determine the mass of the injector and the valves, Equations (3.12) and (3.13) are used respectively. Finally, the nozzle mass is determined with Equation (3.14). Table 3.3 shows the mass and geometry characteristics for the combustion chambers used per stage.

$$M_c = K_g \cdot \frac{\rho_{nozzle}}{\sigma_{nozzle}} \cdot j \cdot P_c \cdot V_c \tag{3.9}$$

$$K_g = \frac{1}{L_c/D_c} + 2 \tag{3.10}$$

$$t_c = \frac{P_c \cdot D_c}{2\sigma_{chamber}} \cdot j \tag{3.11}$$

$$M_{injector} = \frac{1}{3} \cdot M_c \tag{3.12}$$

$$M_{valves} = 0.2\left(F_T \cdot p_c\right)^{0.71} \tag{3.13}$$

$$M_n = \frac{\rho_{nozzle}}{\sigma_{nozzle}} \cdot j \cdot \left(A_i \cdot \left(\frac{\epsilon - 1}{sin(\alpha)}\right) \cdot \left(\frac{D_c \cdot P_c}{2}\right)\right) \tag{3.14}$$

Table 3.3: Final Parameters of one Engine per Stage | Feed System included Pressurisation System

		Stage 1	Stage 2	Stage 3
Amount of engines	[#]	4	1	1
Thrust	[kN]	34.3	48.9	17.3
Vacuum I_{sp}	[s]	352	359	375
Chamber Pressure	[bar]	80	80	23
Expansion ratio	[-]	34	50	150
Throat area	[cm^2]	2.713	3.162	3.63
Exit diameter	[m]	0.343	0.449	0.833
Length Chamber + Nozzle	[m]	0.707	1.02	1.67
O/F Ratio	[-]	3.33	3.36	3.48
Mass flow	[kg/s]	11.9	13.9	4.7
Nozzle + chamber mass	[kg]	21.05	27.14	33.8
Fuel turbo pump mass	[kg]	30.72	38.48	Blow down
Oxidiser turbo pump mass	[kg]	32.04	41.77	Blow down
TVC mass	[kg]	14.96	19.7	23.4
Feed system	[kg]	39.33	15.91	8.6
Total Dry mass Engine	**[kg]**	**138**	**143**	**65.8**

3.3. STRUCTURES

This section deals with the structural and vibrational analysis of the QLS. First, the propellant tanks are structurally sized in Section 3.3.2. The landing legs will be discussed in Chapter 3.8 as part of the recovery subsystem.

3.3.1. MATERIAL CHOICE

The material that is chosen for the tank and structure design is Lithium Aluminium. In comparison with normal aluminium it has a 7-10% lower density, a 10-15% higher Young´s modulus and excellent fatigue and cryogenic toughness properties [14]. All the characteristics makes Lithium aluminium more favourable than normal aluminium.

Carbon fiber reinforced polymers could also be used, but their fatigue behaviour (important for reusability) and cryogenic behaviour are unknown factors. Hence, aluminium lithium is selected.

3.3.2. INTEGRAL PROPELLANT TANK STRUCTURES

Integral propellant tanks are being used in order to combine the pressure loads with the axial body force loads. In this manner, the structure weight can be lowered considerably. Based on the selected propellants for each stage, the propellant tanks will be sized. The rocket uses the fuel LCH_4 with LOX as oxidiser. These propellants are stored in cylindrical and spherical pressure vessels, under a pressure of 28 bar [15]. Based on the rocket diameter of 1m, the thickness of the pressurised propellant tanks is such that it will be able to cope with the hoop stresses, caused by the pressurised propellant inside the tank. It is determined using Equation (3.15) with a safety factor of $j = 1.8$ for the reusable stages and $j = 1.25$ for the expandable ones.

$$\sigma_\theta = \frac{Pr}{t} \Rightarrow t = j \cdot \frac{Pr}{\sigma_\theta} \tag{3.15}$$

The 3rd stage has an amount of propellant, that is capable of being stored in spherical tanks solely, whereas the first and second stage use cylindrical tanks. This amount does not allow for large spherical tanks, which are as wide as the rocket diameter. Hence, a 3rd stage shell is designed in order to carry the axial loads. The height h of the cylindrical parts of the fuel tanks is determined with the required propellant volume, using a cylindrical tank with two hemisphere ends. This is indicated by Equation (3.16). The masses of the fuel tanks are determined by using the tank structure volume and the material density in Equation (3.17). In this equation the subscript cp denotes the cylindrical part of the fuel tank. The material that connects the tanks to the rest of the integral structure in the first and second stage, is evaluated with the radii of the corresponding tank hemisphere end caps, together with equal thickness for perfect integration.

$$h = \frac{V_{prop} - \frac{4}{3}\pi r_t^3}{\pi r_t^2} \tag{3.16}$$

$$M_{Tank} = \rho\left(2\pi \cdot r_t \cdot t_t \cdot h_{cp} + 4 \cdot r_t^2 \cdot t_t\right) \tag{3.17}$$

All the propellant tank masses and their geometries are listed in Table 3.4.

Table 3.4: Propellant Tanks Characteristics

Propellant tank	Mass [kg]	Volume [m^3]	Total length [m]
Oxidiser stage 1	201	2.98	4.13
Fuel stage 1	167	2.42	3.41
Oxidiser stage 2	83	1.75	2.56
Fuel stage 2	69	1.40	2.12
Oxidiser stage 3	35	0.59	1.09
Fuel stage 3	45	0.46	0.96
Totals	**601.02**	**9.60**	**14.26**

3.3.3. FAILURE MODE ANALYSIS

In order to have a proper structure, a failure mode analysis is performed. The structure is checked for Euler buckling with Equation (3.18), shell buckling using Equation (3.19) to (3.22) and compressive yielding, where all axial stresses are combined with Equation (3.23). In Equation (3.21), λ equals the value for which the expression is lowest. This is determined by differentiating and the result is shown by Equation (3.22).

$$\sigma_{euler} = \frac{\pi^2 EI}{AL^2} \tag{3.18}$$

$$\sigma_{shell} = \frac{(1.983 - 0.983e^{-23.14Q})k\pi^2 Et^2}{L^2(12 - 12\nu^2)} \tag{3.19}$$

$$Q = \frac{pR^2}{t^2 E} \tag{3.20}$$

$$k = \lambda + 12\frac{L^4(1-\nu^2)}{\pi R^2 t^2 \lambda} \tag{3.21}$$

$$\lambda = \sqrt{12\frac{L^4(1-\nu^2)}{\pi^4 R^2 t^2}} \tag{3.22}$$

$$\sigma_{vm} = \sqrt{\frac{1}{2}(\sigma_\theta^2 + \sigma_z^2 + (\sigma_z - \sigma_{theta})^2} \tag{3.23}$$

In Equation (3.23), the σ_z is defined as the following:

$$\sigma_z = \sigma_{axial} + \sigma_{longitudinal} \quad (3.24) \qquad \sigma_{axial} = \frac{P}{A} \quad (3.25) \qquad \sigma_{longitudinal} = \frac{Pr}{2t} \quad (3.26)$$

The methodology of using these equations is the follows: all these equations are dependent of the thickness, so the minimum thickness of the tanks can be calculated. By computing the minimum thickness required for all the failure modes, and choosing the biggest value, it is made sure that none of the failure modes will occur in the structure. Once this minimum thickness is found, stiffeners can be added such that the thickness can be lowered. This is done to keep the structural integrity of the structure but to lower its mass.

However, as it turns out, the critical failure mode for every iteration is always the internal tank pressure. This means that the thickness cannot be lowered (even if stiffeners are added) because otherwise the pressure in the tanks will cause the structure to fail. It is concluded that the minimum thickness of the structure is purely determined by (3.15) and this will make sure the structure won't fail under any other mode.

3.3.4. TANK INSULATION

In order to maintain the requested tank pressure in the propellant tanks, the temperature needs to be kept low. This is done by providing sufficient tank insulation, in such a way that the environment does not warm up the tanks by thermal conduction, convection and radiation. The propellant tanks need to keep sufficiently insulated both on the launch pad as well as during the launch, when aerodynamic heating takes place. Additionally, tank insulation protects the skin surface from ice formation. The insulation material that is used is spray on foam insulation (SOFI), which is often used on launchers [16]. The foam is a polyurethane material and is a mixture of the following components: a polyol and an isocyanate, a flame retardant, a surfactant and a catalyst. The blowing agent hydrochlorofluorcarbon (HCFC) then creates millions of small foam cells, which forms the cellular structure of the foam [17]. The amount of insulation that is added to the structure usually varies between 2 and 7 cm, dependent on how the local temperature varies and thus how much is needed. The weight that it adds to the structural mass equals 8% of the tank mass, which is 47.36 kg [18].

3.3.5. INTERSTAGES

Another important aspect of the structure involves the interstages between the rocket stages. These circular structures circumvent the nozzles and are detached together with the previous stage as stages separate. The main purpose is to carry the axial loads and provide an aerodynamic seal of the whole structure. Next to that, interstages provide space and mounting points for different subsystems, such as the EPS, ADCS, FTS and the parachute recovery system. In order to maintain perfect structural integration, the thicknesses of the interstages are equal to the body circumference thickness of the stage below it. This in turn, is again equal to the propellant tank thickness, which dominates the loads by pressure loads. The interstage masses and geometries can be found in Table 3.5.

Table 3.5: Interstage Masses and Geometries

Stage	Mass $[kg]$	Thickness $[mm]$
Interstage 1	25.16	6
Interstage 2	36.54	4
Totals	**61.7**	-

It can be seen that the second interstage is heavier than the first, even though the thickness is smaller. This is because the length of the nozzle of the second stage is smaller than the third stage.

3.3.6. NOSE CONE DESIGN

The nose cone design considerations are discussed in this section. The chosen shape is first justified, then the overall design is presented.

Nose Cone Shape

The Von Karman nose cone was selected previously. This shape is derived from the Sears-Haack body which is designed for the lowest drag in supersonic flow [19]. As the highest drag arises during the rocket breaching the transonic region, designing for this region is prioritised. The relatively small size of the rocket means that any reduction in drag is a greater contribution to the total rocket mass than other nominal rocket missions. The Haack series nose cone governing Equation is [20]:

$$\theta = \arccos(1 - \frac{2x}{L}) \quad (3.27) \qquad y = \frac{R}{\sqrt{\pi}}\sqrt{\theta - \frac{sin(2\theta)}{2} + Csin^3(\theta)} \quad (3.28)$$

Where R is the radius, L is the length and C is a factor which fully determines the final shape. There are a few significant values for C. For $C = 1/3$, called *LV-Haack*, is the minimum drag for a given volume. When C = 0, the minimum drag is given for a certain diameter, called *LD-Haack* also commonly known as Von Karman. Also of note, the Haack series cones do not interface with the body at a tangent. However the offset is so small as to be negligible. The chosen shape is given in Figure 3.11.

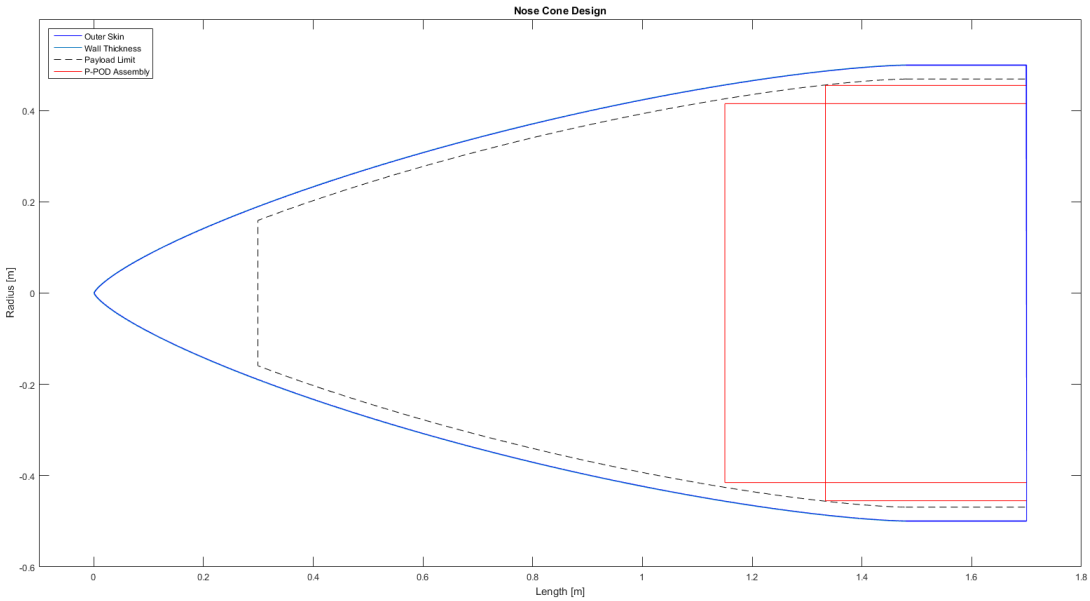

Figure 3.11: QLS Nose Cone

Overall Design

To ensure that the payload is integrable into the fairing, the internal volume is calculated. Dimensions of the nose cone shape are optimised for payload fitting and clearance, as well as mass and drag reduction. From the calculation of volumes, the mass of the total nose cone fairing can also be calculated. The material chosen is carbon fibre reinforced polymer (CFRP). This will allow the the fairing to be as light as possible, as well as sustaining all the required loads and stresses.

The maximum stress induced in the payload fairing is experienced during maximum dynamic pressure. In this region the maximum drag is 15.2 kN and the thrust induced G-load force is 184 N. Total stress within the nose cone is then 4.93 MPa with a wall thickness of 1 mm. Failure stress in CFRP is 110 MPa [3] The nose cone fairing internal is also designed with a 0.03 m clearance distance from the payload to allow for insulation, aero-acoustic dampening, payload integration structures and launch vibrations (Figure 3.11 dotted line). The drag characteristics of the nose cone is simulated using missile DATCOM. Table 3.6 summarises the optimised design parameters of the nose cone fairing.

Table 3.6: Nose Cone Design Parameters

Parameter	Value	Units
Shape	Von Karman	
Wall Thickness	1	mm
Internal Volume	0.5781	m^3
Material Volume	0.00314	m^3
Mass	6.71	kg
Internal Stress	4.93	MPa
Failure Stress (Compression)	110	MPa

3.3.7. TOTAL STRUCTURAL MASS

Now that all the components of the structure have been sized, the total structural mass of the rocket can be found by adding all individual components. The result is displayed in Table 3.7.

[3] https://www.acpsales.com/upload/Mechanical-Properties-of-Carbon-Fiber-Composite-Materials.pdf, visited on: 8-01-2016

Table 3.7: Total Structure Mass

Total mass item	Mass [kg]
Propellant tanks	601.01
Insulation	47.36
Interstages	61.70
Shell	51.00
Fairing	6.00
Totals	**767.08**

3.3.8. VIBRATIONAL ANALYSIS

The following section covers the vibrational analysis of the QLS launcher. The vibrational motion of the three stage rocket will be evaluated regarding to the damping, the stability and the natural frequencies of the system. The analysis of the vehicle will be simplified as a spring-damper vibrational system. The analysis is illustrated in Figure 3.12. The thrust force is acting on the first stage as can be seen in Figure 3.12, noted as T.

The damping coefficient is taken as 65000 Ns/m for all three dampers, as a result from beam damping measurements done by the Goddard Space Flight Center [22]. Firstly, the equations of motion are determined for each stage, shown in Equations (3.29), (3.30) and (3.31).

$$m_1\ddot{x}_1 = -F_{k_1} - F_{c_1} + F_{k_2} + F_{c_2} + T \tag{3.29}$$

$$m_2\ddot{x}_2 = -F_{k_2} - F_{c_2} + F_{k_3} + F_{c_3} \tag{3.30}$$

$$m_3\ddot{x}_3 = -F_{k_3} - F_{c_3} \tag{3.31}$$

The spring forces and the damping forces for each stage are given in equations (3.32), (3.33) and (3.34).

$$F_{k_1} = k_1 x_1 \qquad F_{c_1} = c_1 \dot{x}_1 \tag{3.32}$$

$$F_{k_2} = k_2(x_2 - x_1) \qquad F_{c_2} = c_2(\dot{x}_2 - \dot{x}_1) \tag{3.33}$$

$$F_{k_3} = k_3(x_3 - x_2) \qquad F_{c_3} = c_3(\dot{x}_3 - \dot{x}_2) \tag{3.34}$$

In order to determine the axial stiffness of the rocket, each stage of the rocket is assumed to be an axially loaded beam as can be seen in Figure 3.13. The axial stiffness of each stage is determined using Equation (3.35).

$$\delta = \frac{F \cdot L}{E \cdot A} \qquad F = k \cdot \delta \qquad F = \frac{EA}{L} \cdot \delta \rightarrow K = \frac{E_i \cdot A_i}{L_i} \tag{3.35}$$

Before introducing the state variables the equations of motion are rewritten in the form of Equations (3.36), (3.37) and (3.38).

$$\ddot{x_1} = \frac{(-k_1 - k_2)}{m_1} x_1 + \frac{k_2 x_2}{m_1} + \frac{(-c_1 - c_2)}{m_1} \dot{x}_1 + \frac{c_2}{m_1} \dot{x}_2 + \frac{T}{m_1} \tag{3.36}$$

$$\ddot{x_2} = \frac{k_2}{m_2} x_1 + \frac{(-k_2 - k_3)}{m_2} x_2 + \frac{k_3}{m_2} x_3 + \frac{c_2}{m_2} \dot{x}_1 + \frac{(-c_2 - c_3)}{m_2} \dot{x}_2 + \frac{c_3}{m_2} \dot{x}_3 \tag{3.37}$$

$$\ddot{x_3} = \frac{k_2}{m_3} x_2 - \frac{k_3}{m_3} x_3 + \frac{c_3}{m_3} \dot{x}_2 - \frac{c_3}{m_3} \dot{x}_3 \tag{3.38}$$

The state variables are introduced in Equations (3.39), (3.40) and (3.41). These state variables are then substituted into Equations (3.36), (3.37) and (3.38), thus getting the equations of motion in terms of the state variables.

$$x_1 = y_1 \qquad \dot{x}_1 = y_2 \qquad \ddot{x}_1 = \dot{y}_2 \qquad \dot{y}_1 = y_2 \tag{3.39}$$

$$x_2 = y_3 \qquad \dot{x}_2 = y_4 \qquad \ddot{x}_2 = \dot{y}_4 \qquad \dot{y}_3 = y_4 \tag{3.40}$$

$$x_3 = y_5 \qquad \dot{x}_3 = y_6 \qquad \ddot{x}_3 = \dot{y}_6 \qquad \dot{y}_5 = y_6 \tag{3.41}$$

The state space equations are then written in a matrix form given by the general state space representation in the form of Equations (3.42) and (3.43) [23].

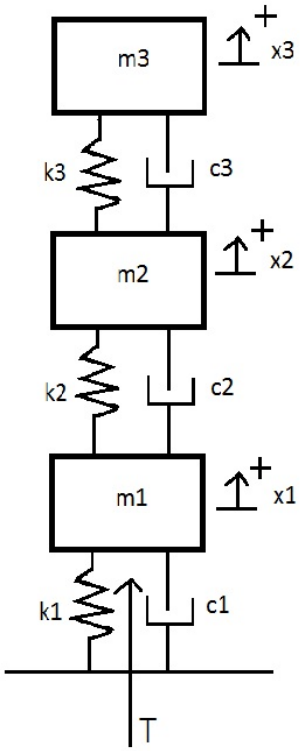

Figure 3.12: Vibrational Analysis of the three stages

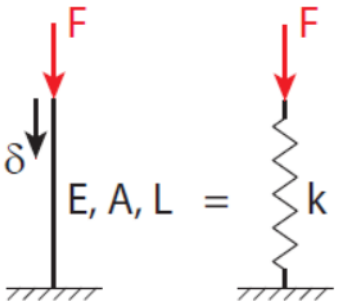

Figure 3.13: Discretising an axially loaded beam [21]

$$\dot{\vec{x}}(t) = A\vec{x}(t) + B\vec{u}(t) \tag{3.42}$$

$$\vec{y}(t) = C\vec{x}(t) + D\vec{u}(t) \tag{3.43}$$

The velocity of the each stage mass is of interest for the output matrix, that is $\dot{x}_1$, $\dot{x}_2$ and $\dot{x}_3$, which are y_2, y_4 and y_6. The following state space arrays in Equations (3.44), (3.45), (3.46) and (3.47), are inserted in MATLAB, after which the poles, the damping ratios and the natural frequencies of the system are received. A step input is inserted in the system and the time response to the step input is received. Figure 3.14 shows the time response of the system.

$$A = \begin{bmatrix} 0 & 1 & 0 & 0 & 0 & 0 \\ \frac{-k_1-k_2}{m_1} & \frac{-c_1-c_2}{m_1} & \frac{k_2}{m_1} & \frac{c_2}{m_1} & 0 & 0 \\ 0 & 0 & 0 & 1 & 0 & 0 \\ \frac{k_2}{m_2} & \frac{c_2}{m_2} & \frac{-k_2-k_3}{m_2} & \frac{-c_2-c_3}{m_2} & \frac{k_3}{m_2} & \frac{c_3}{m_2} \\ 0 & 0 & 0 & 0 & 0 & 1 \\ 0 & 0 & \frac{k_2}{m_3} & \frac{c_3}{m_3} & -\frac{k_3}{m_3} & -\frac{c_3}{m_3} \end{bmatrix} \tag{3.44}$$

$$B = \begin{bmatrix} 0 \\ \frac{T}{m_1} \\ 0 \\ 0 \\ 0 \\ 0 \end{bmatrix} \quad (3.45) \qquad C = \begin{bmatrix} 0 & 1 & 0 & 1 & 0 & 1 \end{bmatrix} \quad (3.46) \qquad D = \begin{bmatrix} 0 \end{bmatrix} \quad (3.47)$$

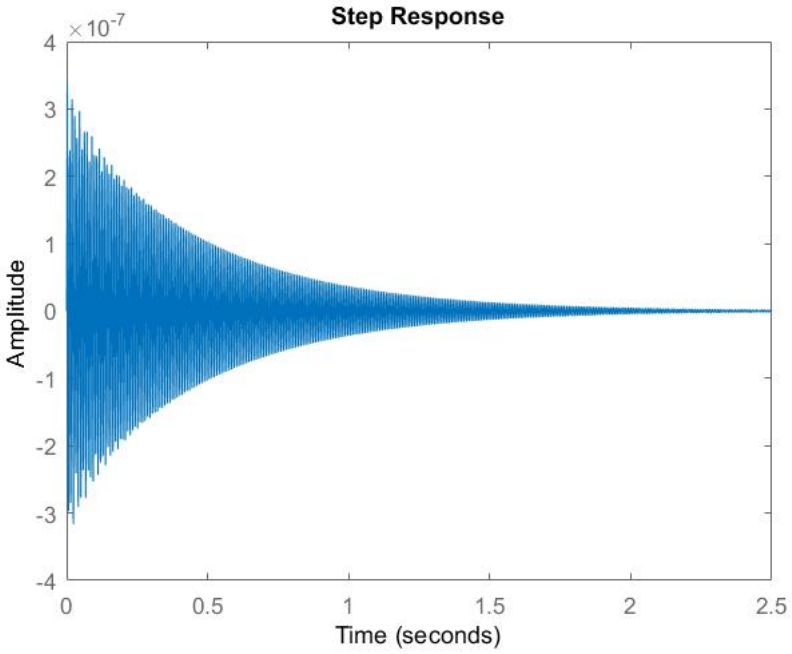

Figure 3.14: Time response to a step input

It can be concluded that the time response to a step input is stable for the system because all poles are negative and the system shows that it is a damped vibration. The settling time is 1.3738s with a threshold of 5%. Table 3.8 gives the poles, damping ratios and natural frequencies of the system by using MATLAB. Figure 3.14 shows the time response of our system to a step input. In order to avoid resonance, the natural frequency of the payload shall not be the same as the natural frequency of the structure. In case of resonance, the vibrational motion will keep increasing in amplitude until the structure fails.

Table 3.8: Time Response to a Step Input

Pole [-]	Damping Ratio [-]	Natural Frequency [rad/s]
$-2.05 \pm 7.17 \cdot 10^2$ i	$2.86 \cdot 10^{-3}$	$7.17 \cdot 10^2$
$-1.09 \cdot 10^1 \pm 1.88 \cdot 10^3$ i	$5.83 \cdot 10^{-3}$	$1.88 \cdot 10^3$
$-4.09 \cdot 10^1 \pm 3.75 \cdot 10^3$ i	$1.09 \cdot 10^{-2}$	$3.75 \cdot 10^3$

3.4. AERODYNAMICS

In this section the aerodynamic characteristics of the launch system will be discussed. First the used software will be discussed in Section 3.4.1 and the results will be presented. Then the aerodynamic performance of the nosecone will be analysed in Section 3.4.2.

3.4.1. MISSILE DATCOM

For estimating the aerodynamic coefficients, Missile DATCOM program is used. Missile DATCOM is a collection of numerical methods implemented in a FORTRAN program, which takes the general rocket shape as input. The input file for this program is cumbersome to manually change, so a program has been written to generate this input file so changes to design parameters can quickly be evaluated. The coefficients can be calculated with body-alone axisymmetric forms, with protuberances(such as landing legs) and with fins. The center of pressure location errors are minimal and body-alone calculations closely match wind tunnel data [24].

In Table 3.15 representative flight conditions (around maximum dynamic pressure and just after liftoff) are shown. The stability derivatives are used to determine if the chosen attitude control is feasible. This is worked out in Section 3.5. The C_D as a function of the Mach number is shown in Figure 3.16, and shows that the transonic region is the most significant region when it comes to drag. In the next section, it is discussed how this nosecone selection. The Reynolds number is kept constant around a representative value. The coefficients show no significant change if the Reynolds number is varied in its expected range.

Figure 3.15: Aerodynamic coefficients for representative flight conditions

	Flight conditions	
	$M_1 = 0.1$	$M_2 = 1.34$
	$Re_1 = 4.4 \cdot 10^7$	$Re_2 = 1.5 \cdot 10^8$
C_D	0.1944	0.3254
C_{m_α}	21.9733	27.0678
$C_{m_{\dot{\alpha}}}$	41.6952	159.5064
C_{m_q}	-126.0912	-494.2010
$x_{c.p.}[m]$	2.28	1.66

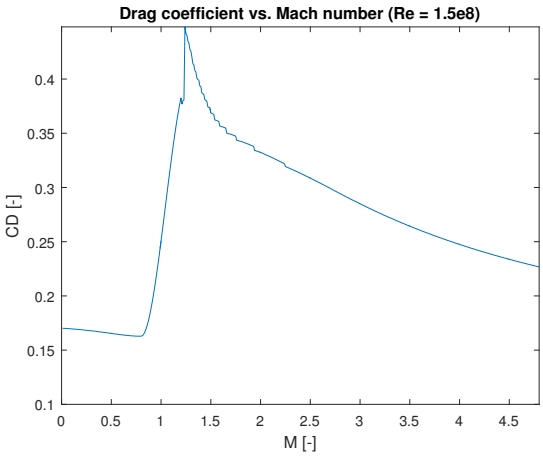

Figure 3.16: Drag coefficient vs. Mach number

3.4.2. NOSE CONE SHAPE

Various nose cone shapes are compared in regards to drag characteristics [19]. Utilising missle DATCOM, the performance of such shapes are shown in Figure 3.17. The best performing nose cone shape throughout the mission velocity profile is the Von Karman shape as shown in Figure 3.18.

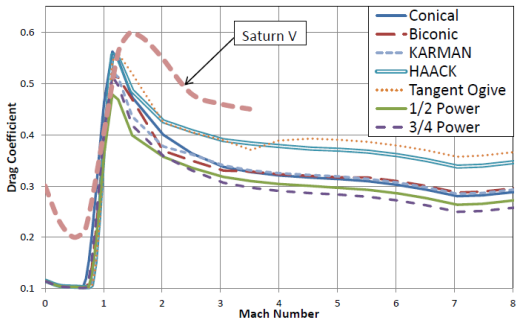

Figure 3.17: Drag Coefficient Profile for Various Nose Cones [20]

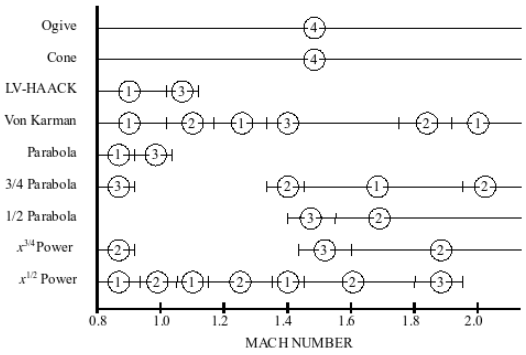

Figure 3.18: Comparison of Nose Cone Geometry

3.5. ATTITUDE DETERMINATION AND CONTROL SUBSYSTEM

In this section the ADCS system will be discussed. Firstly, the part of the system that detects the position of the rocket will be discussed. After that, the control of the rocket will be discussed.

3.5.1. ATTITUDE DETERMINATION

Attitude Determination will be done by different sensors, discussed below. These sensors will not be designed but will be COTS components.

IMU

The IMU will be a LN-200C bought at Northrop Grumman. This IMU consists of three fibre optic gyros and three Micro Electro-Mechanical System (MEMS) accelerometers. It measures the angular velocity and the acceleration in the body reference frame, so it will be strapdown integrated. This unit has a mass of 0.75 kg and needs 12 W power [4].

[4] http://www.northropgrumman.com/Capabilities/LN200FOG/Documents/ln200c.pdf, visited on: 18-12-2015

Two IMU's will be integrated in the rocket. One will be placed in the third stage, which will be used during payload separation. The other one will be placed in the first stage, used during flight back of the first stage.

Sun sensors
Adcole digital sun sensors (64°) [5] are used to determine the yaw and pitch angle for the final stage, since the drifting of the IMU at this stage could be too large and the accuracy for its heading is too low. These angles are measured in the Earth fixed reference frame, so the flight computer has to translate these to the body reference frame. Five sun sensors are used which ensures that always one of the sensors is exposed to the sun. The sun sensors have an accuracy of 0.25 °, which is enough for the requirement of an orbit injection accuracy of 0.25 °. The sun sensors have a mass of 0.3 kg each, and will be placed on the third stage of the rocket.

GPS
A Topstar 3000 D GPS receiver will be used to determine the position. The flight computer can use this data to reduce the drift error of the gyroscopes of the IMU. Next to that, after stage separation, the accelerometers in the IMU could become inaccurate due to high g-loads, so GPS can be used to determine velocity by comparing two position vectors over time. This can also be done for heading of the rocket. However, this will not be accurate enough at orbit injection, so at that point the sun sensors have to be used. The Topstar 3000 D has an accuracy of 10 m [25]. Just as for the IMU, it will be placed in the first and third stage.

Flight Computer
A flight computer has to be used to convert the output data from the sensors into the attitude of the rocket. This data will go through a Kalman filter to reduce the noise. The flight computer has to compute the rocket attitude with a frequency of 10 Hz, as determined in the Midterm Report of this project. The computed attitude will be compared to a desired reference position. To return to this desired position, the flight computer gives control outputs to the actuators of the TVC, which are discussed in the next section. An overview of the in- and outputs of the flight computer is given in Figure 3.19. One flight computer will be integrated in the third stage and one in the first stage. Further explanation of the flight computer is given in Section 3.7. Since no information is available for commercial flight computers, in the next phase of the project a flight computer should be designed as well.

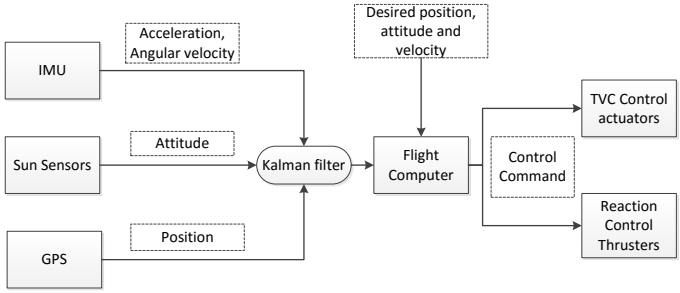

Figure 3.19: Flight computer in- and outputs

3.5.2. STABILITY AND CONTROL

In this section the stability and control of the rocket is discussed.

Stability
For the first stage of the launch in the atmosphere, where aerodynamic forces act on the rocket, the rocket should be stable. For passive stability, the center of pressure should stay under the center of gravity. This can be reached by using fins on the bottom of the rocket. This option was analysed using Missile DATCOM, which can calculate the position of the center of pressure. The center of gravity is calculated using MATLAB, which changes over time, as can been seen in Figure 3.20, for the first stage. As can been seen, the center of gravity shifts slighty donwward and then go upwards. For further analysis, the worst case position of the center of gravity is chosen, which is the most downward position. The other two stages are not analysed, since no aerodynamic forces occur in those stages of the flight and stability is not analysed. The conclusion was made that fins longer than 2 meters long and a span of 0.5 meter has to be used, which will increase the drag up to 25 %. That is why no fins will be used, and the rocket needs to be actively stabilised by the flight computer. The flight computer will use thrust vector control, which is discussed in the section below.

[5] http://www.adcole.com/aerospace/digital-sun-sensors/digital-sun-sensor-64-degree/, visited on: 18-12-2015

In Figure 3.24 and Figure 3.23 the response of the rocket can be seen with the maximum allowable gain of $K = 6$. At this gain, the gimbal angle will not exceed 12 degrees, which is within feasible limits for gimbal angles[4]. Because a proportional controller was assumed, the damping characteristics are not favourable, but it shows that control of the vehicle is possible. In a further design stage different controllers, such as PID-controllers, should be considered to increase the damping performance.

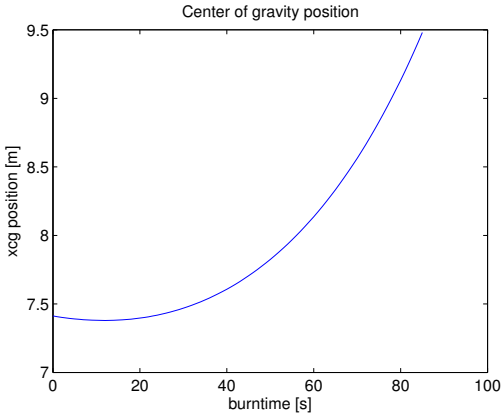

Figure 3.20: Center of gravity change during first stage burn

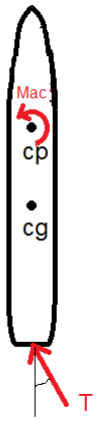

Figure 3.21: Equations of Motion for pitch and yaw control

Thrust Vector Control

The rocket will be controlled with thrust vector control. The first stage consists of four hinge nozzles, so pitch, yaw and roll can be controlled. The configuration is shown in Figure 3.25. The The second and third stage will use one gimbal nozzle each. Roll control for the second and third stage will be done with reaction control thrusters.

As can be seen in Figure 3.21, yaw and pitch motion can be controlled by applying a hinge angle μ of the engine. This will generate a moment around the center of gravity. For simplicity, it is assumed that all the nozzles will add up to one thrust vector. Through the center of pressure, an aerodynamic moment will be present due to aerodynamic moments. This value is calculated using Missile DATCOM and will dependent on disturbance angle of attack, height and speed. The resulting moment will cause an angular motion in pitch or yaw direction.

Pitch/yaw stability/controlability in atmosphere

To investigate the pitch/yaw stability of the rocket, a simplified linearised state-space system for pitching motion is set up (Equation 3.48) [4]. This is a simplified and linearised form of the equations of motion for pitch and yaw, shown in Figure 3.21. Since the rocket is symmetrical for pitch and yaw motion, this state space system is also valid for yaw motion. The model will be valid for small disturbances in angle of attack. The states for this system are pitch rate $\dot{\alpha}$ and angle of attack α. The input is the gimbal/hinge angle μ of the nozzles, which gives a change in pitch rate. The jet damping moment and moment of inertia change can be neglected as together they have a positive effect, and for now only the feasibility of control is checked. A linear controller is assumed, which change the angle of the engine depending on a deviation in angle of attack. The gain cannot exceed $k_{max} = {}^{\mu_{max}}/_{\alpha_{max}}$ For two flight conditions the feasibility is checked: shortly after lift-off, where it is most likely angle disturbances occur and at maximum dynamic pressure, when maximum aerodynamic forces act on the rocket.

$$\begin{bmatrix} \Delta\ddot{\alpha} \\ \Delta\dot{\alpha} \end{bmatrix} = \begin{bmatrix} \frac{1}{I_{yy}}(C_{m_q} + C_{m_{\dot{\alpha}}})\bar{q}_0 Sd & \frac{1}{I_{yy}}C_{m_\alpha}\bar{q}_0 Sd \\ 1 & 0 \end{bmatrix} \begin{bmatrix} \Delta\dot{\alpha} \\ \Delta\alpha \end{bmatrix} + \begin{bmatrix} Tx_e/I_{yy} \\ 0 \end{bmatrix} \mu \tag{3.48}$$

The mass moment of inertia I in this model is calculated analytically. The rocket is assumed to be a solid cylinder, as can been seen in Figure 3.22. With this assumption Equation 3.49 can be used to calculate the mass moment of inertia [6].

[6] http://www.engineersdaily.com/2014/11/basic-concepts-of-moment-of-intertia.html, visited on: 12-1-2015

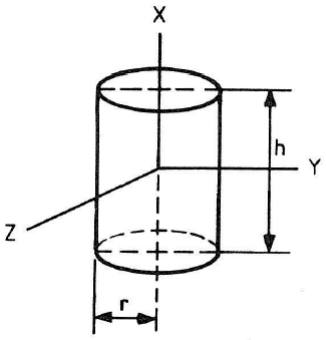

Figure 3.22: Cylinder configuration [26]

$$I_{zz} = \frac{1}{4}MR^2 + \frac{1}{12}ML^2 \tag{3.49}$$

$$I_{xx} = \frac{1}{2}MR^2 \tag{3.50}$$

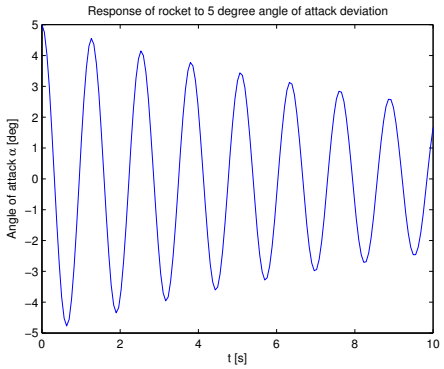

Figure 3.23: Control at launch

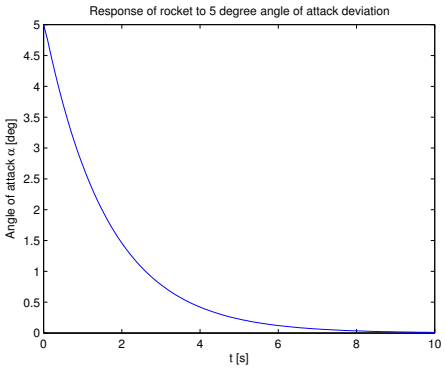

Figure 3.24: Control at maximum pressure

Roll control

In Figure 3.25 the nozzle configuration of the first stage can be seen. The center nozzle is gimballed, and the three around are hinged. Roll control for the first stage can be done with the hinge nozzles, placed around the center nozzle. If the nozzle is placed under an angle, a force will be created which has an arm according to the middle point of the rocket, as in Figure 3.25. The moment of inertia here will be different, as seen in Equation 3.50. The roll control system should ensure the roll speed will be zero, since otherwise it will be impossible to control the rocket for yaw and pitch. A similar control system as for yaw and pitch motion could be made for roll control as well. However, at this point it is not know what kind of roll disturbances will act on the rocket during flight. However, since the mass moment of inertia around this axis is much smaller, it is assumed that the TVC can much easier counteract disturbances in roll than for yaw and pitch.

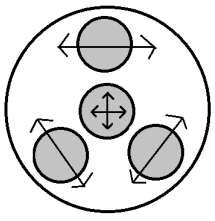

Figure 3.25: First stage nozzle configuration

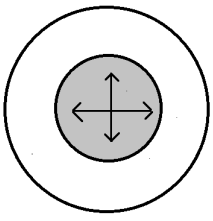

Figure 3.26: Second and third stage nozzle configuration

Actuators

To make the nozzles rotate about their hinge point, actuators are needed. Electromechanical actuators will be used instead of hydraulic ones, since they are beneficial in terms of maintenance costs and implementation [7]. These actuators will be bought of the shelf.

[7] http://www.esa.int/Our_Activities/Space_Engineering_Technology/Mechanisms/Launch_Vehicle_actuators, visited on: 12-1-2016

Recovery turn
In preparation of the first stage landing and recovery, the rocket will have to make a so-called recovery turn. Here, the rocket will perform a 135 degree turn around the y-axis, ending up at a -180 degree pitch angle. It will then initiate a flyback burn to cancel its horizontal velocity. This manoeuvre will allow landing close to the launch site. This manoeuvre is shown in Figure 3.27.

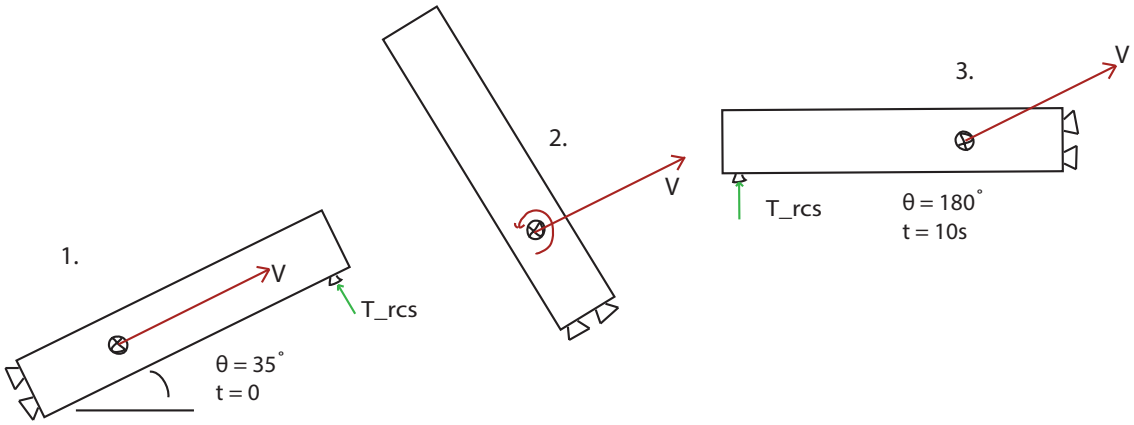

Figure 3.27: Recovery turn

This attitude change is outside the reach of the TVC system. Therefore, a dedicated Reaction Control System (RCS) is needed. First, a trade-off was made to decide between cold gas and catalytic monopropellant thrusters. This is shown in Table 3.9.

Table 3.9: Trade-off table for the first stage RCS.

Item	Cold gas	Monopropellant
Isp	BL	+
Mass	BL	BL
Complexity	BL	-
Cost	BL	-

It is shown that while a monopropellant would offer superior specific impulse, the added complexity and cost would not weigh up to this. Therefore the selected system shall be a cold gas thruster based on nitrogen. It shall contain four thrusters to perform the flip manoeuvre independent of the actual roll angle. As is shown in Section 5.2, the flip takes place at an altitude of 81km, which means drag can be neglected. Furthermore, it is assumed that two one-second burns' will provide the system with the required change in pitch rate. The first stage is modelled as a combination of solid and thin-walled cylinders, with a mass moment of inertia of $\frac{1}{12}m(3r^2+h^2)$ and $\frac{1}{6}m(3r^2+2h^2)$ respectively. The geometric properties of the first stage are shown in Table 3.10.

Table 3.10: First stage geometric properties

Property	Value	Units
Center of gravity	2.45	[m]
MoI	292	[kg m^2]
Flip angle	145	[deg]
Thruster moment arm	4.42	[m]

Based on these values, a thruster force of 72N for two burns of 2s each was calculated. The high-pressure nitrogen used will be drawn directly from the fuel pressurant tank in order to minimise the system weight.

Orbit insertion
Requirement for an orbit at 350 km altitude is that the payload will be injected with an accuracy up to 0.25 °, because

of great differences in orbital life time. As earlier mentioned, sun sensors will detect the orientation of the third stage with an accuracy of 0.25 °. The nozzle of the third stage, as shown in Figure 3.26 will have a gimbal as well, so it can change the orientation of the rocket for orbit insertion. Since no aerodynamic forces are acting, this would not give a problem. Since this one nozzle configuration can not control roll motion, small reaction control thrusters, just as for the recovery of the first stage, has to be used. These will be placed on the third stage, so they can counteract roll disturbance during second and third stage operations. Since it is not known yet what kind of roll disturbances will act on the rocket during these stages, the design of these control thrusters is left for a later phase of the design.

3.6. ELECTRICAL POWER SUBSYSTEM

The EPS design is discussed in this section.

Power Budget

The table of component load requirements are summarised in Table 3.11. Peak power required is calculated per subsystem components and according to their placement in first, second or third stage. The propulsion subsystem is not connected to the EPS. This is due to the fact that the engine nozzles have separate batteries. The quantity of the components are given per stage as the EPS is divided into two separate systems; one for the first stage and one in the third stage. This way, the batteries can be designed separately for the upper and lower stage. This is important for the recovery of the first stage.

Table 3.11: Component Power Budget Per Stage

Item	Quantity			Voltage [Vdc]	Ampere [mA]	Peak Power [W]	
	1	2	3			1	3
Attitude Determination and Control							
Thrust vectoring actuators	5	2	2	28	23000	2576	1288
Cold thruster valves	4		8	-	-	10	20
Guidance and Navigation							
Inertial measurement unit	1		1	5.5	270	24	24
Sun sensor			5	5	70		1.75
GPS	1		1	6	300	1.8	1.8
Tracking Telemetry and Command							
Flight computer	1		1	-	-	150	150
Antenna	3		3	-	-	7.5	7.5
Recovery							
Parachute harness actuators	2			6	1300	15.6	-
Landing legs actuators	3			28	1000	84	-
Structures							
Separation Pyrotechnics	1		2	28	5000	140	280

Primary Battery

The QLS mission duration is much less than one hour. As such, there is no requirement for the EPS to generate electrical power through solar arrays or other alternatives. All electrical power requirements will be met through proper sizing of the primary batteries. The equation to size the batteries is [27]:

$$C_r = \frac{PT}{(DoD)Nn} \tag{3.51}$$

C_r	Capacity	[Wh]
P	Load	[V]
T	Duration	[hr]
DoD	Depth of Discharge	[%]
N	No. of Batteries	[-]
n	Transmission Efficiency	[%]

The mission duration is 1274 s, thus peak power usage is more critical than nominal usage. To properly size the batteries, all components and their peak power usage were analysed and results collated in Table 3.11. Note, however, that not all system components will be used simultaneously. To illuminate the logical flow of component usage, the mission profile 5.8 is consulted.

Largest contributor of power usage are the thrust vectoring actuators. During stage one operations, the maximum thrust vectoring required will be two actuators for the centre nozzle and two for any pair on the hinged nozzles at

once, thus peak power usage is 2576 W. First stage recovery will also give a peak in the power usage profile. No thrust vectoring is required during the landing phase of the first stage, thus the recovery subsystem will provide that peak in power usage. Throughout the entire mission duration, the flight computer will be used. The power usage of the flight computer is estimated to consume 150 W.

Depth of discharge of the batteries represents the amount of battery capacity discharged per charge cycle. This parameter is important in the elongation of battery life cycle. As the first stage is a fully reusable launch platform, there will be some charge cycles. However, battery life cycles are usually in the order of thousands and the first stage reusability is two orders of magnitude lower. Thus the preservation of battery life cycle is non-critical. The nominal transmission efficiency is 0.9, representing harness, distribution and regulation losses. Table 3.12 summarises the results of the battery capacity calculation

Table 3.12: EPS Load Profile and Battery Capacity Calculation

Item	Peak Power [W]		Duration [s]		Battery Load [Wh]	
	Stage 1	Stage 3	Stage 1	Stage 3	Stage 1	Stage 3
Thrust Vector Actuators	2576	1288	85	173 (x2)	60.82	123.79
Cold Thrust	10	20	85	173 (x2)	0.24	1.92
IMU	24	24	1274	531	8.49	3.54
Sun Sensor	-	1.75	-	531	-	0.26
GPS	1.8	1.8	1274	531	0.64	0.27
Flight Computer	150	150	1274	531	53.08	22.13
Antenna	7.5	7.5	1274	531	2.65	1.11
Separation Pyrotechnics	140	280	<0.01	<0.02	<0.01	<0.01
Parachute Harness	15.6	-	976	-	4.23	-
Landing Legs	84	-	30	-	0.7	-
				Total	130.86	153.01
Parameter	Stage 1		Stage 3			
N	2		2			
n	0.9		0.9			
DoD	0.75		0.75			
C_r	96.93		113.34			

From the required capacity of the launcher primary batteries, the selection of the battery cell can take place. Lithium-ion cells have high energy density, allowing a lower EPS mass. The specific energy of lithium-ion cells is 139 Wh/kg [8]. The mass of the battery with 2 cells is then 2 kg.

Distribution and Control

From the load profile in Table 3.12, it can be concluded that all components require DC voltage and can be interfaced with the 28 Vdc battery source. A decentralized approach is taken for the regulation and distribution. Power is distributed through an unregulated main bus and converters are in place per subsystem connected to the EPS for interface. Complex regulation is not required for interfacing with a solar array. This essentially simplifies the EPS into batteries, distribution and regulators. The electrical block diagram (Figure 3.28) further elaborates the design philosophy of the EPS. A typical distribution system circuit is shown in Figure 3.29. The QLS distribution is modelled after such a system. The safe mode is integrated into the distribution subsystem which will provide monitoring capabilities and fault isolation circuits.

3.7. COMMUNICATION SUBSYSTEM

In this section the communication subsystem will be discussed. It contains the chosen antennas and the communication link budget. Next to that, it also describes the command and data handling subsystem, which is responsible for managing the data the communication system transmits.

3.7.1. ANTENNA SELECTION

The ground station contains a dish antenna. As the antenna on the rocket should be as small as possible, a turnstile antenna is used. This contains four whips. The advantage of this antenna is that it is lightweight. This type of antenna is also used on the Delfi mission. It operates at a frequency smaller than 0.3 GHz, so a frequency of 0.2 GHz is chosen

[8] http://www.eaglepicher.com/li-ion-3, visited on: 19-01-2016

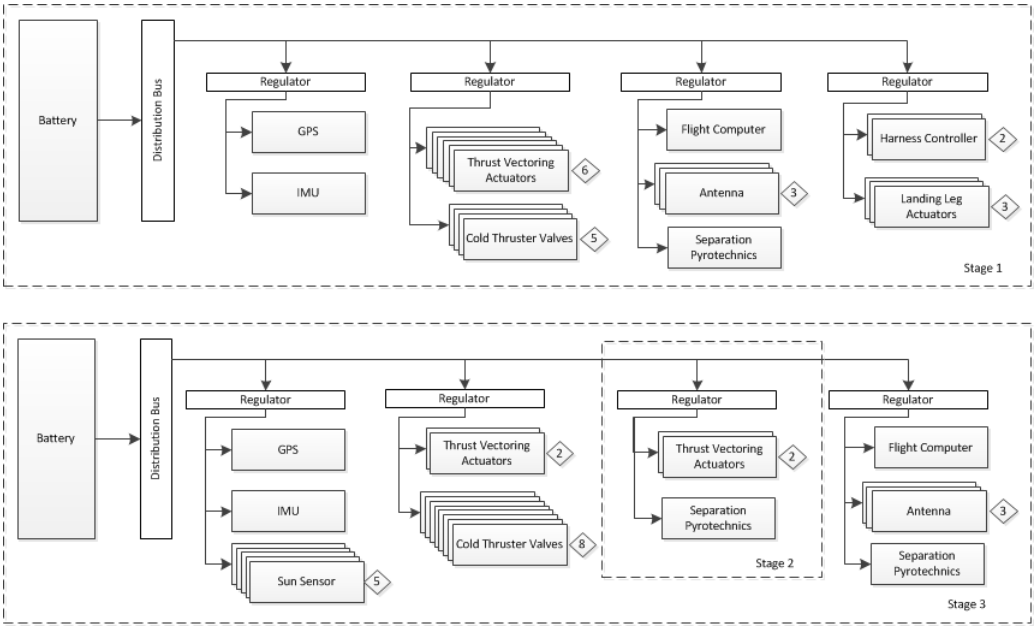

Figure 3.28: Electrical Block Diagram

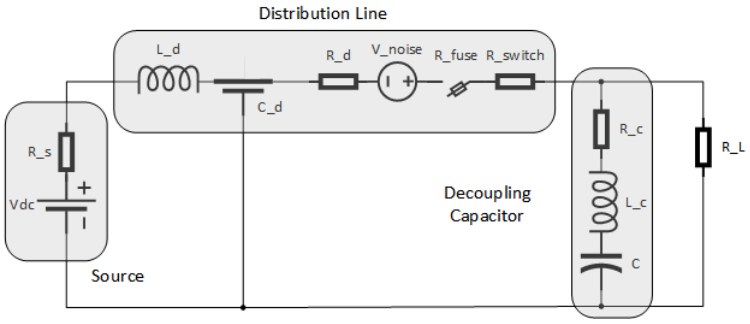

Figure 3.29: Power Distribution System Equivalent Circuit [27]

(VHF band) [28]. For the Delfi mission, the turnstile antenna had a transmitter power of 0.28 W and a gain of 4.9 dB, given by [29]. Since no further information is available, these values are assumed for this mission as well. The ground antenna can be designed by iteration, until the required SNR is reached. In total six antennas will be used, three on the first and three on the third stage on the outer body of the rocket.

3.7.2. COMMUNICATION LINK BUDGET

The required signal to noise ratio (SNR) is 10 dB for a spacecraft [30], so this value will be assumed for the launcher. The SNR can be calculated with Equation 3.52. The input values can be found in Table 3.13. The system noise temperature, loss factors, system noise temperature and antenna efficiency are estimated using [31] and [30].

$$\frac{Eb}{N_0}[dB] = P_T + L_i + L_R + G_T + L_a + G_R + L_s - 10log_{10}(R) - 10log_{10}(k) - 10log_{10}(T_s) \tag{3.52}$$

Table 3.13: Communication inputs

P_T	Transmitter power	0.28 [W]
L_i	Transmitter loss factor	0.9
f	Downlink frequency	0.2 [GHz]
η	Antenna efficiency	0.6
A_R	Receiver antenna diameter	2 [m]
L_R	Receiver loss factor	0.9
R	Data rate	8 [Mbit/s]
T_s	System noise temperature	221 [K]

The transmitter power, loss factors, data rate and system noise temperature are converted to dB, after which they are implemented in Equation 3.52.Transmitter and receiver gain can be calculated with Equation 3.53 and 3.54 respectively. The signal lost in space can be calculated with Equation 3.55. Here λ is the wavelength of the signal. Atmospheric loss is estimated at -0.04 dB. [31]

$$G_T = \frac{4\pi\eta A_T}{\lambda^2} \quad (3.53) \qquad G_R = \frac{4\pi\eta A_R}{\lambda^2} \quad (3.54) \qquad L_s = \left(\frac{4\pi r}{\lambda}\right)^2 \quad (3.55)$$

The communication link budget can be found in Table 3.14. Here the downlink budget is shown. The uplink budget would look similar, and will only be used for the flight termination system, so a smaller data rate would be sufficient. Choosing a ground antenna with a diameter of 2 meter, a downlink rate of 8 Mbit/s can be reached, and a SNR margin of 5 dB is obtained. The equipment on board of the rocket should stay quite fixed, because of restricted mass and power available. However, if the customer requires a higher bit rate, a ground antenna with a greater diameter could be chosen.

Table 3.14: Communication budget

Symbol	Parameter	
P_T	Transmitter power	-5.53 [dBW]
G_T	Transmitter gain	4.9 [dB]
G_R	Receiver gain	10.23[dB]
L_T	Transmitter loss	0.46 [dB]
L_R	Receiver loss	0.46 [dB]
L_S	Free space loss	129.35 [dB]
L_a	Atmospheric loss	0.04 [dB]
k	Boltzmann constant	-228.6 [dB(J/K)]
T_s	System noise temperature	23.44 [dB-K]
R	Data rate	69.03 [dB-Hz]
$\frac{E_b}{N_0}$	Received SNR	15.42 [dB]
$\frac{E_b}{N_0}$	Required SNR	10 [dB]
	Margin	**5.42 [dB]**

3.7.3. DATA HANDLING

This section contains the design of the command and data handling subsystem. This system can be seen as the 'brains' of the launcher. Its purpose is to transfer and process the data flows between subsystems within the launcher, maintain onboard autonomy and manage commands that come in from the ground station. Therefore, all the data gathered by the different sensors in the system will pass through the data handling system. In this section, a preliminary component architecture is presented, as well as a visual representation of the data flows in the system.

The command and data handling subsystem is based on the use of an on-board computer, a data bus system and point-to-point links[32]. As opposed to spacecraft, which are not constantly in contact with the ground station and thus have a need to store lots of data, QLS will remain in constant contact with the ground at all times during the mission operation[27]. Therefore, the design of on-board memory is not driven by the data rate of the communication subsystem. With a mission duration of approximately 600 seconds and a communication data rate of 8Mbit/s, the total communication data handled by the system in any one mission equals approximately 4800Mbit or 600 MB.

From a mission point of view, the Command & Data HandlingC&DH subsystem can be split in two parts. One part is located in the first stage and will be closely integrated with the Guidance, Navigation & Control (GNC) and recovery subsystems. The other will be located in the third stage, and will handle command and data flow in the top two stages. This split is necessary to allow full mission control of both parts of the launcher after the first stage separates for recovery manoeuvres.

In order to ensure safe operations during the entire mission profile, the system needs to tolerate a certain level of radiation damage. The system can either be either made out of radiation-hardened parts or be radiation-tolerant as a system, having enough redundancy to continue operations regardless of radiation-induced errors. The advantages and disadvantages are given in Table 3.15.

Based on the information above, a radiation-tolerant, redundant system was opted above a radiation-hardened system. The use of COTS components significantly eases software development. This does necessitate the use of redundant computer- and CPU blocks. These blocks will be set up in a so-called triple modular redundancy setup. In

Table 3.15: Radiaton hardened and radiation- tolerant redundant advantages and disadvantages

Radiation hardened	
Advantages	Disadvantages
Resistance to glitching Proven in flight	Low availabilty High development cost Low processing power High price
Radiation-tolerant redundant	
Advantages	Disadvantages
High availability Low development cost Low unit cost High processing power	Redundancy needed Slightly higher mass

this setup, each microcontroller that controls, for example, an engine will receive commands from three computers constantly checking each other in a majority vote system. The microcontroller then executes the command if all three agree, but if one of them is different, the system will go with the strings that have previously been correct. This setup gives the system fault tolerance without the use of expensive radiation hardened components. However, the size of the data flows in the rocket are still unknown. Therefore, as suggested by [33], a definite choice for a processor will be left for a later phase of the design. A preliminary architecture of the C&DH system is shown in Figure 3.31. In Figure 3.30 the communication flow diagram is shown, which shows which data is transferred to which subsystem. The flight computer will send the necessary information to the ground system.

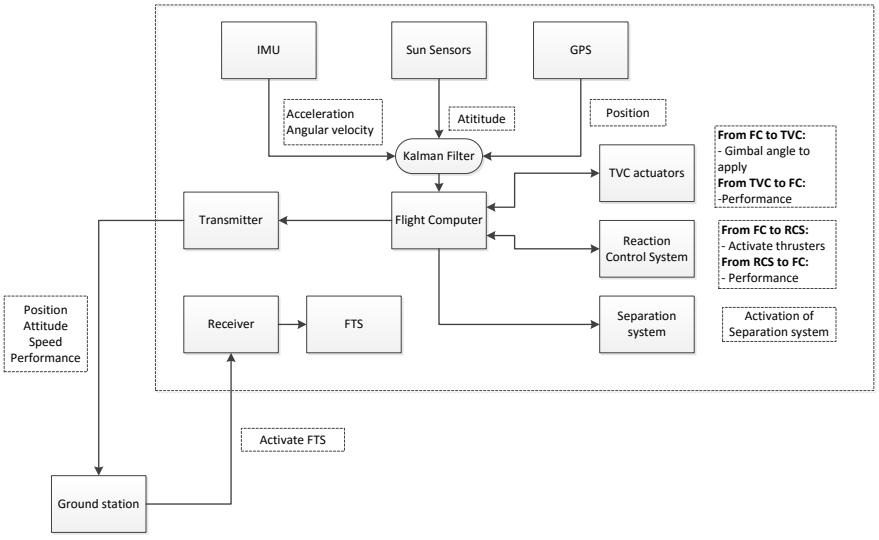

Figure 3.30: Communication Flow Diagram

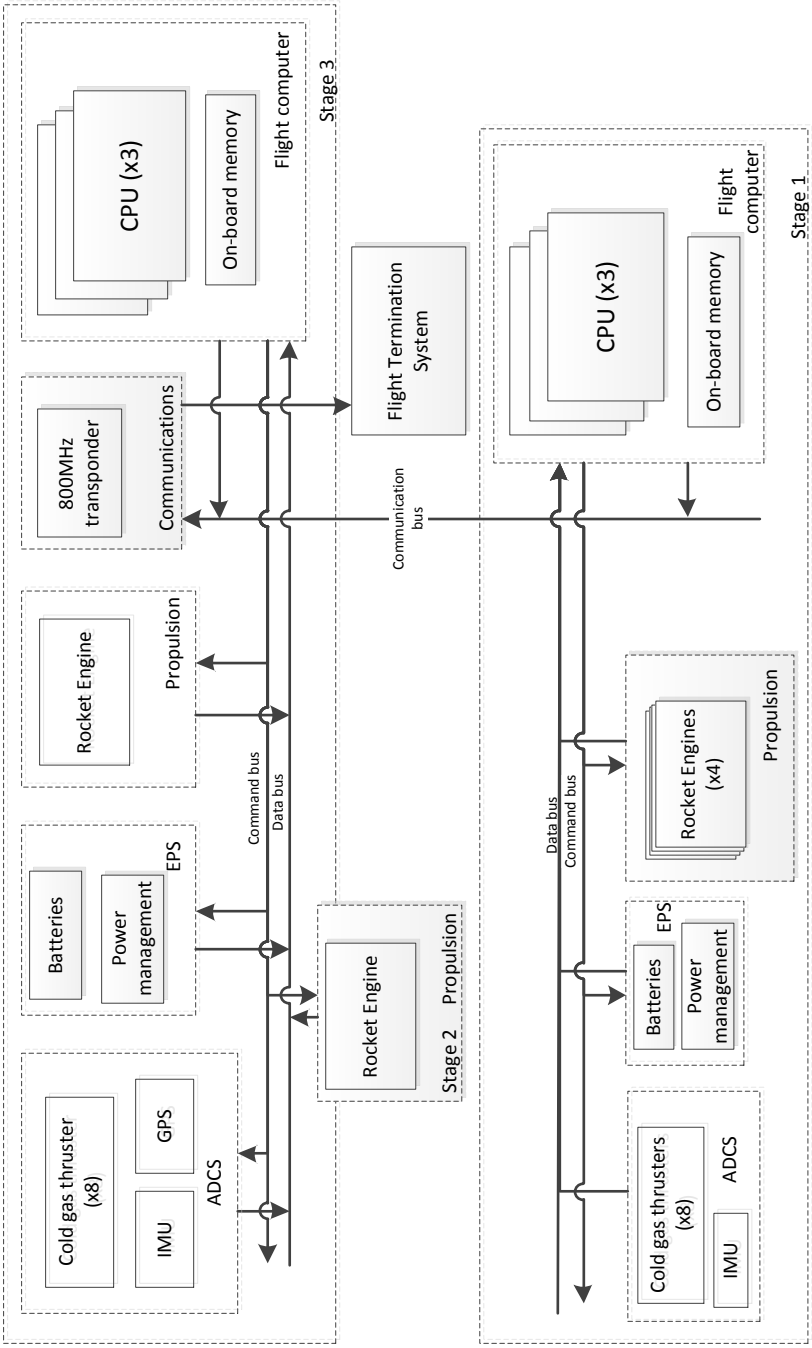

Figure 3.31: Architecture of the Command and Data Handling subsystem

3.8. RECOVERY SUBSYSTEM

After the first stage of the launcher has brought the remaining stages and payload to 27 km altitude, it will separate. But that is only half of its predetermined job. After the separation, the first stage will be recovered. The recovery part of the first stage is explained in this section. The entire first stage recovery mission profile is shown in Figure 5.9.

3.8.1. TRAJECTORY

The empty first stage has a certain altitude, velocity and direction after separation. If no action is taken to intervene after first stage separation, the first stage will continue to go up to about 55 km altitude before gravity will take it down. During this uncontrolled trajectory, the first stage will travel to about 600 km horizontal distance from the launch site. To land back in the neighbourhood of the launch site, the separated first stage makes a boost-back-manoeuvre (as explained in Section 3.1). After the boost back manoeuvre, the engines will turn off and the parachutes will guide it to the desired landing side.

3.8.2. DROGUE PARACHUTE

When the first stage has decreased in altitude to 12 km, a drogue parachute will be deployed to decrease the velocity of the first stage from its supersonic terminal velocity to a subsonic velocity of 77 m/s.

The drogue chute is a ribbon conical parachute and is shown in Figure 3.33, the relations regarding the sizing of the drogue chute are displayed in Equation 3.56. The final inputs and results are displayed in table 3.16. At the moment the main chute will be deployed, the drogue chute will be separated from the stage.

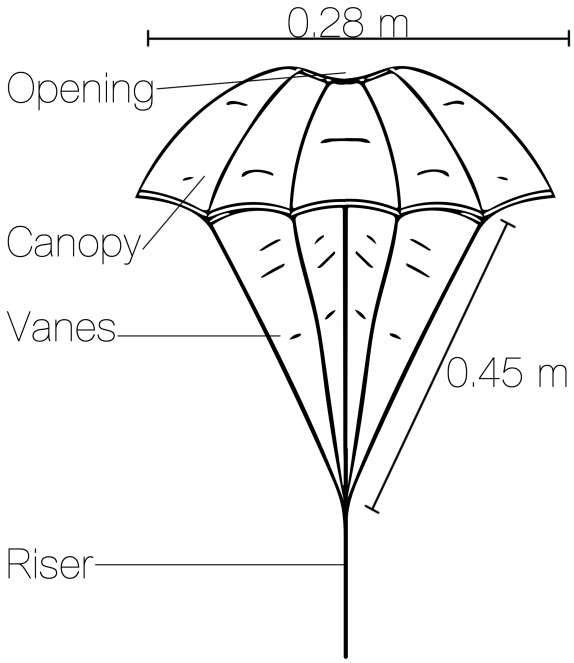

Figure 3.32: MA-1 Drogue Pilot Chute

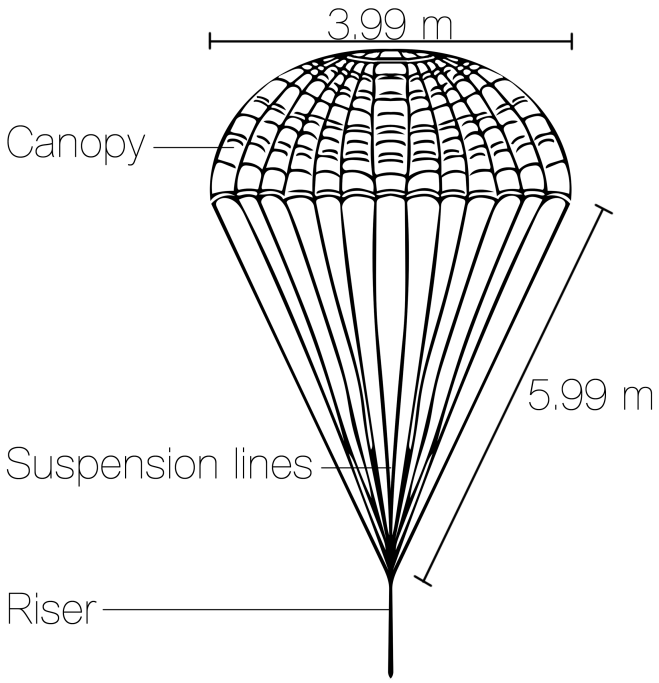

Figure 3.33: Ribbon Conical Drogue Chute

$$S_c = \frac{g(M_s + M_{mc})}{2\rho v_t^2 C_D} \qquad D_c = \sqrt{\frac{4S_c}{\pi}} \qquad L_l = 1.5 D_c$$

$$n_l = \frac{S_c}{0.3} \qquad M_t = S_c M_{sp_{canopy}} + L_l n_l M_{sp_{line}} \qquad V_t = \frac{M_t}{480.6} \tag{3.56}$$

In which S_c is the canopy surface area, M_s is the mass of the empty first stage, M_{mc} is the mass of the main parachute, v_t is the terminal velocity, D_c is the diameter of the canopy, L_l is the length of the lines, n_l is the number of lines, M_t is the total mass of the parachute including canopy and lines and V_t is the total packed volume of the parachute when it is pressure packed.

The number of lines per parachute are determined by the snatch forces the chute needs to handle during deployment and the number of lines needed to keep the shape of the parachute. Since the number of lines needed to keep the preferred shape is many times higher than the number of lines needed to handle the snatch forces, the shape determines the number of lines. This is the case for all parachutes used. The material used for both the lines and the webbing is Kevlar [34] (The specific material properties are displayed in the specification table under 'input').

3.8.3. MAIN PARACHUTE

To control the landing of the first stage without the engines and therefore with parachutes alone, controllable parachutes need to be used. Examples are a Sailwing, a Parawing and a Parafoil [34]. Since Parafoils (or Ram-Air-Parachutes)

Table 3.16: Inputs and results of the Drogue Chute

Input		Results	
C_D	0.55 [34]	Area	12.53 m^2
Terminal velocity	1100 m/s	Diameter	3.99 m
Deployment height	12 km [34]	Suspension line length	5.99 m
End Velocity	77 m/s [34]	Number of suspension lines	35
Line Diameter	0.0025 m [35]	Total Mass	2.00 kg
Specific Line strength	2.55e+9 N/m^2 [34]	Total Volume	0.0015 m^3
Specific Canopy mass	0.056 kg/m^2 [34]		

have the highest lift-over-drag coefficients (L/D) and have been used successfully for many years with manned jumps [34], the parafoil is the most interesting. The Parafoil Main Parachute is displayed in Figure 3.35. The relations used to design the main chute are shown in Equation 3.57. And the final inputs and results for the Main Parafoil Parachute are displayed in Table 3.17. Right at landing (when the legs touch the ground) the main parachute is disconnected from the rocket to prevent sudden winds inflating the chute and tipping the stage over.

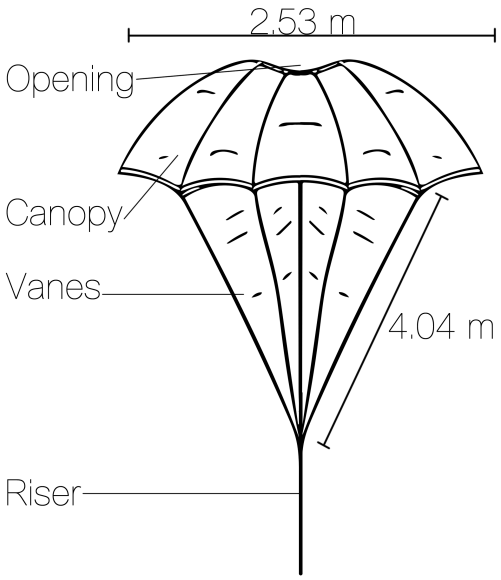

Figure 3.34: MA-1 Main Pilot Chute

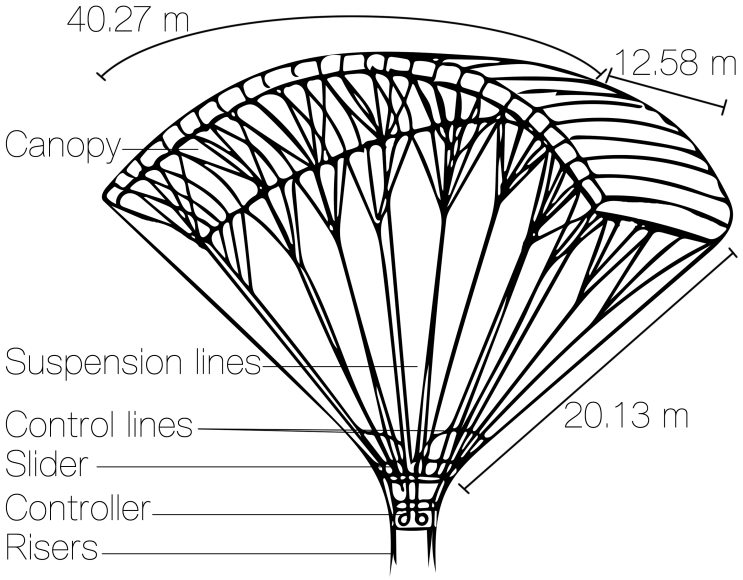

Figure 3.35: Main Parafoil (Ram-Air) Parachute

$$k = \frac{2\pi AR}{a_0} tanh\left(\frac{a_0}{2\pi AR}\right) \qquad a_{02} = a_0 k$$

$$a = \frac{\pi AR a_{02}}{\pi AR + a_{02}(1+\tau)} \qquad C_L = a(\alpha - \alpha_{zl}) \qquad C_r = \sqrt{C_L^2 + C_D^2}$$

$$S_c = \frac{2M_s g_0}{\rho_0 C_r v_l^2} \qquad W_c = \sqrt{S_c AR} \qquad L_c = \frac{S_c}{W_c} \qquad R_{manoeuvre} = h_d \frac{L}{D}$$

$$L_l = \frac{1}{2} W_c \qquad n_l = \frac{S_c}{\frac{1.11 S_c}{300}} \qquad \phi = \frac{45 W_c}{\pi L_l} \qquad \psi = atan\left(\frac{1}{\frac{L}{D}}\right) \tag{3.57}$$

In which AR is the aspect ratio, a_0 is the two dimensional lift curve slope, α is the angle of attack, α_{zl} is the zero lift angle of attack, τ is a small positive factor that increases the induced angle of incidence, v_l is the preferred landing speed, W_c is the width of the canopy, L_c is the length of the canopy, h_d is the deployment altitude, $R_{manoeuvre}$ is the radius in which the parafoil can manoeuvre, ϕ is the arc-anhedral angle and ψ is the approach angle.

3.8.4. PILOT CHUTES

Since both the drogue chute and the main chute have a diameter larger than 1.5 m, pilot chutes are needed to deploy the drogue and main chutes evenly. A pilot chute also decreases the high snatch forces, possible line entanglements and partial canopy deployment which can lead to damages [34]. The pilot chutes will be deployed with a gun and will, when deployed, pull out the main/drogue chutes from their bags. Both pilot chutes are MA-1 Pilot Chutes and

Table 3.17: Input and Results of the Main Parafoil Chute

Input		Results	
L/D	3.2 [34] [35]	Area	506.72 m^2
AR	3 [34] [35]	Length	12.58 m
α	6 deg	Width	40.27 m
α_{zl}	-0.1222 rad [35]	ϕ	28.65 deg
v_l	5 m/s	ψ	17.35 deg
a_0	6.89 rad^{-1} [35]	Suspension line length	20.134 m
τ	0.097 [35]	Number of suspension lines	271
Specific Line strength	2.55e+9 N/m^2 [34]	Total Mass	56.87 kg
Specific Canopy mass	0.056 kg/m^2 [34]	Total Volume	0.059 m^3
		Braking Velocity	4.92 m/s

are shown in Figures 3.32 and 3.34. The relations regarding to the size of the pilots are shown in Equation 3.58 and the final inputs and results are displayed in Table 3.18 and Table 3.19.

$$S_{pc} = \frac{0.03 C_d S_c}{C_{D,p}} (when V \leq 150 knots) \qquad S_{pc} = \frac{0.02 C_d S_c}{C_{D,p}} (when 150 \leq V \leq 250 knots)$$

$$S_{pc} = \frac{0.005 C_d S_c}{C_{D,p}} (when V \geq 250 knots) \qquad L_{pl} = 1.6 D_{pc} \tag{3.58}$$

In which the subscript c and l denote the drogue/main canopy and the subscript pc and pl denote the pilot canopy and pilot lines. The diameter and mass relations are the same as in 3.56 and are therefore note repeated.

Table 3.18: Input and results of the Drogue Pilot Chute

Input		Results	
C_D	0.55 [34]	Area	0.063 m^2
Drogue Chute Diameter	2.96 m	Diameter	0.28 m
Drogue Chute Area	6.88 m^2	Suspension vane length	0.45 m
Line Diameter	0.0025 m [35]	Number of suspension vanes	8
Specific Line strength	2.55e+9 N/m^2 [34]	Total Mass	0.0040 kg
Specific Canopy mass	0.056 kg/m^2 [34]	Total Volume	7.37e-06 m^3

Table 3.19: Input and results of the Main Pilot Chute

Input		Results	
C_D	0.55 [34]	Area	5.03 m^2
Main Chute Area	402.21 m^2	Diameter	2.53 m
Main Chute width	34.74 m	Suspension vane length	4.05 m
Main Chute length	11.58 m	Number of suspension vanes	8
Line Diameter	0.0025 m [35]	Total Mass	0.64 kg
Specific Line strength	2.55e+9 N/m^2 [34]	Total Volume	0.00059 m^3
Specific Canopy mass	0.056 kg/m^2 [34]		

3.8.5. CONTROL

To steer the empty first stage towards its desired landing location, the main parafoil parachute needs to be controlled. During manned jumps with parafoil parachutes, the person controls the parachute by pulling on a left and right control cable. Those cables are connected to the back ends of the parachute. Pulling on those cables would deflect the right and/or left trailing edge of the parachute as a form of ailerons or flaps. Deflecting the trailing edge 'flaperons' can make the parachute turn or brake. The person controlling the parachute can be replaced by a electrical/mechanical controller which consists of two servo motors pulling the control lines, a GPS-antenna to monitor the trajectory and a computer that controllers the servos due to the GPS input. This configuration (Automatic Controlled Parafoil Recovery System), has not been used for the recovery of space vehicles yet. The US army has plans to use such a system for the accurate dropping of goods in combat areas [35]. And NASA's X-38 Prototype Crew Return Vehicle had a similar system. But due to budget cuts, the X-38 program was cancelled after a few droptests [9].

[9] https://www.nasa.gov/centers/armstrong/news/FactSheets/FS-038-DFRC.html, visited on: 17-01-2016

Figure 3.36 shows a schematic drawing of such a controller and Figure 3.37 shows the feedback form of such a system. Table 3.20 shows the input and results of the sizing of the controller due to the size of the flaperons of the main parachute and the line length they have to reel-in for a 90 degrees flaperon deflection. Equation 3.59 displays the relationships involved.

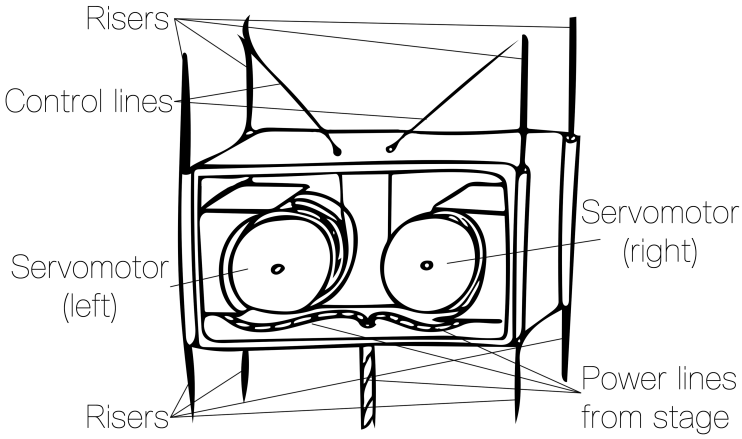

Figure 3.36: Schematic drawing of the main parafoil parachute controller

Figure 3.37: Controller feedback control system

$$\gamma = atan\left(\frac{1}{\frac{L}{D}}\right) \qquad Turnrate = -\frac{C_{n,\delta}}{C_{n,r}}\delta\frac{2v_l}{W_c}$$

$$Turnradius = \frac{v_l cos(\gamma)}{TurnRate} \qquad S_w = 0.27S_c \tag{3.59}$$

In which γ is the flight path angle, δ is the flap deflection angle, $C_{n,delta}$ is the yawing coefficient due to control deflection, $C_{n,r}$ is the yaw damping coefficient due to yaw rate and S_w is the wetted area of the main chute.

Table 3.20: Input and results of the Main chute controller

Input		Results	
$C_{n,\delta}$	0.0124 [35]	Max Turn Rate	7.27 deg
$C_{n,r}$	-0.0441 ($-C_D/6$) [35]	Min Turn Radius	37.61 m
L/D	3.2 [34] [35]	Max line reel-in length	5.15 m
		Servo Rounds	25
		Servo Diameter	0.0656 m
		Servo Length	0.0625 m

The turn rate and turn radius are influenced by the size of the flaperons, the size of the parachute and the deflection angle. These turn rates and turn radii are plotted as a function of deflection in Figure 3.38.

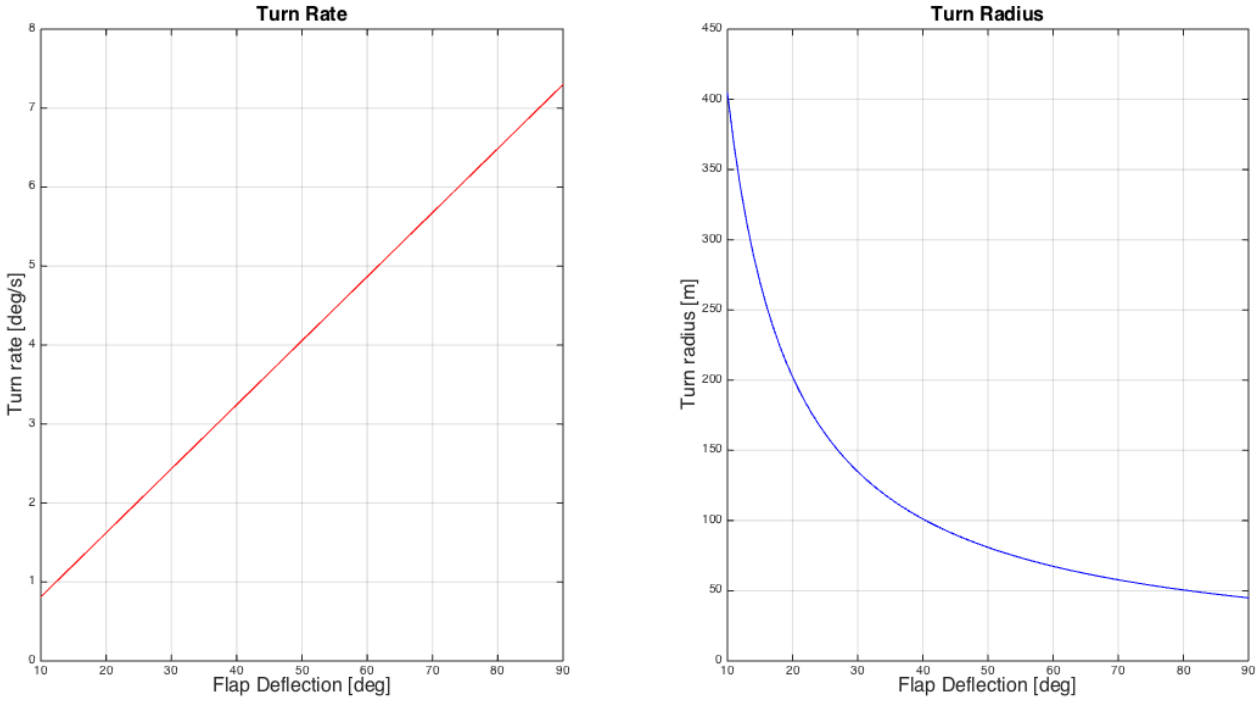

Figure 3.38: Turn rate and turn radius of the Main Parafoil Parachute

Detailed flight dynamics of the return of the first stage, starting with the boost-back-manoeuvre and ending with the parachutes decelerations, are shown in Figure 5.6 in Section 3.1. This includes the change in velocities due to the engines and the parachutes, as well as the change in altitude over time and the ground track.

Figure 3.39 gives a total overview of the all the parachutes and controllers of the recovery system.

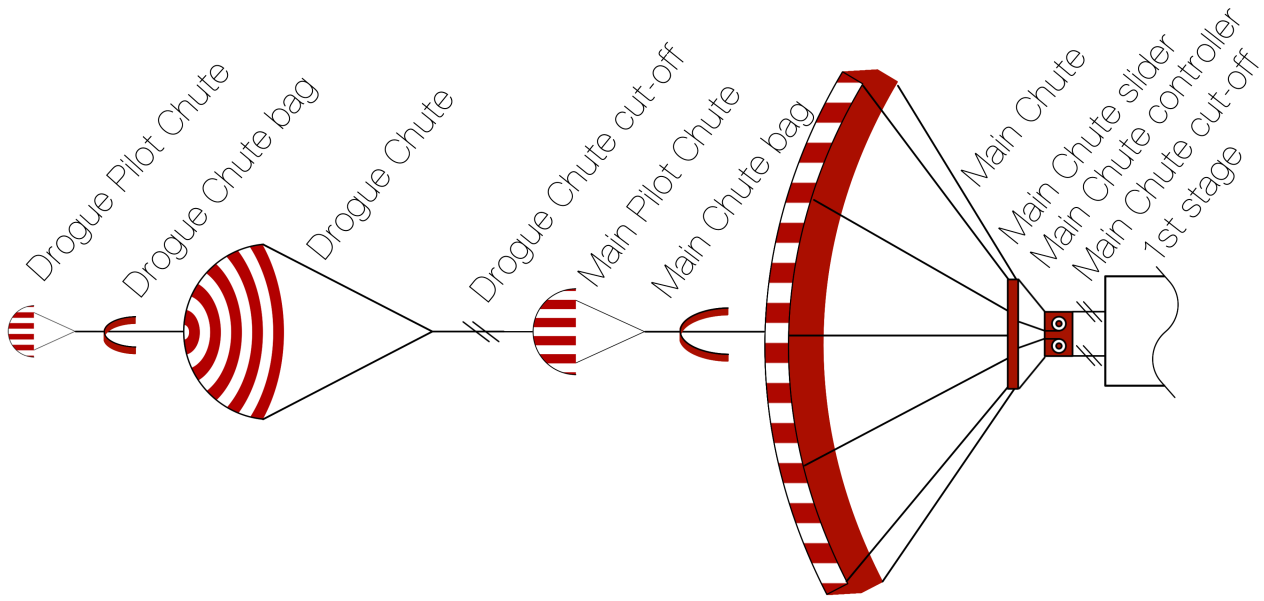

Figure 3.39: Schematic overview of the controllable parachute recovery system

The accuracy of the landing system depends on the accuracy of the Global Positioning System (GPS). Current GPS has a horizontal accuracy of 3 meters and a vertical accuracy of 5 meters [25]. If the control system would try to correct for diverging trajectories of 3-5 meters, the system would keep pulling on the parachute, which can lead to unstable situations [35]. Therefore a deadband has to be introduced. This deadband is a region of a few meters divergence in which the controller will not make corrections to keep the entire system stable. This region diameter should be the width of the parafoil chute [36]. Therefore, only if the trajectory of the first stage landing is half the width of

the parafoil off course, the system will act and correct. This then also determines the accuracy of the landing. The controllable parachute system can land the empty first stage with a 20.14 m accuracy.

3.8.6. LANDING LEG SYSTEM

In order to prevent the nozzles from hitting the ground during the landing, landing legs will be used. This will insure that there is a certain distance from the ground to the nozzles (clearance length). In order to increase the stability of the rocket during the landing and when it has landed, the upper attachment points of the landing legs will be above the centre of gravity of the first stage. This will prevent the rocket from tilting over. The lower attachment points will be on the rocket just above the nozzles to prevent any damage to the nozzles and the burning of the legs during the flight as can be seen in Figure 3.40.The three landing legs will be retracted during launch, side by side against the rocket stage. The top of the leg will be covered with a fairing to give it an aerodynamic shape. The vertical and the horizontal landing legs are attached to the rocket stage with means of pin connections. A rail on the side of the rocket stage will enable the upward and downward movements of the vertical and horizontal legs. The rocket has a constant approach velocity of 5 m/s when it hits the ground. Shock absorbers inside the landing legs will be used to absorb the impact velocity, while the the landing legs' outer structure will carry the structural loads of the rocket. Supporting legs will carry only tensile stresses and prevent horizontal movement of the vertical landing legs.

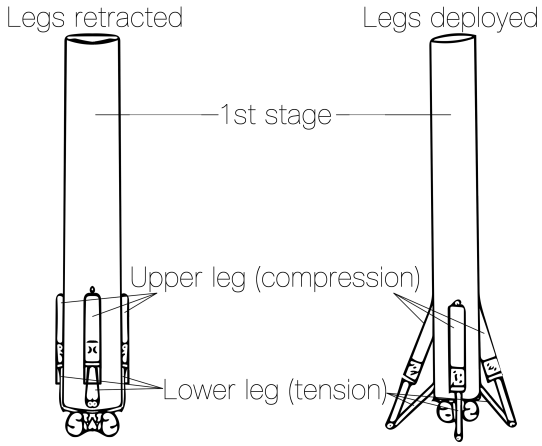

Figure 3.40: Landing Legs

The centre of gravity is obtained using Equation (3.60). The distances are measured from the nozzles towards the nosecone.

$$x_{cg} = \frac{m_{eng} \cdot x_{eng} + m_{struct} \cdot x_{struct}}{m_{eng} + m_{struct}} \rightarrow \frac{552.3 \cdot 0.35 + 493.2 \cdot 4.16}{552.3 + 493.2} = 2.15m \tag{3.60}$$

The landing legs' length and thickness depend upon the angle θ, its ability to carry the structural loads without buckling and having enough space inside it to allow for shock absorbers. A schematic representation of the legs is given in Figure 3.41. Where L_A is the length of lower to upper attachment points and must be higher than the centre of gravity, $L_{Nozzles}$ is length of the nozzles, $L_{Clearance}$ is the clearance length, L_V is the length of the landing leg and L_h is the length of the supporting leg.

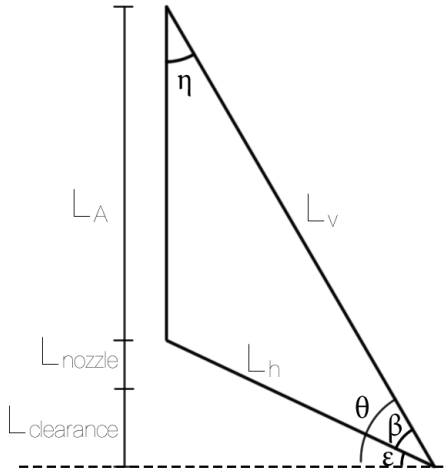

Figure 3.41: Schematic Representation of the Legs

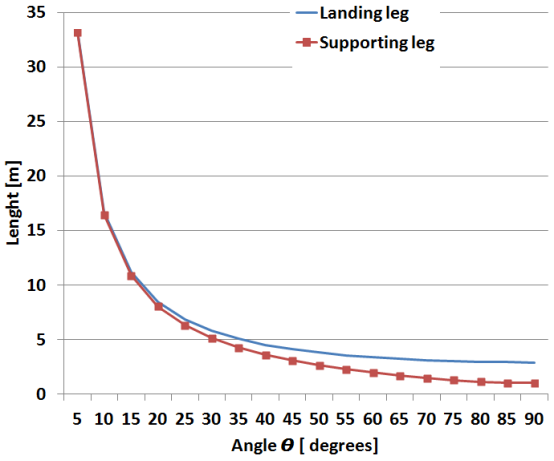

Figure 3.42: Length of the Landing Legs

The length of L_V can be determined using Equation (3.61).

$$L_V = \frac{H}{\sin(\theta)} \qquad H = L_A + L_{Clearance} + L_{Nozzles} \tag{3.61}$$

Using the law of cosines, the length of the supporting leg can be determined by Equation (3.62)

$$L_h = \sqrt{L_A^2 + L_V^2 - 2 \cdot (L_A \cdot L_V) \cdot \cos(\eta)} \qquad \eta = 90° - \theta$$

$$\epsilon = \arcsin\left(\frac{L_{Clearance} + L_{Nozzles}}{L_h}\right) \qquad \beta = \theta - \epsilon \tag{3.62}$$

As can be seen in Figure 3.42, the length of the landing leg and supporting leg decreases with increasing angle θ.

The choice of angle θ determines the stability margin of the rocket during the landing as well. The critical situation is when the rocket hits the ground on one leg only. This means the rocket will be under angle η. In order to increase the stability of the rocket during landing, this Angle need to be increased. As it can be seen in Figure 3.42, after 70° the landing leg length changes are very small. Thus keeping θ at 70° gives a η of 20°. This means that the rocket can land even when it is approaching the ground with angle of 20°.

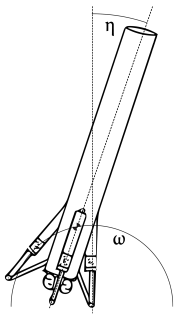

Figure 3.43: Maximum Landing Angle

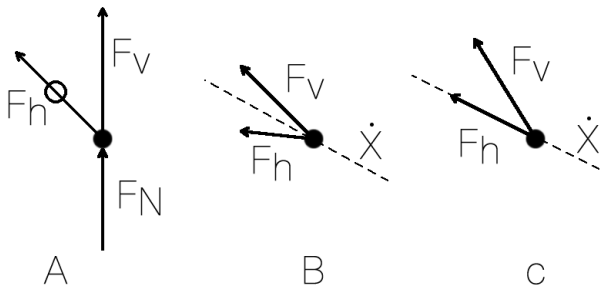

Figure 3.44: Forces Acting on the Landing Legs

The input and the results of the landing and supporting legs can be seen in Table 3.21.

Table 3.21: Input and Results of Landing and Supporting Legs

Input		Substituted in Equation	Results	
θ	70°	(3.62) and (3.61)	H	3.4 m
η	20°	(3.62)	L_V	3.1 m
L_A	1.9 m	(3.62) and (3.61)	L_h	1.5 m
$L_{clearance}$	0.5 m	(3.62) and (3.61)	ϵ	43.45°
$L_{Nozzles}$	0.5 m	(3.62) and (3.61)	β	26.55°

The landing legs are designed for the worst case scenario, which is hitting the ground with one leg with a approach velocity of 5 m/s. This means that one Landing leg should be able to absorb the initial velocity and withstand the structural loads as well. Using method of joints as can be seen in Figure 3.44 the maximum loads, which acts on the Landing and supporting legs can be determined.

From Figure 3.44 A, The vertical landing force F_V can be determined. In the worst case scenario the Normal force F_N is equal to the applied force $F_{applied}$, which is safety factor multiplied by weight.

$$\sum F_{vertical\uparrow+} = 0 : F_N + F_V = 0 \rightarrow F_V = -F_N \quad (3.63) \qquad F_{applied} = S.F. \cdot m \cdot g \quad (3.64)$$

After changing the axis to $\dot{x}$ axis (see Figure 3.44 B and C), the force on supporting leg can be determined.

$$\sum F_{horizontal\rightarrow+} = 0 : -F_h + F_v \cdot \cos(\beta) = 0 :\rightarrow F_h = F_V \cdot \cos(\beta) \quad (3.65)$$

where η and β are determined using Equation (3.62)

The input and the results of the loads of the landing and supporting legs can be seen in Table 3.22

Table 3.22: Input and Results of Loads acting on Landing and Supporting Legs

Input		Results	
Mass	1045.5 kg	$F_{applied}$	15384.5 N
Safety factor (S.F.)	1.5	F_V	-15384.5 N
g	9.81 $\frac{m}{s^2}$	F_h	13762.2 N
β	26.55°		

In order to prevent buckling in the Landing legs, the critical loads (P_{cr}) should not be higher than the applied load ($F_{applied}$). The critical load can be calculated using Equation (3.66)

$$P_{cr} = \frac{n \cdot \pi^2 \cdot E \cdot I}{L^2} \quad (3.66)$$

where E is young modulus, I is moment of inertia, L is the length of the column and n is the buckling mode. For a simply supported beam, which is the case here n= 1

The moment of inertia can be determined using Equation (3.67)

$$I = \frac{\pi}{4} \cdot (R_0^4 - {R_i}^4) = \frac{\pi}{4} \cdot (R_0^4 - (R_{0-t})^4) \quad (3.67)$$

Where R_0 is the outer radius and R_i is the inner radius and t is thickness of the cross-section. R_0 depends on shock absorber bore diameter and wall thickness of the chamber, which can be determined by Equation (3.86). The value of R_0 is given in the Table 3.28.

The supporting leg L_h carries only tensile stresses. In order to prevent failure the normal stress in L_h, should be lower than the yield stress of the material. This is given by Equation (3.68), where A_h is the cross-sectional area of the supporting leg.

$$\sigma_{normal} = \frac{F_h}{A_h} \qquad A_h = \pi \cdot (R_0^2 - R_i^2) = \pi \cdot (R_0^2 - (R_{0-t})^2) \quad (3.68)$$

The choice of material for the landing legs are based on high performance, weight reduction and affordable price. the optimal option is Aluminum-lithium (Al-Li) 2099 alloy. This alloy has the lowest density, high young modulus, ultimate strength and yield stress. Although the price is slightly high, this material results in low weight and less required material for production. Al-Li 2099 alloy has been chosen [37].

Using the above relations and the material properties of Al-Li 2099 alloy as can be seen in the Table 3.23, Figures 3.45 and 3.46 have been obtained.

Table 3.23: Aluminum-Lithium (Al-Li) 2099 T-83 Properties [37]

Input	
E	78.6 GPa
$\rho_{Aluminum}$	2630 kg/m^3
σ_{yield}	490 MPa
$\sigma_{ultimate}$	545 MPa

As can be seen in Figures 3.45 and 3.46, the landing and supporting legs will not fail even at a thickness of $1mm$. Therefore, the critical thickness for the landing leg depends upon wall thickness of the shock absorber fluid chamber given Equation (3.82). But there is no shock absorber inside the supporting leg. Therefore, the optimum value for radius R_h is found after numerous iteration. The thickness of the supporting leg is limited by manufacturability. In order to simplify manufacturability slightly higher thickness is chosen than required from normal stress point of view. The results are give in Table 3.24

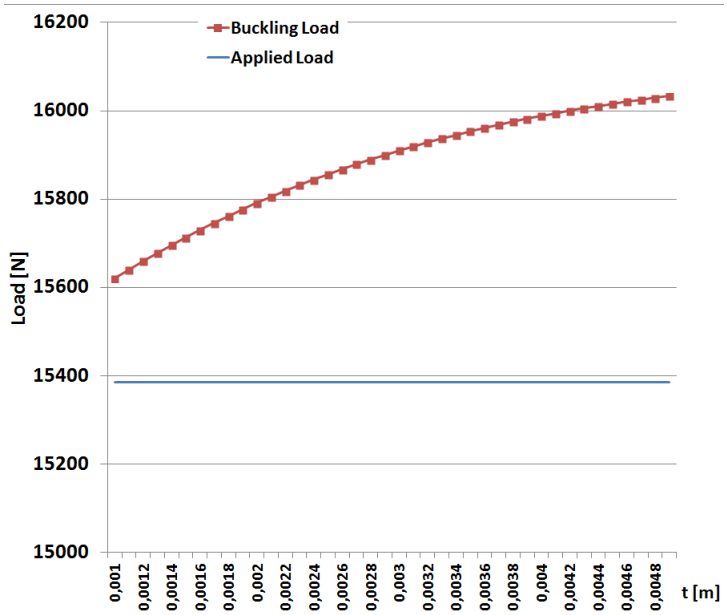

Figure 3.45: P_{cr} and $F_{applied}$ of the Landing Leg

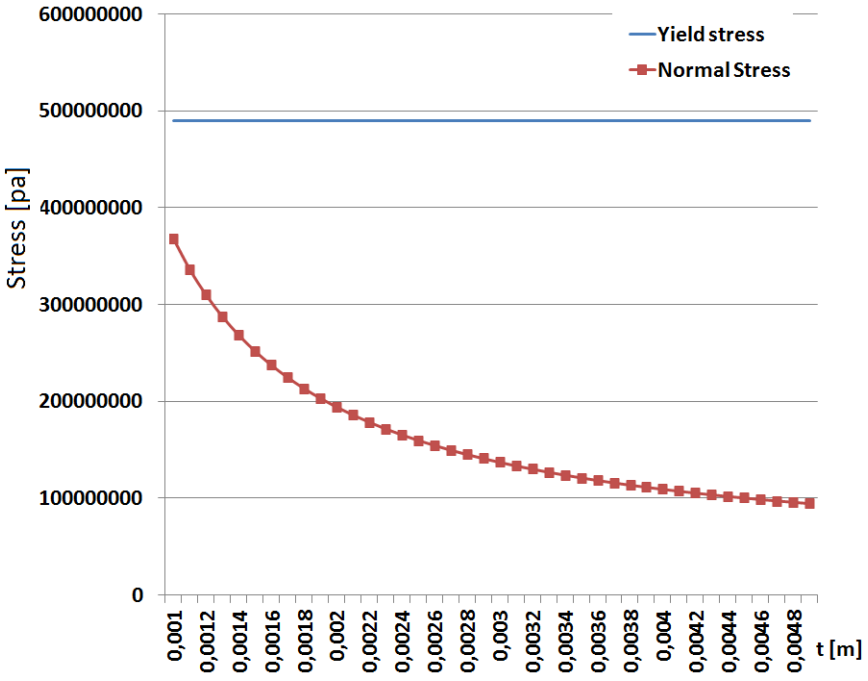

Figure 3.46: σ_{Normal} and σ_{yield} of the Supporting Leg

3.8.7. OIL-SPRING SHOCK ABSORBER SYSTEM

Each landing leg will include shock absorbers to absorb the impact forces during landing as it was mentioned in the beginning of this section. The sizing of the shock absorbers is done by a series of equations and approximations [38]. Firstly the kinetic energy, thus the energy required for the shock absorber to absorb has to be calculated by

Table 3.24: Landing and Supporting Leg Results

	L_V	L_h
Length [m]	3.1	1.5
Outer radius R_0 and R_h [m]	0.0459	0.01
Thickness [m]	0.002	0.002

Equation (3.69). After calculating the kinetic energy of the impact during landing the stroke is calculated for the shock absorber by using Equation (3.70). The stroke is a measure of how much the piston will move towards the oil chamber in order to absorb the impact forces. The shock force of the shock absorber is calculated after this by using Equation (3.71).

$$E_k = \frac{1}{2}mv^2 \quad (3.69) \qquad x_s = \frac{v^2}{\eta 2gN} \quad (3.70) \qquad F_{ps} = \frac{E_k}{x_s \eta} \quad (3.71)$$

where m is the empty mass of the first stage, v is the approach velocity, g is the gravity constant 9.81m/s^2, η is the shock absorber's efficiency and N is the load factor.

Table 3.25: Kinetic Energy, Stroke and Shock Force of the Shock Absorber

Input		Substituted in Equation	Output	
m	1045.5kg	(3.69)	E_k	13059.8J
v	5m/s	(3.69), (3.70)	x_s	0.283m
η	0.9	(3.70), (3.71)	F_{ps}	51240.4N
g	9.81m/s^2	(3.70)		
N	5	(3.70)		
E_k	13059.8J	(3.71)		
x_s	0.283m	(3.71)		

Equations (3.72) and (3.73) give the relations to determine the bore area and the bore diameter respectively of the shock absorber. The rod area needs to be estimated firstly after which the Johnson formula, Equation (3.74) is used to find the most optimal choice for the rod diameter. The safety factor is equal to F_c/F_{ps}, thus the ratio between the shock force and the column force. When the safety factor is around 1.3 the most optimal choice for the rod diameter has been found. After this, the area of the rod can be determined using Equation (3.75).

$$A_B = \frac{F_{ps}}{psp} \quad (3.72) \qquad D_B = \sqrt{\frac{4A_B}{\pi}} \quad (3.73) \qquad F_c = S_y A_{rod}\left[1 - \frac{S_y L_e^2 A_{rod}}{4\pi^2 EI}\right] \quad (3.74) \qquad A_{rod} = \frac{D_{rod}^2 \pi}{4} \quad (3.75)$$

where F_{ps} is the shock force, psp is the peak shock pressure, S_y is the yield strength of the rod material, L_e is the effective column length assumed at 0.7L_{rod}, where L_{rod} is the entire column length, A_{rod} is the rod area, D_{rod} is the rod diameter, E is the Young's modulus of the rod material, which is the same, the aluminium-lithium alloy 2099, as for the landing legs mentioned in Table 3.23, and I is the moment of inertia of the rod.

Table 3.26: Bore Area, Bore Diameter, Column Force and Rod Area of the Shock Absorber

Input		Substituted in Equation	Output	
F_{ps}	51240.4N	(3.72)	A_B	$3.72{\cdot}10^{-3}$m^2
psp	13.79MPa	(3.72)	D_B	0.069m
A_B	$3.72{\cdot}10^{-3}$m^2	(3.73)	F_c	67630.3N
S_y	490MPa	(3.74)	A_{rod}	$1.11{\cdot}10^{-3}$m^2
A_{rod}	$1.11{\cdot}10^{-3}$m^2	(3.74)		
L_e	0.7m	(3.74)		
E	78.6GPa	(3.74)		
I	$9.811{\cdot}10^{-8}$ m^4	(3.74)		
D_{rod}	0.0376m	(3.75)		

Assuming a maximum pressure of 40,000psi (≈ 2757.9bar) and a preload pressure of 2000psi (≈ 137.9bar) the compressibility of a liquid-spring fluid gives the following values for the slope, Equations (3.76) and (3.77). The change in deflection of the fluid under the given pressure can be calculated by Equation (3.78).

$$\delta_p = \frac{\Delta V}{V}\Big|_{2000psi} = 0.015 \quad (3.76) \qquad \frac{\Delta V}{V}\Big|_{40{,}000psi} = 0.14 \quad (3.77) \qquad \Delta\delta = 0.14 - 0.015 = 0.125 \quad (3.78)$$

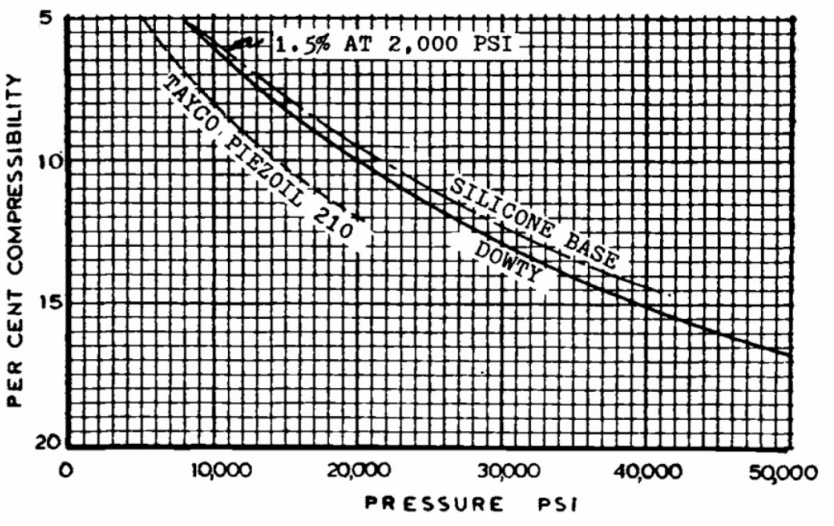

Figure 3.47: Compressibility of a liquid-spring fluid [38], page 88

After computing the change in fluid deflection the total fluid volume can be computed by Equation (3.79). The geometric volume of the fluid chamber can be computed after this by using Equation (3.80), which takes into account some existing precompression of the shock absorber, (3.76). Finally, the length of the chamber can be calculated by using Equation (3.81) and the thickness of the chamber wall by using Equation (3.82).

$$V_t = \frac{A_{rod} x_s}{\Delta\delta} \quad (3.79) \qquad V_{geo} = \frac{V_t}{1+\delta_p} \quad (3.80) \qquad L_{ch} = \frac{V_{geo}}{\pi(D_B/2)^2} \quad (3.81) \qquad T_{wall} = \frac{R}{(S/P)-1} \quad (3.82)$$

where R is the bore radius, P is the end load spring pressure of 50,000psi (≈ 3447.4bar) and S is the cylinder stress of 200,000psi (≈ 13,789.5bar) [38], page 93.

Table 3.27: Fluid Volume, Geometric Volume, Chamber length and the Chamber Wall Thickness of the Shock Absorber

Input		Equation	Output	
A_{rod}	$1.11{\cdot}10^{-3}\text{m}^2$	(3.79)	V_t	$2.52{\cdot}\ 10^{-3}\text{m}^3$
x_s	0.283m	(3.79)	V_{geo}	$2.48{\cdot}10^{-3}\text{m}^3$
$\Delta\delta$	0.125	(3.79)	L_{ch}	0.667m
V_t	$2.52{\cdot}10^{-3}\text{m}^3$	(3.80)	T_{wall}	0.0115m
δ_p	0.015	(3.80)		
V_{geo}	$2.48{\cdot}10^{-3}\text{m}^3$	(3.81)		
D_B	0.069m	(3.81)		
R	0.034m	(3.82)		
S	13,789.5bar	(3.82)		
P	3447.4bar	(3.82)		

Equation (3.83) gives the relation to compute the fluid velocity of the shock absorber. Equations (3.84) and (3.85) give the relations to compute the orifice area and the piston area respectively.

$$V_F = \sqrt{\frac{2gp}{3\rho}} \quad (3.83) \qquad A_O = A_B \frac{V_P}{V_F} \quad (3.84) \qquad A_P = A_B - A_O \quad (3.85) \qquad R_0 = \frac{D_B + 2\cdot T_{wall}}{2} \quad (3.86)$$

where V_P is taken equal to the approach speed, v, used in relation (3.69), ρ is the silicone oil density which is assumed equal to $0.97\rho_{water}$, where ρ_{water} is the density of water ($\approx 1000 kg/m^3$), g is the gravity constant equal to 9.81m/s^2, p is the peak shock pressure 40,000psi or 5,760,000psf (≈ 2757.9bar).

It is important to analyse the heat development during the shock absorption. Assuming a frictionless, adiabatic flow and constant pressure, the temperature inside the fluid chamber can be determined using the energy equation. This is given by Equation (3.87), where C_p is specific heat of Silicone oil [10] $1370 J/kgK$ and V_1 is fluid velocity given in the table 3.28, noted as V_F.

[10] http://www.matbase.com/material-categories/other-materials/liquids/material-properties-of-silicone-oil.html, visited on: 20-01-2016

Table 3.28: Fluid Velocity, Orifice Area, Piston Area and the Outer radius of the Shock Absorber

Input		Equation	Output	
g	9.81m/s^2	(3.83)	V_F	435.74m/s
p	2757.9bar	(3.83)	A_O	4.263·10^{-5}m^2
ρ	970kg/m^3	(3.83)	A_P	3.67·10^{-3}m^2
A_B	3.72·10^{-3}m^2	(3.84)	R_0	0.0459m
V_P	5m/s	(3.84)		
V_F	435.74m/s	(3.84)		
A_O	4.263·10^{-5} m^2	(3.85)		
D_B	0.069m	(3.86)		
T_{wall}	0.0115m	(3.86)		

$$C_p \cdot T + \frac{1}{2} \cdot V^2 = constant \qquad C_p \cdot T_1 + \frac{1}{2} \cdot V_1^2 = C_p \cdot T_2 + \frac{1}{2} \cdot V_2^2 \tag{3.87}$$

At the end of the absorption process velocity (V_2) is zero. Assuming an initial temperature of $T_1 = 25°C$, will result in a $T_2 = 94.3°C$. This is way below the boiling temperature of the silicone oil [11], which is $230°C$. Therefore, the design is deemed safe to operate.

3.8.8. LANDING LEGS WEIGHT ESTIMATION

The weight of the landing legs consist of shock absorbers, the structure of the landing and supporting legs and the actuators. During launch the legs are retracted next to each other and at the moment of landing a linear actuator will jolt the vertical landing leg and push it downward. The specifications of the actuator chosen are given in Table 3.29. Three actuators are required in total for the first stage recovery system, one for each landing leg.

Table 3.29: Specifications of the Model 310 Linear Actuator [12]

Specifications	
Size [m]	0.051 x 0.085 x 0.214
Force [N]	1334.5 (Rated) ; 4448.2 (Peak)
Stroke [m]	0.076
Weight [kg]	2.0
Power [W]	28

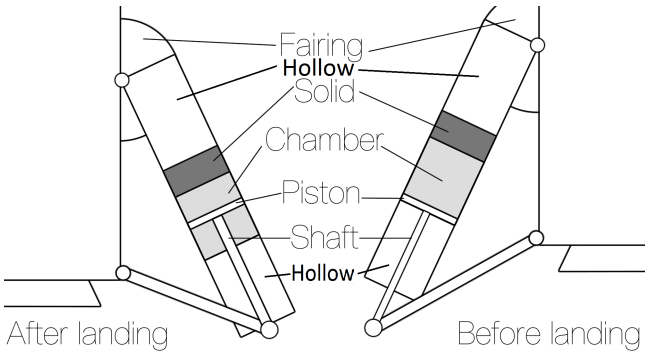

Figure 3.48: Detail Sketch of Landing and Supporting Legs

A detailed sketch of the landing and supporting legs can be seen in Figure 3.48. The length of the shock absorber, is smaller than the entire length of the landing leg. In order to keep the shock absorber at a fixed location inside the landing leg, a small solid part is introduced there. The remainder of the part is hollow. This is done in order to reduce the weight of the landing system. Furthermore, the hollow part has a different thickness (see Table 3.24) compared to the wall thickness of the chamber (see Table 3.28). The weight of each segment is determined separately and added together in order to get the total weight of the landing leg. The weights are determined using Equations (3.88) up to (3.96), where the length of the solid part $L_{solid} = 6cm$, length of the piston $L_{piston} = 6cm$, length of the

[11] http://www.sigmaaldrich.com/catalog/product/sial/175633, visited on: 20-01-2016
[12] http://www.moog.com/products/actuators-servoactuators/multi-purpose/linear-actuators/model-310/, visited on: 15-01-2016

rod $L_{rod} = 1m$, W_{ch} is the chamber structural weight and R_h is the radius of the supporting leg. Using the values of Tables 3.21, 3.23, 3.24, 3.26, 3.27, 3.28 and 3.29, the total weight of the landing system can be calculated. The results are given in Table 3.30.

$$W_{Solid} = L_{solid} \cdot \rho_{aluminum} \cdot \pi \cdot R_0^2 \quad (3.88)$$

$$W_{piston} = L_{piston} \cdot \rho_{aluminum} \cdot A_{piston} \quad (3.89)$$

$$A_{piston} = A_{bore} - A_{orifice} \quad (3.90)$$

$$W_{rod} = L_{rod} \cdot \rho_{aluminum} \cdot A_{rod} \quad (3.91)$$

$$W_{fluid} = \rho_{oil} \cdot V_t \quad (3.92)$$

$$W_{hollow} = \rho_{aluminum} \cdot L_{hollow} \cdot \pi \cdot (R_0^2 - (R_0 - t)^2) \quad (3.93)$$

$$L_{hollow} = L_V - L_{solid} - L_{ch} \quad (3.94)$$

$$W_{ch} = \rho_{aluminum} \cdot L_{ch} \cdot \pi \cdot (R_0^2 - (R_0 - T_{wall})^2) \quad (3.95)$$

$$W_h = \rho_{aluminum} \cdot L_h \cdot \pi \cdot (R_h^2 - (R_h - t)^2) \quad (3.96)$$

Table 3.30: Landing Legs Weight

landing leg subsystem	Weight [kg]
W_{rod}	2.92
W_{piston}	0.58
W_{fluid}	2.44
W_{hollow}	3.52
W_{solid}	1.04
$W_{chamber}$	5.07
W_h	0.43
$W_{actuator}$	2
one landing and supporting leg	18
Total weight of the landing system	54

3.9. FLIGHT TERMINATION SUBSYSTEM

In this section the design of the flight termination system is discussed. First safety regulations regarding the FTS are discussed in Section 3.9.1. Then the options for the FTS are discussed and selected in Section 3.9.2. Finally the design of the subsystem is given in Section 3.9.3.

3.9.1. SAFETY REGULATIONS

In order to ensure safety, there are several regulations a flight termination system must adhere to. The most important safety concern is that the maximum casualty expectation of any launch cannot exceed 0.000003 in case of vehicle failure [39]. The flight termination system plays a big role in this as it has to make sure this value is respected. Therefore a flight termination system must operate completely independently of any other system. A failure of another system must not interfere with the FTS. Regulations allow the FTS to share components with another system, only if it can be demonstrated that this will not affect the FTS's reliability. Furthermore, the flight termination system should be able to terminate the flight of any propulsion system capable of reaching a populated or protected area. In case of solid propulsion systems, it should be able to destroy the pressure integrity of solid propellant systems in order to terminate thrust as quickly as possible. On the other hand, in case of liquid propulsion systems, it should be able to disperse all the remaining liquid propellant and to start the burning of any toxic propellant. The FTS must however not cause any of the (liquid or solid) propellants to detonate. [40]

3.9.2. POSSIBLE OPTIONS AND SELECTION

There are several options for the flight termination system, these are listed below.

1. **Thrust Termination System (TTS)** - This ends the propelled stage of the flight by stopping the thrust. It is only applicable to liquid propulsion systems, as the thrust can be controlled in these systems by shutting the valves for example. Solids propulsion systems burn until depleted and there is no possible way to stop the thrust while keeping the stage intact. This system can be activated manually by range safety officers (RSO) to prevent the rocket from leaving the designated fly zone. [41] It can also be triggered automatically by the FTS computer when design parameters, such as propellant pressure, vary outside safety ranges.

2. **Flight Destruction System (FDS)** - This destroys the launch vehicle. When a rocket failure occurs that will affect public safety, the rocket can be destroyed in order to not bring harm to people. This can be done by

mounting linear shaped charges onto the propellant tanks. When detonated, the propellant will disperse and thrust will stop. This is an effective way of terminating solid propulsion systems.

3. **Vehicle Recovery System (VRS)** - This will attempt to soft land the vehicle. The most common way to do this is by using parachutes. It is useful for example in case of a failure in the ability of the vehicle to maintain controlled flight along its path. By terminating the thrust, dumping the fuel and using the parachutes the launch vehicle can be brought relatively intact back to Earth. It also safe because the vehicle will have a velocity much lower than free-fall when falling back to Earth.

Thrust termination on itself is not an effective way to ensure safety as a flight termination system, but it is a step to be taken before continuing with other flight safety activities. The QLS FTS will therefore implement a TTS. A FDS will be needed as well, in case of critical situations where the launcher veers into an unexpected flight path. Before launch boundaries are set, in case the vehicle flies outside of those boundaries or becomes uncontrollable within it should be destroyed in order to minimise the damage and maximise the safety on the ground. Boundaries are determined to minimise the danger debris will bring to people on the ground. Since the launch system will have parachutes in order to recover the first stage, these can be used as well in order to attempt a soft landing in case of failure and act as VRS. The landing speed will be too high to recover the whole rocket with the parachute, as it is designed to only recover the first stage. A hard landing with the rocket still carrying propellants will also be extremely dangerous. Stage separation to separate the first stage from the rest of the rocket must therefore be performed first. The first stage will then be attempted to recover while the second and third stage will be destroyed with the FDS to minimise impact.

All three options will therefore be implemented in the launch system. It will strongly depend on the stage of flight and other crucial circumstances which of the three systems will be used in case of critical failure. The design of the systems follows in the next section.

3.9.3. FTS DESIGN

Since the FTS is a completely independent subsystem, it needs to have its own batteries and antenna (receiver). The other components of the system are an encoder, a safe and arm device and explosive charges. Based on reference data, the following uplink properties have been selected. [42] [43] [44]

- Carrier frequency: UHF 406 - 460 Mhz
- FM modulation: ranging from 10Hz to 100kHz
- EIRP: between 56 and 90 dBm
- Link margin: between 9 and 12 dB
- Antenna gain: between 0 and 8 dBi
- Standard RCC tones as inputs

The standard RCC tones are standards set by the Inter-Range Instrumentation Group (IRIG). Monitor (tone 5), flight destruction (tone 3) and arm (tone 1) have a frequency of 500, 750 and 1250Hz, respectively. [45] [46] There are no standard tones for vehicle recovery (tone 4) and thrust termination (tone 3), so these have to be fixed to a certain bandwidth. After a tone has been received, it is encoded by the FTS encoder. The logic of the FTS can be seen in Figure 3.49.

As can be seen from Figure 3.49, the FTS will have a fail-safe mechanism in case of any failure to receive tones from the ground. This fail-safe mechanism is activated if no tone is received, or a tone that is not recognised. The main blocks will be briefly explained below.

Monitor - Tone 5 is continuously sent to the FTS in case everything is proceeding as expected. It means that the flight operations continue as planned.

Arm - When in addition to tone 5 also tone 1 is sent, the charges are armed. This happens when an anomaly has been found. It does not necessarily mean that the system has failed critically and that the mission has to be aborted. When the RSO decides that the flight can continue, tone 1 will not be sent anymore, and the FTS goes back to monitor block, while continuously receiving tone 5. In case the RSO decides that the anomaly is critical and the mission has to be aborted, either tones 2, 3 or 4 are sent in order to activate the Thrust Termination (TT), Flight Destruction (FD) or Vehicle Recovery (VR) processes. More on that below.

Thrust Termination - When tone 3 is received together with 1, right after tones 1 and 5 were received together, the TT system is activated. This means the valves of the engines are shut down. Propellants will no longer go to the combustion chamber and no thrust will be generated.

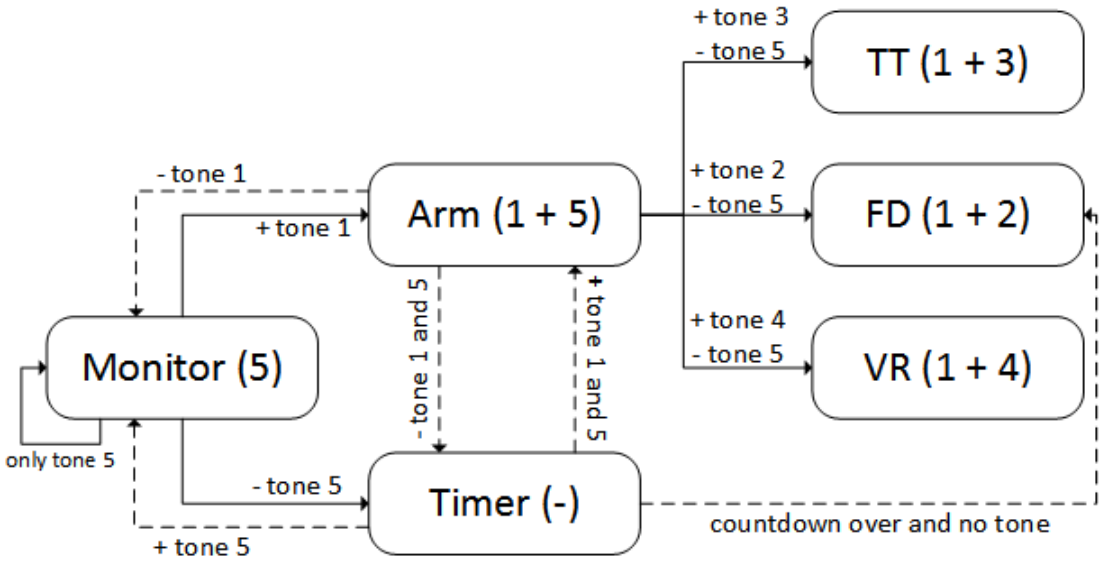

Figure 3.49: FTS Logic Diagram

Flight Destruction - In case tone 2 is received in addition to tone 1, and the charges are armed, the FD system will be activated. This means that the charges attached to the propellant tanks are ignited in order to destroy the tanks and let the propellant out of the rocket as quickly as possible.

Vehicle Recovery - On the other hand, if tone 4 is received simultaneously as 1, and the system is armed, the VR system is activated. This means that the interstage charges are ignited, in order to separate the first stage to the rest of the rocket. The first stage will then deploy its recovery parachute and attempt a landing. The other stages will continue with flight destruction by igniting the charges on the propellant tanks, as there is no recovery possibility for these stages.

Timer - The timer is the fail-safe mechanism of the FTS, as already mentioned above. In case no or an unknown tone is received, the timer starts a countdown. If in this timeframe tone 5 is received, the system will go back to monitoring. In case tones 1 and 5 are received, the charges are armed. In case nothing happens and the countdown ends, the charges are armed (not shown in the logic diagram) and the FD system is activated.

Important is to note that the TT, FD and VR systems will not be activated if the respective tones are received, without receiving the activation tones first. The only exception to this is when the fail-safe timer countdown reaches zero. Another important note is that the IRIG tones are sent automatically to the FTS receiver, but the RSO can also decide to do this manually, in case of some failure.

If the launch proceeds as expected, and there is no need to activate the FTS, the system will be safed. This means that the system is shut down so that the charges cannot be ignited. The subsystem itself will be placed on the first stage, as it will only be used for critical failures during the first phase of the launch. The charges are on the other hand located on every stage. Once a certain altitude is reached, it will be too dangerous to use the FTS since it will be unpredictable how the debris will scatter, and it will be safed. It will therefore not be a concern that after the first stage separation it will be impossible to detonate the charges, since the FTS computer is located on the first stage.

3.10. PAYLOAD INTEGRATION

It was determined from the market analysis that the launcher has to be able to carry several different kinds of payloads of minimum mass of 60 kg into orbit. These payloads are: a package of several CubeSats, one custom made small satellite or a combination of both. And additionally, if the current miniaturisation of CubeSats continues, the launcher should also be able to put a package of smaller Pico- or FemtoSats in orbit.
Sketches of these concepts can be seen in Figure 3.50. On the left a custom made satellite can be seen. In the middle an assembly of P-PODS that can carry a total of 14 3U CubeSats. The CubeSats will be stored in a P-POD, and once in orbit they are pushed out of their slot using a spring. On the right an impression is given on how to carry 136 PicoSats of 3 cm by 10 cm in orbit.
The left and middle options are viable possibilities at present time, the right one is more a possibility for the fu-

ture.

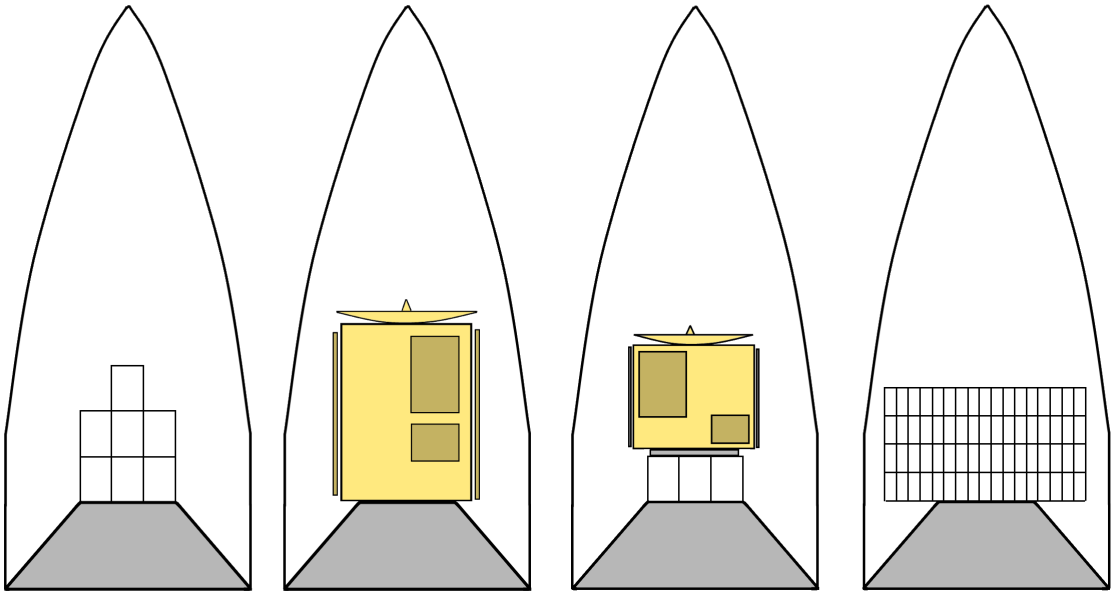

Figure 3.50: Four of the Possible Payload Configurations

3.10.1. PAYLOAD MASSES AND DIMENSIONS

In the P-POD assembly there are 14 3U CubeSat slots available. This means that a 1Ux3U CubeSat can be placed in one slot but also 3 times a 1Ux1U etc. The average mass per slot should be not higher than 4.29 kg, but the mass per slot can be determined on a mission to mission basis, i.e a few slots carry less and others more.
For the custom made small satellite the minimum mass is 60 kg, but the maximum depends on the orbit characteristics, see Section 3.1. The maximum dimensions are determined by available volume in the nosecone, which can be seen in Figure 3.51.
On a mission to mission basis it can also be determined to launch a few CubeSat in their P-PODS and a (smaller) custom made satellite together. Then a separation mechanism should be added on top of the P-POD assembly where the satellite will be placed.

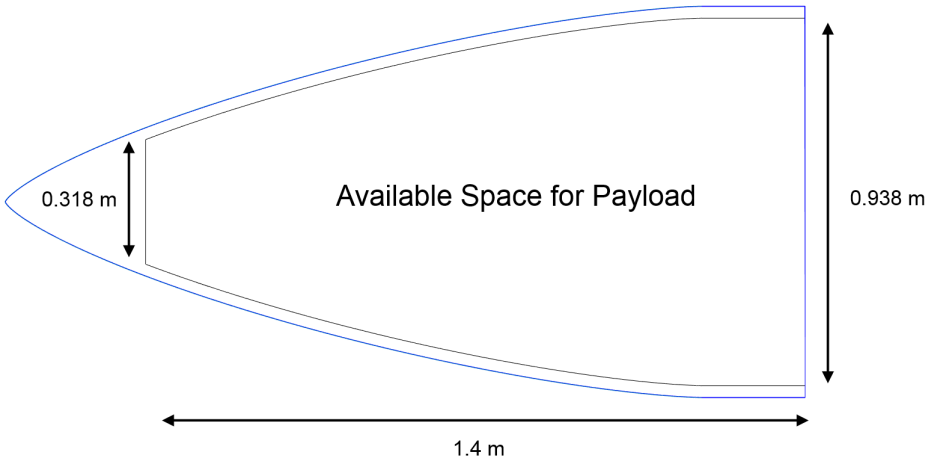

Figure 3.51: Available Space for a Custom Made Satellite

3.10.2. CUBESAT ORBIT INJECTION

To make sure the third stage keeps its orbit during CubeSat deployment, two CubeSats of the same mass have to ejected from opposite P-PODS at the same time, hence the lay out of the P-POD assembly. This means that it should be determined for every mission which slot is occupied by which CubeSat.

3.10.3. PAYLOAD ADAPTER

To ease payload integration all payloads will be placed on the same payload adapter ring. This ring has a base of 1 meter diameter and a top diameter of 40 cm. On this top part the payload or P-POD assembly, including separation system if required, can be mounted.

3.11. DESIGN PROCESS

In this section the design process of the launcher will be discussed in Section 3.11.1 and the applied optimisation in Section 3.11.2

3.11.1. ITERATIVE DESIGN PROCESS

In Figure 3.52 a simplified model of the iterative design process can be seen. The governing equation of every block are described in the above sections in this chapter. Then the outputs of those programs are always inputs for other programs. In short: everything depends on everything. This makes optimisation of the rocket a complex and time expensive process. The main optimisation that occurred was changing the ΔV contribution of stages to achieve a lower total mass, which will be described in the next section.

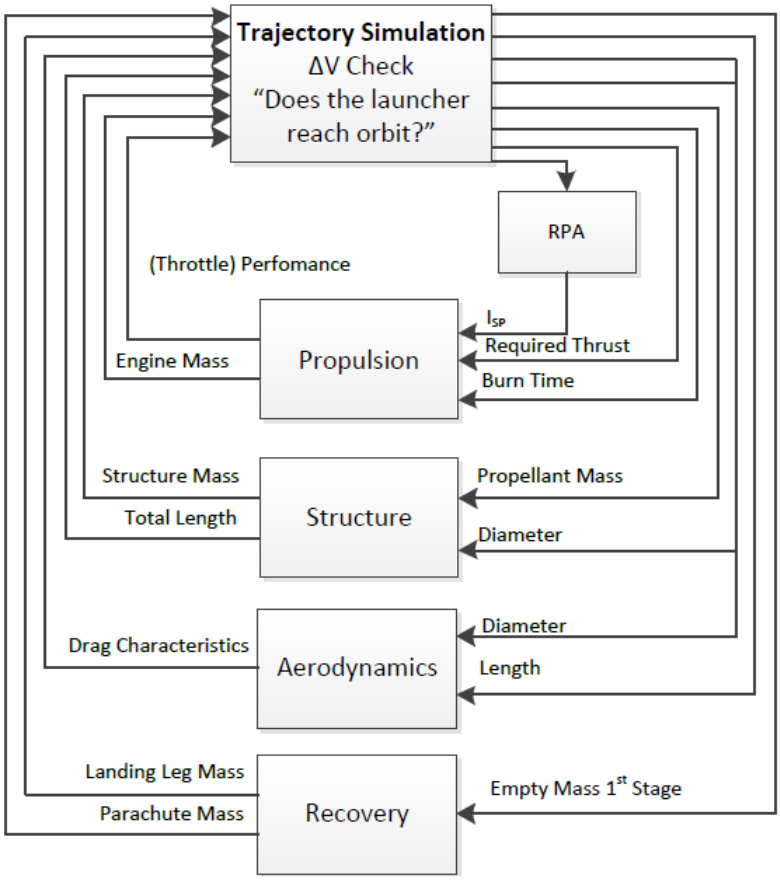

Figure 3.52: A simplified flow chart of the iterative process to determine the launcher performance

3.11.2. OPTIMISATION WITH RELATIVE DELTA V CONTRIBUTION

ΔV contribution per stage is varied to investigate the effect on the total rocket mass. A coefficient matrix is devised in Table 3.31 to cover all possible combinations of ΔV variation. The scaling factor increases or decreases the stages by a factor of 0.25,0.33, 0.4 or 0.5. Table 3.32 is the result of increasing or decreasing the stage contributions by 0.33. For example, in row 2 of the Table 3.32, stage 1 contributes 33% more than stage 2 or 3. For each scaling factor the total launcher mass is then recorded in Table 3.33, while keeping the total ΔV constant. The lowest three ratios are further investigated for other scaling factors, it is shown that the larger a difference the stage differs from each other, the lower the mass. Also the optimum configuration is given when the ratio of stage 3 provides 50% of the total ΔV and stage 1 provides 50% of the ΔV of stage 2. Giving the ΔV ratio of 1/2/3 for stages 1,2 and 3 coincidentally. This optimum is shown not to change depending on scaling factor.

The mass of 8951 kg is the optimum baseline for the launcher and the inclusion of the boostback calculations is based on this ΔV configuration. From here, the target ΔV is then varied to find the optimum mass configuration from the iteration process.

Table 3.31: Coefficient Matrix

Coefficient Matrix		
1	2	3
0	0	0
1	0	0
0	1	0
0	0	1
-1	0	0
0	-1	0
0	0	-1
-1	0	1
-1	1	0
0	-1	1
0	1	-1
1	-1	0
1	0	-1

Table 3.32: Stage ΔV Ratio

Stage ΔV Contribution		
1	2	3
0.3333	0.3333	0.3333
0.3994	0.3003	0.3003
0.3003	0.3994	0.3003
0.3003	0.3003	0.3994
0.2509	0.3745	0.3745
0.3745	0.2509	0.3745
0.3745	0.3745	0.2509
0.2233	0.3333	0.4433
0.2233	0.4433	0.3333
0.3333	0.2233	0.4433
0.3333	0.4433	0.2233
0.4433	0.2233	0.3333
0.4433	0.3333	0.2233

Table 3.33: Launcher Mass with Varying Scaling Factors

Scaling Factors / No Boostback			
0.25	0.33	0.45	0.5
	13208		
	16007		
	12465		
	12040		
11496	10995	10621	10100
	14589		
	15234		
10877	10336	9970	**8951**
11198	10752	10465	10136
	12983		
	14061		
	15097		
	14599		

3.12. LAYOUT

In this section the layout of the rocket is depicted. Firstly the overall rocket system is shown, after which the payload integration and recovery system layout are shown. After that, a mass budget and a hardware diagram are given.

3.12.1. ROCKET LAYOUT

The 18 m high and 1 m wide rocket can be seen in Figures 3.53 and 3.54, which give both a schematic overview and conceptual impression. The internal layout can been seen, with the fuel tanks, nozzles, and payload integration.

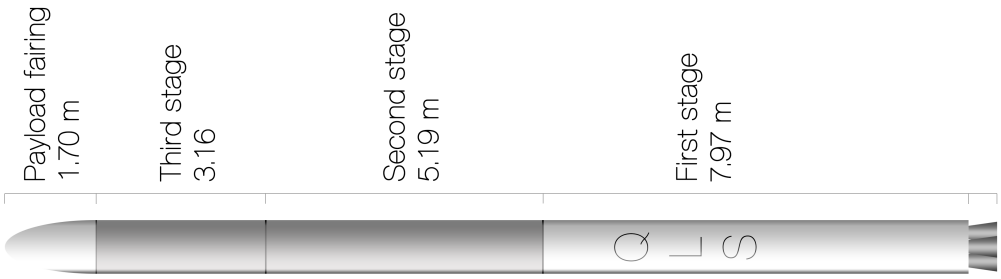

Figure 3.53: Rocket Schematic

3.12.2. PAYLOAD INTEGRATION AND DEPLOYMENT

The Quantum launch system has a payload adapter in the form of a 45 degrees circular prism. In this way, multiple type of payloads can be allocated in the payload bay under the nosecone. The payload can either consist solely out of multiple nano-satellites, a small micro satellite or a combination of both. Figure 3.55 displays how the payload is integrated under the nosecone. Figure 3.56 shows a illustration of deployment of multiple 1U and 3U CubeSats. The cutouts indicate how they are integrated in their ISIPODS[13]. A detailed view can be seen in fig 3.57.

[13] CubeSat housing prior to deployment

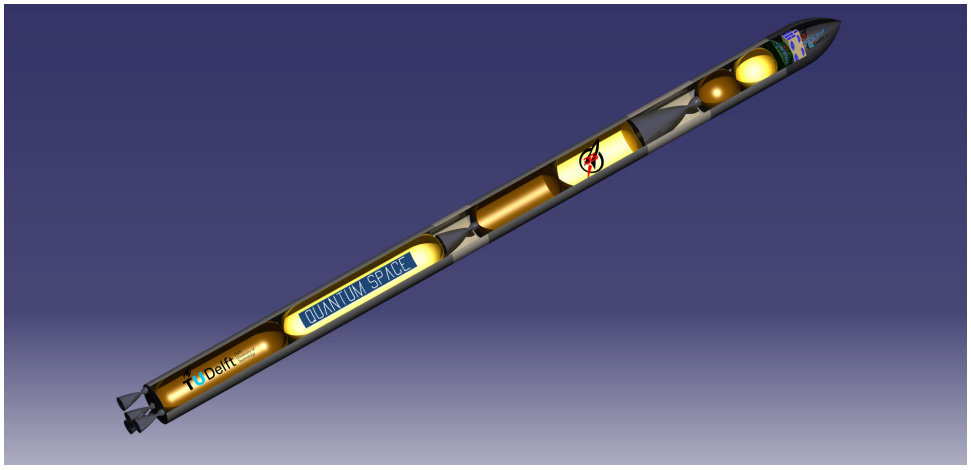

Figure 3.54: Graphical Illustration Rocket

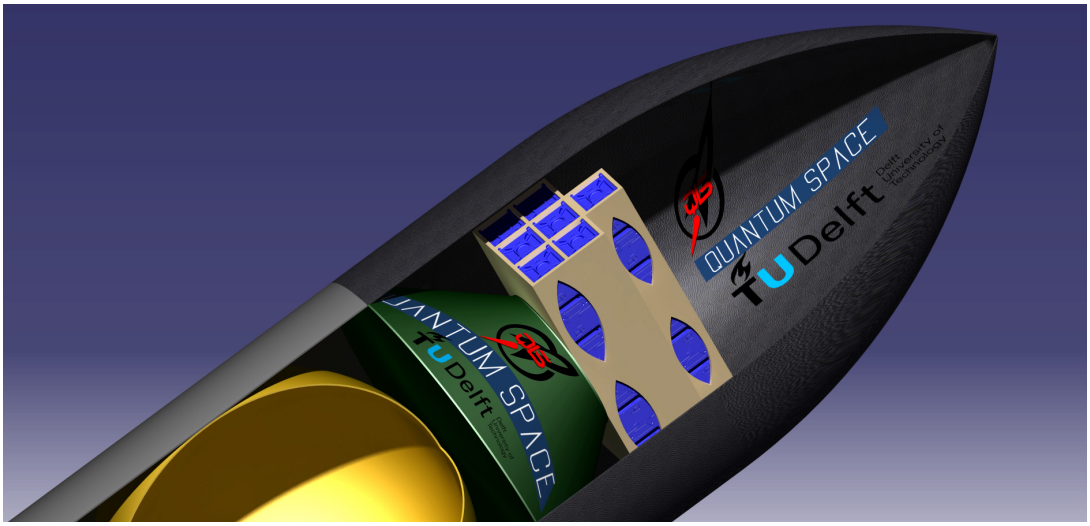

Figure 3.55: Integrated Payload under Nosecone

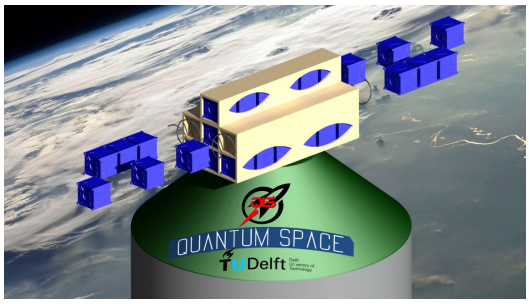

Figure 3.56: Deployment of Multiple CubeSats

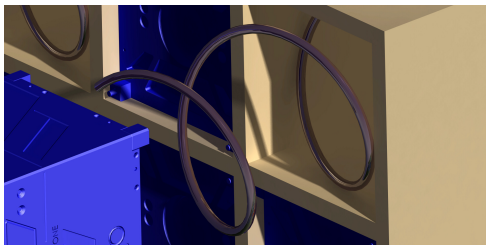

Figure 3.57: Detail View Deployment

3.12.3. RECOVERY SYSTEM

The drogue chute and the ram air parafoil are shown in Figures 3.58 and 3.59.

3.12.4. MASS BUDGET

In Table 3.34 the mass budget of the whole system is shown. All the masses for the different subsystems are shown, and added up to give the total mass per stage. The total rocket mass will be 9202 kg.

3.12.5. HARDWARE BLOCK DIAGRAM

The interfaces between all hardware in the QLS is shown in Figure 3.60.

Figure 3.58: Graphical Illustration Drogue Chute

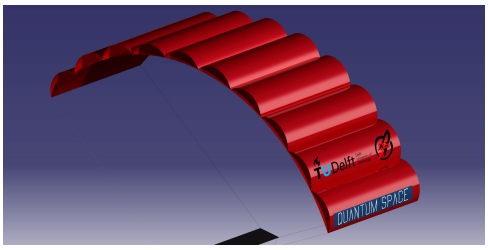

Figure 3.59: Graphical Illustration Ram Air Parafoil

Table 3.34: Mass budget

	Stage 1	Stage 2	Stage 3
Structure	471	203	87
Propellant	4212	2461	826
Engine	503	143	66
ADCS	2	-	3
EPS	5	-	5
Communication	1	-	1
Recovery	112	-	-
Payload	-	-	60
PPOD	-	-	28
Payload adapter	-	-	2
Total	**5306**	**2807**	**1078**

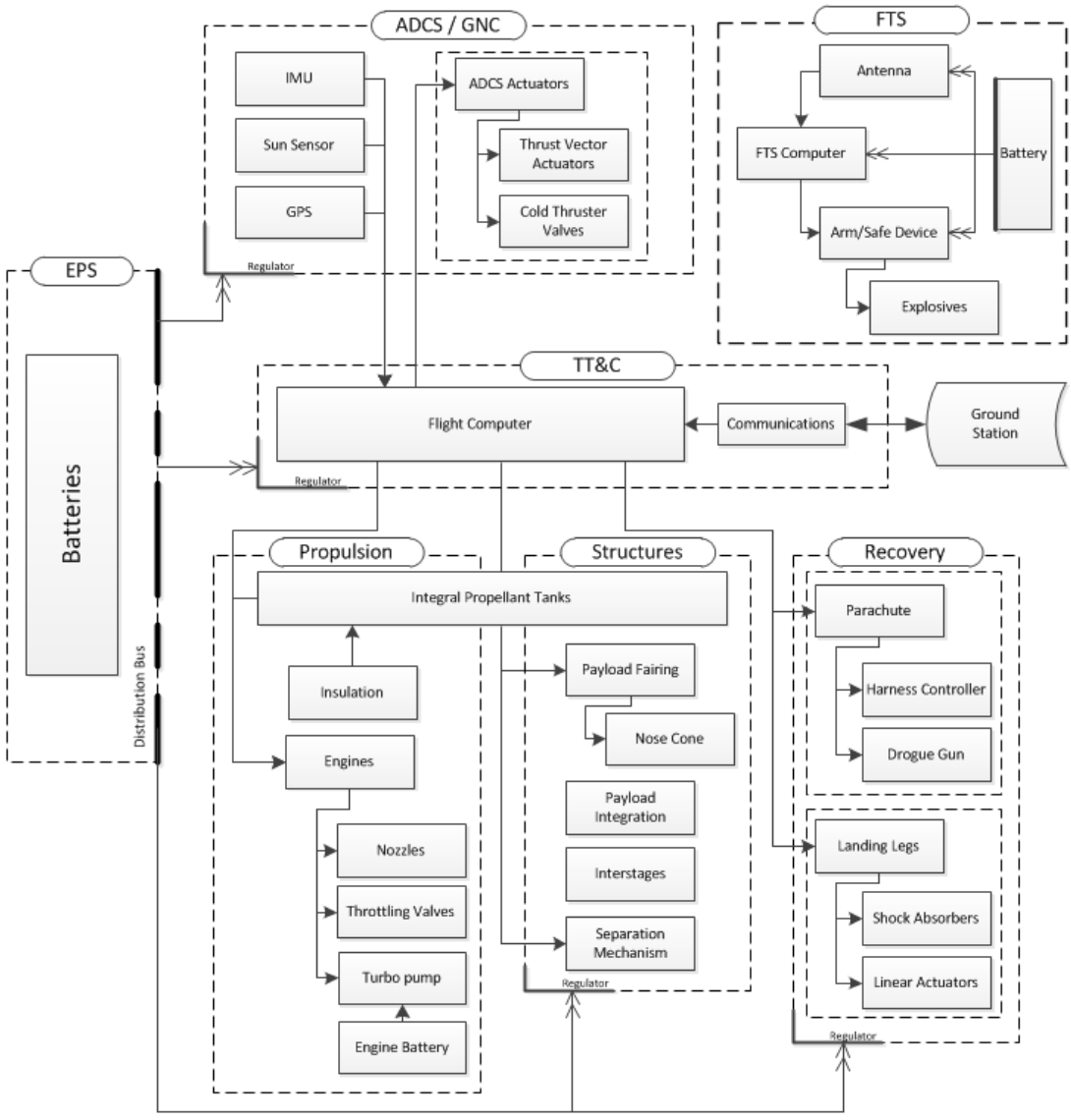

Figure 3.60: Hardware Block Diagram

4

Design Analysis

In this chapter an analysis will be performed in order to check the determined design. First all the subsystems will be verified and validated in Section 4.1. Then it will be checked whether the design meets all the requirements in Section 4.4 and finally a sensitivity analysis will be performed in Section 4.5.

4.1. Verification and Validation

In this chapter the verification and validation process is discussed. First the V&V method for the numerical model is explained in section 4.2 and then the models will be verified in the sections after it. The requirementst verification and validation is discussed in Section 4.3.

4.2. Numerical Model Verification and Validation

Built numerical models have to be verified and validated to determine and prove the credibility of the model. Verification determines if a computational model accurately represents the underlying mathematical model and its solution. Validation is the process of determining the degree to which a model is an accurate representation of the real world from the perspective of the intended uses of the model [47] All models built in the DSE project will have to be verified [48], validation is not required but definitely recommended.

4.2.1. Verification

Verification of numerical models consists of two parts: code verification and calculation verification. Code verifications makes sure that there are no programming errors in the code, such a syntax errors or loops that are not working [47]. Tools that can be used for this are the compiler and unit tests on small blocks of code.
Calculation verification happens ones the code verification has been completed. Its purpose is to determine whether the numerical model does not contain any errors [47]. Tools that can be used for this are solving a simplified model or use an analytical solution and compare the results. If these results are within the beforehand set error bound the program passes the verification. Furthermore a convergence test can be used.
It might be possible that these errors cancel each other out for a specific situation but not for others. So it is advisable to apply code and calculation verification to individual blocks of code, so called unit testing.

4.2.2. Validation

The goal of validation is to determine the predictive capability of a computational model for its intended use. This is done by comparing the results from the numerical code to actual to actual observations [47]. These results can be obtained from experiments or from reference data. Since experiments are costly and time consuming, they will not be used in the DSE. If, however, data on already performed experiments are found these could be used to validate the program. Secondly data from actual flight operations can be used. Finally simulations from more advanced and already validated models could be used.

In the next sections the used numerical models will be verified and validated.

4.2.3. Verification of Flight Dynamics Tools

For Flight Dynamics two tools were developed that form the basis for the iteration process.

Staging Analysis Tool

The SAT uses ΔV calculations that can easily be replicated by hand, which allowed for easy verification of the code.

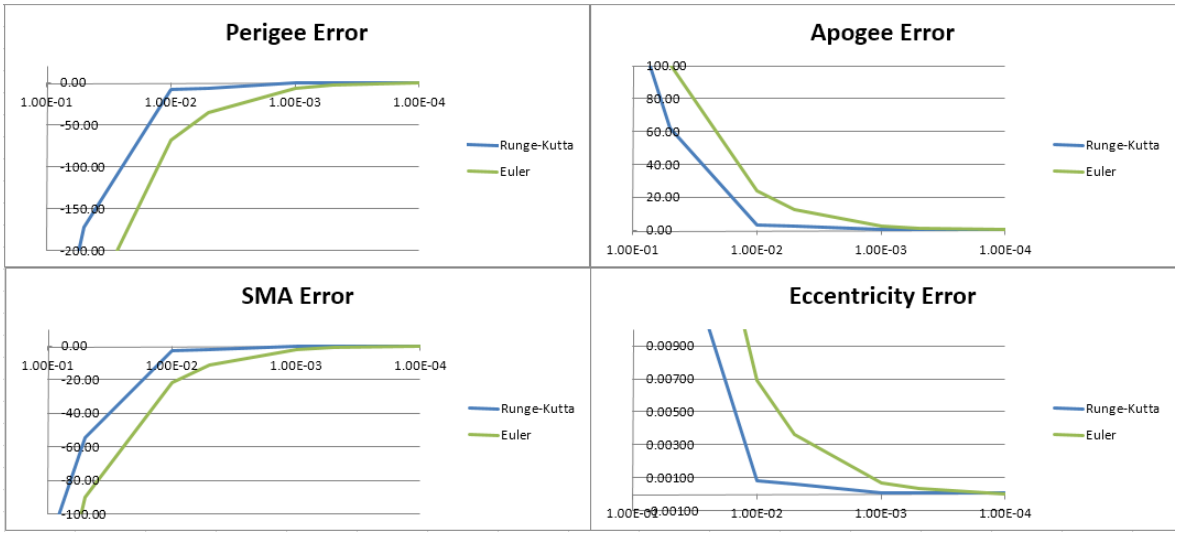

Figure 4.1: Convergence of Interpolation Errors: Runge-Kutta vs Euler

TRAJECTORY SIMULATION TOOL

The trajectory simulation tool was verified in numerous ways. The mass profile could easily be shown to be correct, as the mass of the following stage is known in advance, and it can be checked that the code progresses from the start-of-stage mass through the end-of-stage mass reached the correct value for the following stage. For gravity and drag calculations several points were taken for which the gravity and drag could be compared to manual calculations showing both the direction and magnitude were accurate.

One major criterion used for verification was the total ΔV from the launch trajectory, which was calculated as the sum of the losses due to drag, the losses due to gravity and the final total velocity. This value was compared to the projected ΔV from the SAT, which matched to within one metre per second.

Validation of the model progression was possible by comparing an object placed in initial conditions for which the Kepler orbit elements were known, and comparing the model progression to the expected orbit based on widely used calculations for Kepler orbits. This model was then further improved by moving from the Euler method to a Runge-Kutta (RK4) method for solving the second order differential equation. These two methods could then be compared to each other for varying timesteps to show their convergeance behaviour. This was done by designing a launcher trajectory for a high accuracy, i.e. small timestep RK4, trajectory simulation. Next the same launch conditions were run for varying time-steps to show the gradual deviation from optimal performance. There was no need to change the design between the RK4 method and the Euler method, because it was observed that for small enough time-step they were nearly identical in outcome. The resulting graphs are shown in Figure 4.1

4.2.4. VERIFICATION OF ROCKET PROPULSION ANALYSIS

The developers of RPA have verified their own program and this verification is available on [1]. The verification focuses on four different aspects of the code: the equilibrium properties, liquid propulsion performance analysis, solid and hybrid propulsion performance analysis and finally thermal analysis.
The equilibrium properties have been verified using NASA's Chemical Equilibrium with Applications 2 (CEA2), a widely used and validated program. The maximum error between the two programs is 0.002% [2].
The performance of liquids and solids and hybrids rockets is validated by comparing RPA results with several existing rocket engines. The maximum error found is 2% for liquids and 1.7% for hybrids and solids.
The verification of the thermal analysis tool of RPA is not needed since no thermal analysis is performed in this project.

Now RPA is verified, it can be used to verify the propulsion performance calculations, this will done in the next section.

4.2.5. VERIFICATION OF THE PROPULSION CALCULATIONS

The propulsion code calculates thrust for different ambient pressures (i.e altitudes) and throttle values. RPA can do this as well, so this is an easy way to verify this part of the code. The error in the thrust calculations can be seen in

[1] http://www.propulsion-analysis.com/verification.htm, visited on: 20-01-2016
[2] http://www.propulsion-analysis.com/verification_1.htm, visited on: 20-01-2016

Table 4.1. It can be seen that the maximum error is 0.13%. This specific test also confirms the correct use of the other equations used in the propulsion code, mainly Equation (3.5).

Table 4.1: Comparison between the calculated thrust in [N] with RPA for different ambient pressures

P_a [Pa]	RPA	Calculated	Error [%]
101325	5244	5256	0.24
3749	6758	6750	0.12
1196	6798	6789	0.13
821	6804	6795	0.13

The comparison in throttling for one engine can be seen in Figure 4.2. The maximum error occurs at a throttle value of 0.8 and equals 12.1%. The errors are caused by the assumption that T_c, M_w, γ and O/F ratio are constant. This error is accepted since the effort to implement varying gas properties would be high. How the properties vary can be seen in Table 4.2.

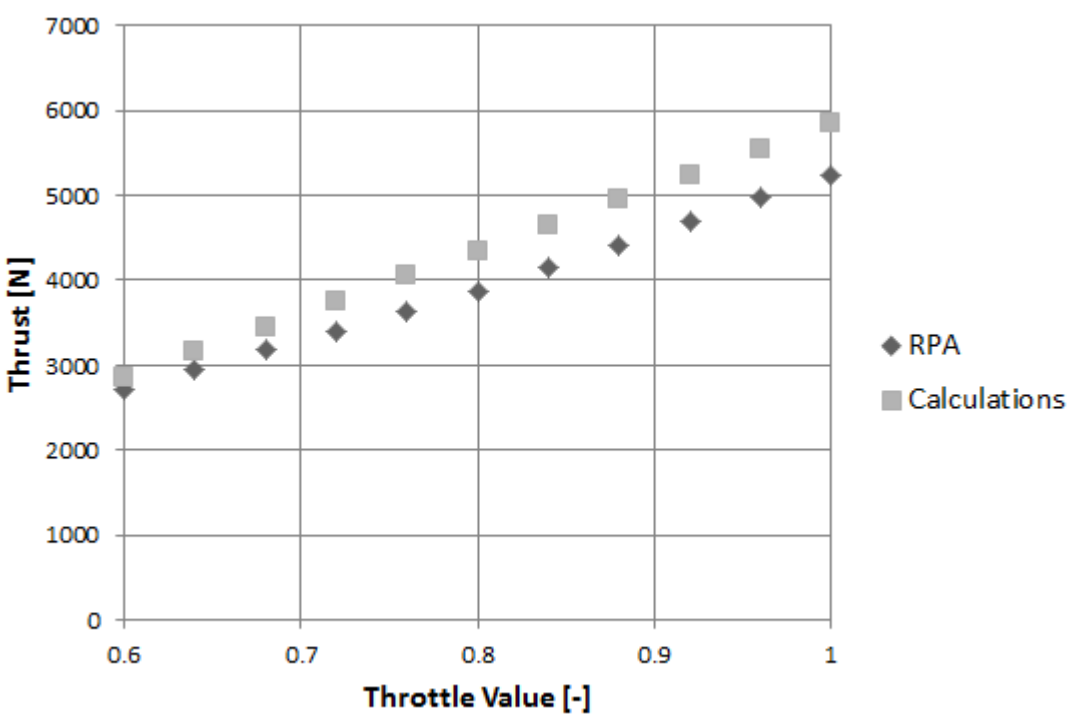

Figure 4.2: Comparison between calculated thrust and thrust given by RPA

Table 4.2: The maximum differences in gas properties for different throttle values

	Throttle value	$P_c[bar]$	γ	$T_c[K]$	Optimum O/F	Γ
	0.6	48	1.7400	3496	3.3535	0.736472979
	1	80	1.1736	3564	3.3581	0.643354053
Difference [%]			32.6	1.95	0.14	12.6

4.2.6. ADCS VERIFICATION AND VALIDATION

The MATLAB script for ADCS is verified by comparing the numerical determined eigenvalues for pitch stability with analyitically calculated ones. The program is verified by checking if it outputs the expected eigenvalues with the calculated eigenvalues. The characteristic equation of the state-space system (3.48) is:

$$\begin{aligned} 0 &= A\lambda^2 + B\lambda + C \\ A &= 1 \\ B &= -\tfrac{1}{I_{yy}}(C_{m_q} + C_{m_{\dot{\alpha}}})\bar{q}_0 Sd \\ C &= -\tfrac{1}{I_{yy}}\bar{q}_0 SdC_{m_\alpha} \end{aligned} \tag{4.1}$$

The analytically determined eigenvalues for the maximum pressure are are: $\lambda_1 = -0.2816$ and $\lambda_2 = 0.1353$. And the computed eigenvalues are: $\lambda_1 = -0.2816$ and $\lambda_2 = 0.1353$. These are excactly the same. The MATLAB tool has thus been verified for correct use of the equations. The mass moment of inertia I_{yy} calculation is verified by checking if it produces correct results in simple input cases. For zero mass, the result is zero. For unit inputs of 1 kg and 1 meter radius, the result corresponds with manually calculated values. The stability derivatives have been obtained by Missile DATCOM (see Section 3.4. The Missile DATCOM methods have been validated with wind tunnel data in the case of body-alone calculations[24].

The program is linearised on an angle of attack of zero degrees, and without disturbance input, the rocket should stay stable and show no motion. This input of zero angle of attack is verified and the program shows indeed that the rocket will not move in pitch and yaw direction for this case. The program was also run with a gain of 0, to verify the pitch/yaw motion will not go back to initial state and will deviate continuously from its initial state. Next to that, different initial angles were given as input, to check if the disturbances grow harder for greater disturbance angles, which is expected.

4.2.7. PARACHUTE VERIFICATION AND VALIDATION

The parachute design software has been verified by comparing it to other parachute design calculations, taken from [35]. The source gives two example parachutes for a 217 kg payload and a 1808 kg payload. The source uses $\alpha = 2.9°$, $AR = 2.5$, $\frac{L}{D} = 4.5$ and $v = 13.9\ m/s$. These values are used as inputs in the self-developed code. The results are shown in Table 4.3.

Table 4.3: Verification of the Parachute software

Input	[35]	QLS	Error
C_L	0.5	0.5	0%
C_D	0,06	0,11	46%
Area (217 kg)	36 m^2	35,00 m^2	3%
Area (1808 kg)	300 m^2	291,56 m^2	3%

The overall error in the final area of the chutes is very small and due to the differences in C_D. This error is quite large. The C_D value is depending on a lot of factors from a lot of parts of the parachute. The chute itself, the lines and the payload contribute to the total C_D. Regretfully, the source [35] does not specify their C_D values, so an exact answer to this divergence can not be given.

The total parachute concept can actually only be compared with the recovery system of NASA's X-38 as that is the only large controllable parachute ever been designed [49]. The X-38 lands with the same speed as the empty QLS first stage but weighs more (about 6500 kg), The total chute area of the X-38 is about 600 m^2. This is rather small compared to QLS' parachute area, which 507m^2. One of the reasons is that the X-38 has a lifting body, while the QLS empty first stage is dead weight. Another reason for the difference is that the QLS chute is designed to be larger on purpose to be able to have a large manoeuvrable radius for the controlled landing.

4.2.8. SHOCK ABSORBER VERIFICATION & VALIDATION

In order verify the right implementation of the governing equations, the example values of the book [38], which gives the equations, on page 90-93 will be used to see if the same results are obtained. Using Equations (3.69), (3.70), (3.71) and (3.72) the result that can be seen in Table 4.4 are obtained. Once the calculated values are converted into inches, pound and inch-pound it can be seen that the obtained values are exactly the same as the example of the book. Thus the implementation of the equations is done correctly.

Table 4.4: Verification of the Shock Absorber

Kinetic energy [J]	126.2
Stroke [m]	0.18
Shock Force [N]	800.7
Bore Area [m^2]	$2.90 \cdot 10^3$

In order to validate the properties of shock absorber, it will be compared with commercially available shock absorbers on the market. The Automation Control Equipment (ACE) Company is well recognised as the global leader in industrial absorption technology worldwide. On their website shock absorber calculation software can be downloaded [3]. Using this software the QLS shock absorber will be validated. Using the model "Mass lowered at controlled

[3] http://ace-ace.com/wEnglisch/pages/Support/berechnungsprogramm.php, visited on: 10-01-2

speed", which is similar to QLS constant approach velocity and input values according Table 4.5. After choosing the option "calculate propelling force", the Shock force can be calculated. This will give a shock force of 51602 N, which is 363 N more than QLS shock force. So there is an error of 0.7%. This means yhat the QLS shock absorber performance is estimated rather precise.

Table 4.5: Validation of the Shock Absorber

Inputs	Values
Maximum mass [kg]	1045.5
Velocity at time of impact [m/s]	5
Cycles per hour	1
Number of sock absorber	1
peak shock pressure [bar]	138
Piston diameter [m]	0.069

4.2.9. STRUCTURES VERIFICATION & VALIDATION

In order to verify the software program that sizes the propellant tanks and estimates the mass of the structure and the length of the rocket, all the inputs are set to zero one by one. By doing this, the mass of the calculated structures should become zero as well.
When the yield stress is put to zero, the thicknesses become infinite and the program blows up, as expected. If the different densities (oxidiser, fuel and material density) is set to zero, the mass of the structure components all become zero, as expected. If the Young's modulus is set to zero, all the stresses and masses become zero, again, as expected. In case the internal tank pressure is set to zero, the internal pressure is no longer the critical failure mode and the failure thickness becomes extremely small, which is as expected since the other failure modes were not as critical as the internal pressure failure mode. As a last check the calculated thicknesses are overwritten by a value of zero to see what happens. As a consequence, the structure fails in all modes, which is as expected. The verification of the software is now complete.
Furthermore, the results are compared to reference data from similar existing rockets in order to validate these results. It turns out the length and the mass are close to the regression line generated by reference data, which means the result is completely verified and validated.

4.3. VERIFICATION & VALIDATION OF THE REQUIREMENTS

In systems engineering the definitions or verification and validation for requirements are as follows. Verification: proof of compliance with design solution specifications and descriptive documents, i.e. it meets the requirements. Validation: proof that the product accomplishes the intended purpose based on stakeholder expectations [50]. NASA uses the following methods to verify the requirements of the Space Launch System: analysis, inspection, demonstration, test, validation of record (VoR), similarity or any combination of these methods [50].
Testing is always preferred when it is practical, cost effective and safe [50]. So for the V&V on the requirements, first testing or demonstration is considered. If this is not feasible due to budget constraint, practicality or effectiveness the other methods are considered.

4.3.1. MISSION REQUIREMENTS

Most of the mission requirements have to be verified using analysis, because the other option, demonstration, is too costly. However the first (commercial) launch can also demonstrate the achievement of the requirements. So this means that verification does not stop at lift off of the first launch but continues during (the beginning of) the vehicles operational life. But before the first flight, analysis has to be used. The analysis methods are described below.
Requirement **QR-MIS-010** until **QR-MIS-030** and **QR-MIS-050** can be analysed at this stage of the project with the self-developed trajectory simulation tool. It was found that all these four requirements are met. **QR-MIS-040** will have to be analysed in a later stage of the project. However, the preliminary design is finished on time so it is likely that this requirement will be met.

QR-MIS-060 can be definitely analysed in the future after several launches. Then a good estimation of the reliability can be determined. However it is recommended to find ways to analyse the launcher during the whole design process to see what the estimated reliability is.

4.3.2. ASTRODYNAMICS REQUIREMENTS

All astrodynamics requirements (**QR-AST-010** to **QR-AST-04 0**) can be verified by using the self-developed trajectory simulation tool, so analysis. All parameters of the rocket are input for this program and then the performance of the

rocket is an output.

4.3.3. COMMUNICATIONS

The communication requirements can be verified by testing the communication system in a relevant environment. A mockup of the rocket can be created and then the power of the signal can be determined and possible occurring interferences can be discovered. Furthermore it can be checked if the systems do what they should do, a 'it either works or it does not work test'. This data can then also be used to analyse the performance during the flight. It is also possible to analyse what happens during fight if some systems stop working.

4.3.4. FLIGHT TERMINATION SYSTEM

The FTS requirements can be verified using analysis. There should be looked closely at the design and flow of the FTS system. From this it can be determined that it has no activation at false positives (**QR-FTS-020**) and that it works as independent system (**QR-FTS-030**). **QR-FTS-010** can also be tested by similarity testing. The way to do this is to build a FTS system and activate it once, with relevant inputs. So for example, power of the signal should correspond with the minimum power it will have during flight.

4.3.5. MTI REQUIREMENTS

In this stage of the project **QR-MTI-010** and **QR-MTI-030** can be analysed, by having a close look at the manufacturing process. During the actual process it should be continuously inspected. Also **QR-MTI-020** can be inspected by having a look at the manufacturing process. **QR-MTI-040** and **QR-MTI-050** should also be inspected once production starts.

4.3.6. ELECTRICAL POWER SYSTEM

Requirement **QR-PWR-010** can be verified using inspection, just see if there is a system available that can store electrical energy. **QR-PWR-020** , **QR-PWR-030** and **QR-PWR-050** can be verified by demonstration on a test system and/or the actual flight version. For example before placing it on the launch pad. **QR-PWR-040** will have to be tested on a test model of the whole rocket. This means it will be an expensive and time consuming test and therefore it has to be combined with other tests. **QR-PWR-060** has to be verified by inspection of the system and then compare it with the safety regulations.

4.3.7. PROPULSION REQUIREMENTS

All propulsion requirements will be verified by testing, this is of such high importance that there is a separate test plan for it, see Section 7.2.3

4.3.8. STABILITY, CONTROL AND NAVIGATION REQUIREMENTS

Requirements **QR-SCN-010**, **QR-SCN-020**, **QR-SCN-040**, **QR-SCN-050** and **QR-SCN-060** can be verified using analysis of the control system. The whole control system can be modelled including better characteristics of the launcher (e.g. masses, inertia, drag, thrust etc.) and then see what the control system can achieve. **QR-SCN-030** can be verified by inspection.

4.3.9. STRUCTURE REQUIREMENTS

The structure of the rocket can be verified by (similarity) testing. This is of such a high importance that a separate test program is set up for it, see Section 7.2.6

4.3.10. SUSTAINABILITY REQUIREMENTS

Requirements **QR-SUS-010** can be verified using analysis to see what happens to the non recoverable stages. If they burn up in the atmosphere they contribute a minimum amount of pollution. If they do not burn up it should be analysed what happens then. If they quickly sink, then pollution is also minimal. Requirement **QR-SUS-020** can be verified by analysis with the trajectory simulation tool, and depends mainly on the altitude of the orbit.

4.3.11. RECOVERY REQUIREMENTS

The requirements of the recovery system can be verified by testing first the subcomponents and then later the whole system. A more elaborated test plan is set up for this, see Section 7.2.5

4.3.12. USER GUIDE REQUIREMENTS

All user manual requirements can be verified by inspection of said manual and see if these information is in there.

4.4. COMPLIANCE CHECKS

In the previous phase of the project, all requirements were listed. In Table 4.6 the compliance matrix is shown, which checks if the requirements are met. If the requirements are not met or partially met, comment has been given on what has to be done.

Requirement Code	Requirement	Compliance	Comment
QR-MIS-010	The minimum total payload that the launcher shall bring to the designated orbit is 10 kg	✓	Price per kg is cheaper when more payload is launched together.
QR-MIS-020	The launcher shall bring the payload into a circular orbit around Earth of 350 km altitude	✓	
QR-MIS-030	The launcher shall bring payload into orbit inclinations between 0° and 90°	✓	Rocket is designed for a polar orbit. A lower inclination can bring more payload into orbit.
QR-MIS-040	The first launch shall take place in 2021	-	Can not be verified until first launch is performed.
QR-MIS-050	The launch shall have a ground track over sea	✓	Rocket will land on launch platform.
QR-MIS-060	Launch success rate shall be 90% or higher	-	Cannot be said until some launches have been performed.
QR-MIS-090	The propellant system shall not exhaust toxic substances into the environment	✓	
QR-MIS-100	The first stage shall be recoverable without increasing cost	✓	First stage recovery will decrease production costs, but increases operational costs.
QR-MIS-110	The targeted price per launch shall be competitive with the current piggyback-launch cost of approximately $\$50,000/kg$	✓	
QR-MIS-120	A test program shall be set up per subsystem	✓	For the propulsion and recovery subsystem dedicated test programs are set up.
QR-MIS-130	The mission shall be unmanned	✓	
QR-AST-010	The variation in orbit lifetime of the delivered payloads due to orbital injection shall be less than 30% of the variation due to the solar activity cycle	✓	
QR-AST-020	The error in ΔV that vehicle delivers shall be less than 5 m/s	✓	
QR-AST-030	The error in insertion altitude of the delivered payload shall be less than 1 km	✓	
QR-AST-040	The error in flight path angle shall be less than 0.25°	✓	
QR-COM-010	The communication system shall be able to receive signals throughout the entire mission from the ground station	✓	FTS can be controlled from ground
QR-COM-020	The communication system shall be able to send signals throughout the entire mission to the ground station	✓	
QR-COM-030	The communication system shall be able to store data throughout the entire mission	✓	
QR-COM-040	The communication system shall be able to handle signals throughout the entire mission	✓	
QR-COM-050	Communication components shall be flight-proven	✓	
QR-FTS-010	The FTS shall be able to abort the mission instantly	✓	
QR-FTS-020	The FTS shall make sure it is not activated in case of false positives	✓	
QR-FTS-030	The FTS shall function as an independent subsystem	✓	
QR-MTI-010	Waste resources shall be limited during the manufacturing process	✓	
QR-MTI-020	Manufacturing shall conform to industry safety standards	✓	
QR-MTI-030	Manufacturing shall not release toxic substances into the environment	✓	
QG-MTI-040	New possibilities to increase the sustainability of the manufacturing process should be explored continuously	✓	
QG-MTI-050	New possibilities to limit the waste of resources should be explored continuously	✓	
QR-PWR-010	The EPS shall incorporate an electrical storage capacity	✓	
QR-PWR-020	The EPS shall be able to be charged via an external power source	✓	
QR-PWR-030	The EPS shall distribute electrical energy over all the required subsystems	✓	
QR-PWR-040	The EPS shall not interfere with other subsystems and components	-	This will be verified in the testing campaign with an Electromagnetic Compatibility Test
QR-PWR-050	The EPS shall incorporate a monitoring system	✓	
QR-PWR-060	The EPS shall have a safe mode	✓	
QR-PWR-070	The EPS shall comply to the international electrical safety standards	✓	
QR-PRP-010	The propulsion system shall have a controlled ignition system	-	Not designed in this phase of the project
QR-PRP-020	The propulsion system shall provide a minimum ΔV of $9.3 km/s$	✓	
QR-PRP-030	The propulsion system shall store the required propellants	✓	
QR-PRP-040	The amount of fuel available shall be measurable	✓	
QR-PRP-050	The propulsion system design shall prevent risks due to leakages	✓	
QR-SCN-010	The control system shall point the vehicle at injection parallel to the required orbit of its payload up to an accuracy of 0.25 degrees	-	Actuators have not been designed yet
QR-SCN-020	The control system shall ensure stability during the entire flight	-	The feasibility of control has been proven in Section 3.5.2
QR-SCN-030	The control system shall control the stage separation	✓	
QR-SCN-040	ADCS shall ensure a deviation of maximum 100 m from predefined flight path	✓	
QR-SCN-050	ADCS shall update the vehicle's position with a frequency of 10 Hz	✓	
QR-SCN-060	ADCS shall have an attitude pointing accuracy of 0.25° for yaw and pitch	✓	
QR-STR-010	The launch system shall be structurally mountable to the launch platform	✓	
QR-STR-020	The structure of the launch system shall integrate the payload	✓	

Requirement Code	Requirement	Compliance	Comment
QR-STR-030	The structure shall protect the payload from the environment	✓	
QR-STR-040	The structure shall withstand mission profile vibrations	✓	
QR-STR-050	The structure shall withstand mission profile temperatures	✓	
QR-STR-060	The structure shall withstand mission profile loads	✓	
QR-STR-070	The structure shall accommodate communication signals	✓	
QR-REC-010	The recovery system shall land the first stage with a maximum velocity of 5 m/s	✓	
QR-REC-020	The recovery system shall land the first stage within 20 km of the launch site	✓	
QR-SUS-010	Stages that are non-recoverable shall prevent environmental pollution	✓	
QR-SUS-020	Launcher space debris shall not stay in orbit for more than 25 years	✓	Orbit of 350km is self-cleaning.
QR-USE-010	The user shall be provided with the vibration/acoustic loads that occur during launch	-	The user guide cannot be written before the system characteristics have been measured in the test campaign. The user guide will be written as soon as they can be quantified.
QR-USE-020	The user shall be provided with expected accelerations in longitudinal and lateral direction	-	”
QR-USE-030	The user shall be provided with a payload mass-range diagram	-	”
QR-USE-040	The user shall be provided with a payload mass-inclination diagram	-	”
QR-USE-050	The user shall be provided with the expected life time of the orbit	-	”
QR-USE-060	The user shall be provided with accuracies that can be achieved in orbit characteristics	-	”
QR-USE-070	The user shall be provided with mission profiles	-	”
QR-USE-080	The user shall be provided with maximum payload dimensions	-	”
QR-USE-090	The user shall be provided with available electrical interfaces on the launcher	-	”
QR-USE-100	The user shall be provided with a cost per payload mass for a launch	-	”
QR-USE-110	The user shall be provided with the launch operation schedule	-	”

4.5. SENSITIVITY ANALYSIS

The sensitivity analysis is performed by first varying key parameters for the design in Section 4.5.1 and inspecting the impact on achievable ΔV. Next the effect of a change in target ΔV will have on the total launcher mass is investigated in Section 4.5.2 and general conclusions are made in Section 4.5.3

4.5.1. VARIATION OF DESIGN PARAMETERS

Firstly three key design parameters are varied, and then the launch trajectory is varied to match the nominal value for injection angle and orbit altitude. The resulting launch will have a change in finally reached velocity upon injection, and these can be compared.

PAYLOAD MASS

For the payload mass variation it is taken to be from the absolute minimum, 0 kilograms payload, up until the payload where the total ΔV is within 500 metres per second of the nominal design. It is varied with steps of 10% of the nominal payload. Table 4.7 shows the resulting values.

TARGET ALTITUDE

For the target altitude a range is taken starting from a 310 kilometers, which is deemed minimal due to the very short orbital life at this altitude, and again up to the altitude where the total ΔV is within 500 metres per second of the nominal design. It is varied with steps of 20 kilometers of the nominal target altitude, as shown in Table 4.8.

Table 4.7: Change of Payload Versus Change in ΔV

Payload Mass	Delta ΔV
0	877.2
6	779.53
12	683.33
18	591.35
24	499.8
30	412.16
36	324.62
42	241.19
48	160.21
54	80.81
60	0
66	-72.3
72	-152.48
78	-224.3
84	-294.6
90	-366
96	-438.4

Table 4.8: Change of Target Altitude Versus Change in ΔV

Target Altitude	Delta ΔV
310	177.97
330	88.58
350	0
370	-90.89
390	-181.34
410	-280.93
430	-377.38
450	-475.95

TARGET INCLINATION

The change in inclination has an effect on the launcher because the launcher velocity at the start of the launch is equal to the rotational velocity of the earth. Due to this, a launch in the direction of the rotation of the earth would require less ΔV equal to the rotational velocity of the earth surface. For launches with a nonzero inclination the launcher must be launched to a apparent higher inclination orbit, as the added vectors of injection velocity and rotational velocity must give rise to the desired inclination. The difference in length of the actually required injection velocity and the normal orbital velocity can be both a gain and a loss, depending on the inclination of the target orbit. This effect is lessened when launching from a higher declination, as the earth rotational velocity is less at the surface of these launch locations. Simultaneously the available inclinations are reduced due to the need for the ground-track to pass over the launch site. The effect of inclination on ΔV is therefore calculated for a number of launch site declinations, and shown in Figure 4.3

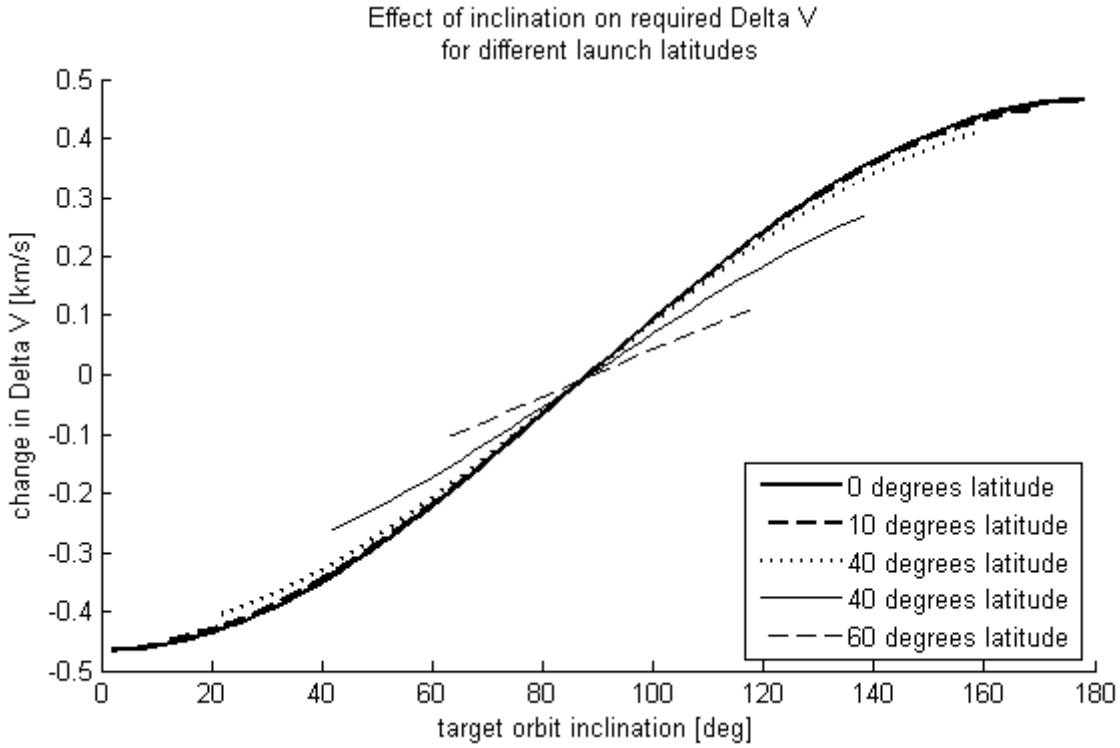

Figure 4.3: Effect of Inclination on ΔV

4.5.2. VARIATION OF TARGET ΔV

The ΔV is an over-arching parameter that determines the outlines of the launcher. An increase in target ΔV increases the total mass of the launcher but improves the structural efficiency. This shows that, indeed, larger launchers are able to achieve a higher structural efficiency. Due to the ratio of ΔV amongst the stages, it is shown that the structural efficiency of stage one has the highest propensity to vary with increasing or decreasing target ΔV. The results of varying target ΔV is summarised in Table 4.9.

Table 4.9: Design Dependency on Target ΔV

ΔV [$^m/_s$]	Total Mass [kg]	Stage Structural Efficiency			
		Total	1	2	3
9832	8089.77	0.1933	0.2245	0.1322	0.1992
9932	8350.99	0.1898	0.2202	0.1299	0.1964
10032	8622.94	0.1863	0.2160	0.1276	0.1936
10132	8906.69	0.1830	0.2119	0.1254	0.1909
10232	9201.74	0.1797	0.2079	0.1233	0.1882
10332	9509.07	0.1765	0.2039	0.1212	0.1886
10432	9829.98	0.1734	0.2001	0.1192	0.1830
10532	10163.83	0.1704	0.1964	0.1172	0.1804
10632	10511.91	0.1674	0.1928	0.1153	0.1779

4.5.3. CONCLUSION

The payload mass, inclination and target altitude are all dependant on the target ΔV. varying them after the design is completed has an impact on the final velocity upon injection. These impacts can be counteracted by an opposite change in one of the other parameters. In this way an interchange of the three parameters can be combined for a certain target ΔV. For instance, if the client should desire more payload mass, an exchange for inclination and target altitude can be made to still meet the target ΔV, i.e. a similar launcher size and configuration for a decreased mission altitude. This gives insight in both the sensitivity of these parameters, as well as showing possible avenues to resolve the issue. The payload mass, target altitude and target inclination are looked into.

Finally these changes in final velocity can also be compensated for by the target ΔV of the design itself. In this way it can be seen what the impact on the total mass would be if the increased payload made possible by up scaling the rocket, or if the inclination range is lowered how much rocket mass can be reduced.

5

PERFORMANCE ANALYSIS

This chapter gives more information about the performance of the launch system. Section 5.1 shows the results from running the final design through the Trajectory Simulation Tool. Section 5.2 summarises this information schematically in the mission profile of the launch system. Section 5.3 explains the emissions throughout the mission duration.

5.1. SIMULATION RESULTS

The results of the simulation programs are shown and discussed in this section.

5.1.1. MAIN LAUNCH TRAJECTORY

The resulting launcher configuration from the iteration is now simulated in the TST. Figure 5.1 shows the internal parameters of the launcher during the flight. It can be seen that the mass profile gradually decreases throughout engine operation and that at the end of a stage the stage construction mass is ejected. It is also visible that there is a considerable coast time between the second and third stage to allow for gravity to curve the trajectory more tangential to the earth surface, allowing for a more efficient third stage burn. A final key indication is the increase in first stage engine specific impulse, due to the large variation in atmospheric conditions. Due to this large increase, in combination with the reducing launcher mass, the g-limits are exceeded before stage separation occurs. To compensate the first stage engines are throttled down at this point, as can be seen in the mass flow profile, which directly affects the thrust and g-loads.

The next main outputs are the external parameters, shown in Figure 5.2, including the flightpath angle, the velocities, both tangential and radial to the Earth surface as well as total velocity, the altitude and the groundtrack. For a circular injection it is required that the radial velocity must go to zero at the end of the flight, which is confirmed in the graph. The total velocity, then equal to the tangential velocity, must be the circular orbital velocity at this altitude, which for the target orbit of 350 kilometers is calculated to be 7.69 kilometers per second. Other key points are the altitude and groundtrack profiles, which determin the requirements for several subsystems, e.g. communications system, for each stage.

The last main outputs of the TST are the losses, including drag and gravity, incurred during flight, shown in Figure 5.3. This information is crucial for the design process, as these can not be accurately estimated, unlike circular orbit velocity, while having a major impact on the design ΔV requirements. They allow for tuning of the design to the optimum combination of losses and stage ΔV contributions.

5.1.2. BOOST BACK TRAJECTORY

The second set of figures collects the same data during the boost back manoeuvre of the first stage. The actual return trajectory of the manoeuvre is shown in Figure 5.4. This shows the return trajectory passing up and above the launch trajectory, and landing within 300 metres of the launch site. The data recorded during this simulation is shown in Figures 5.5 and 5.6, which are internal and external parameters respectively. Most relevant to the internal parameters is the large mass-drop, constituting the second and third stage 'dropped' by the returning first stage, a separate coast time, and the g-loads. The high g-loads can be sustained, because the stage is no longer carrying the upper stages, and only needs to carry internal loads. The most relevant external parameters are the altitude, the ground track, and the tangential velocity.

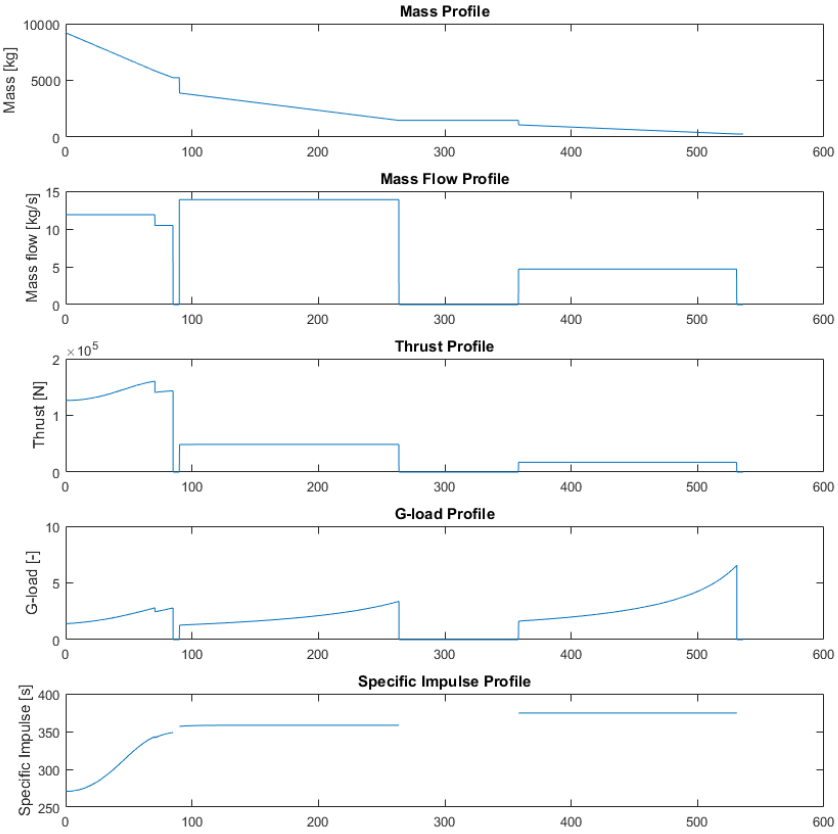

Figure 5.1: Mission Simulation Internal Parameters, including Mass, Mass Flow, Thrust

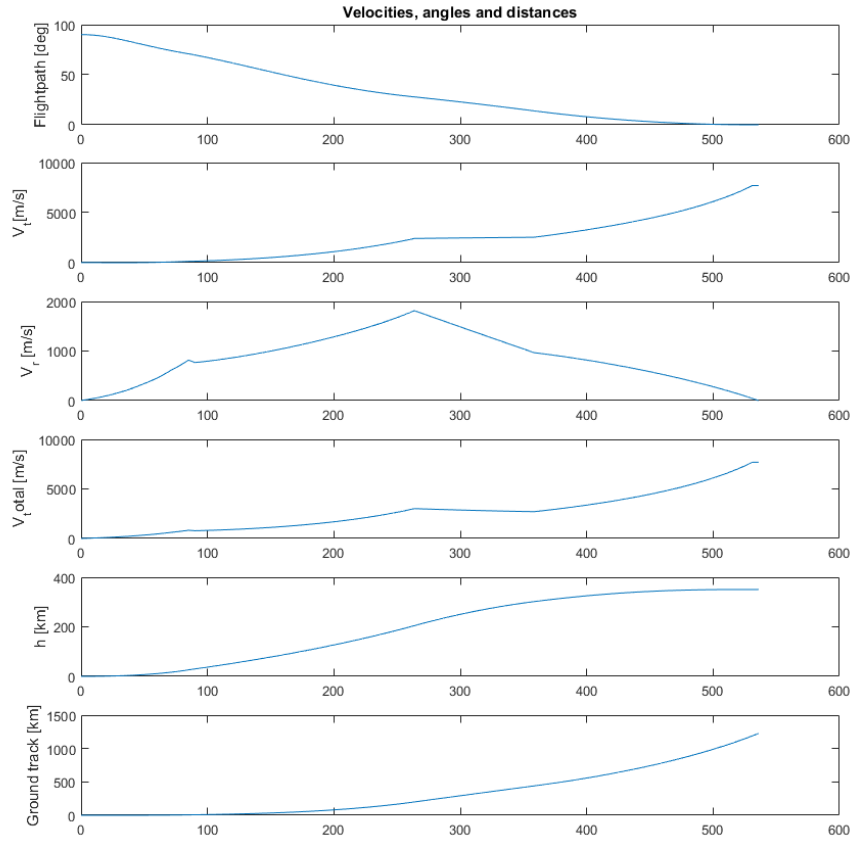

Figure 5.2: Mission Simulation Internal Parameters, Including Flight Path Angle, Velocities, Altitude, and Ground Track

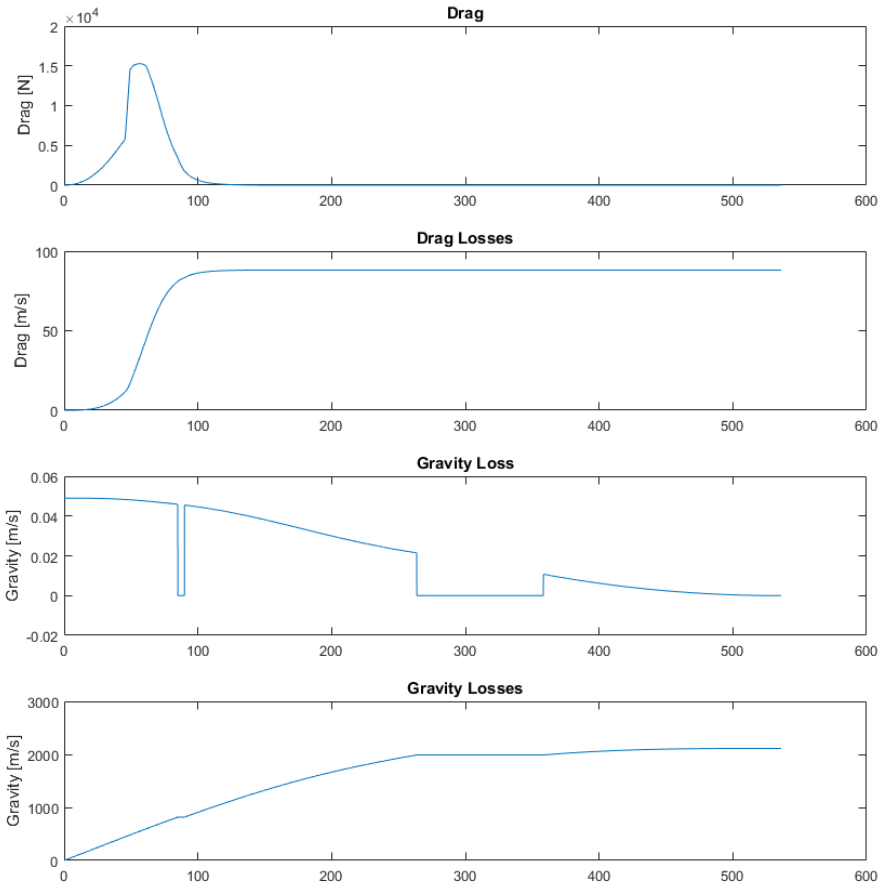

Figure 5.3: Mission Losses Simulation

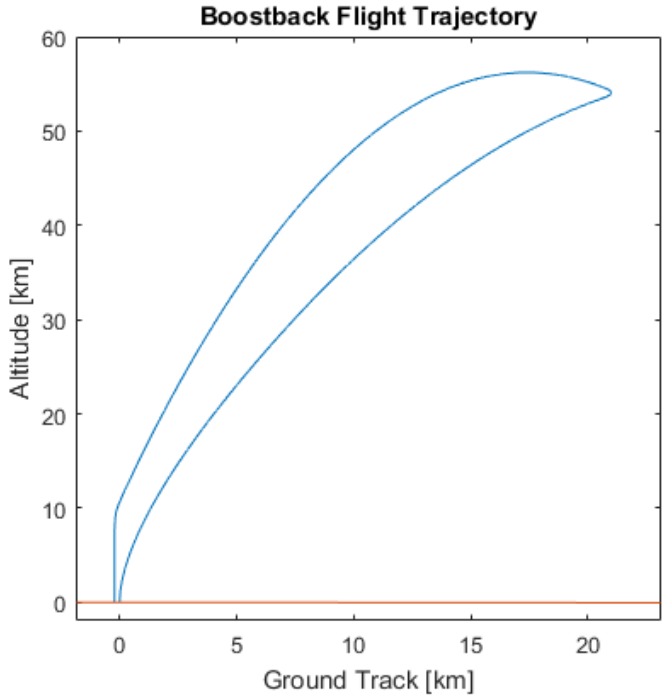

Figure 5.4: Boostback Trajectory Simulation

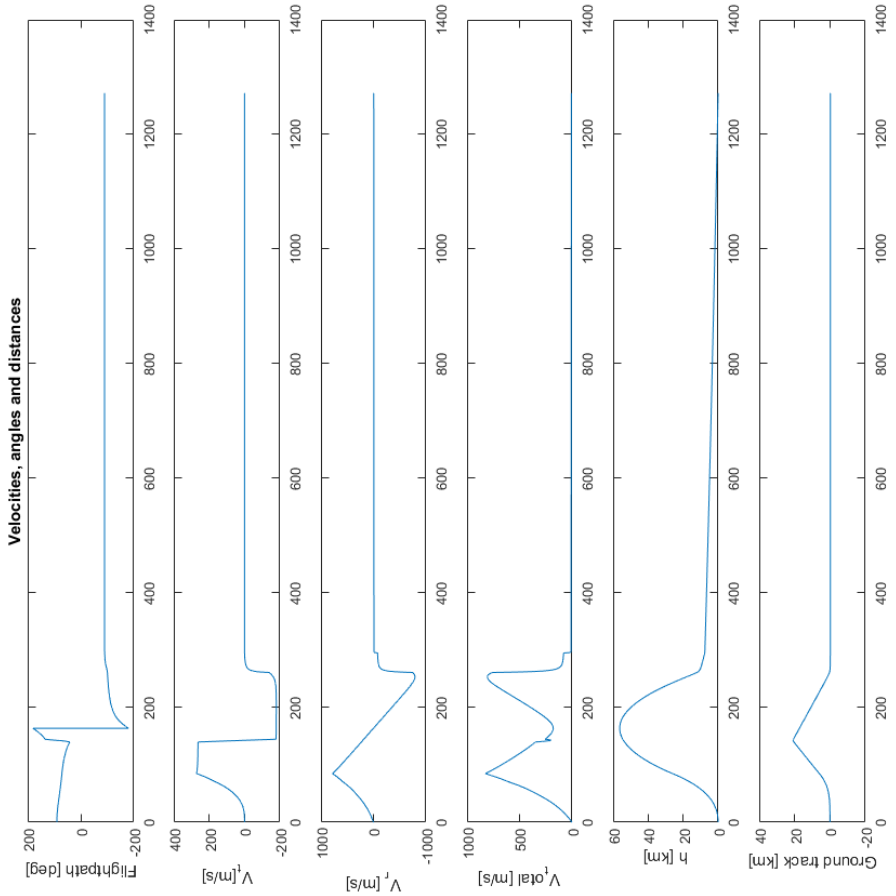

Figure 5.6: Boostback Velocity, Altitude, Ground Track Simulation

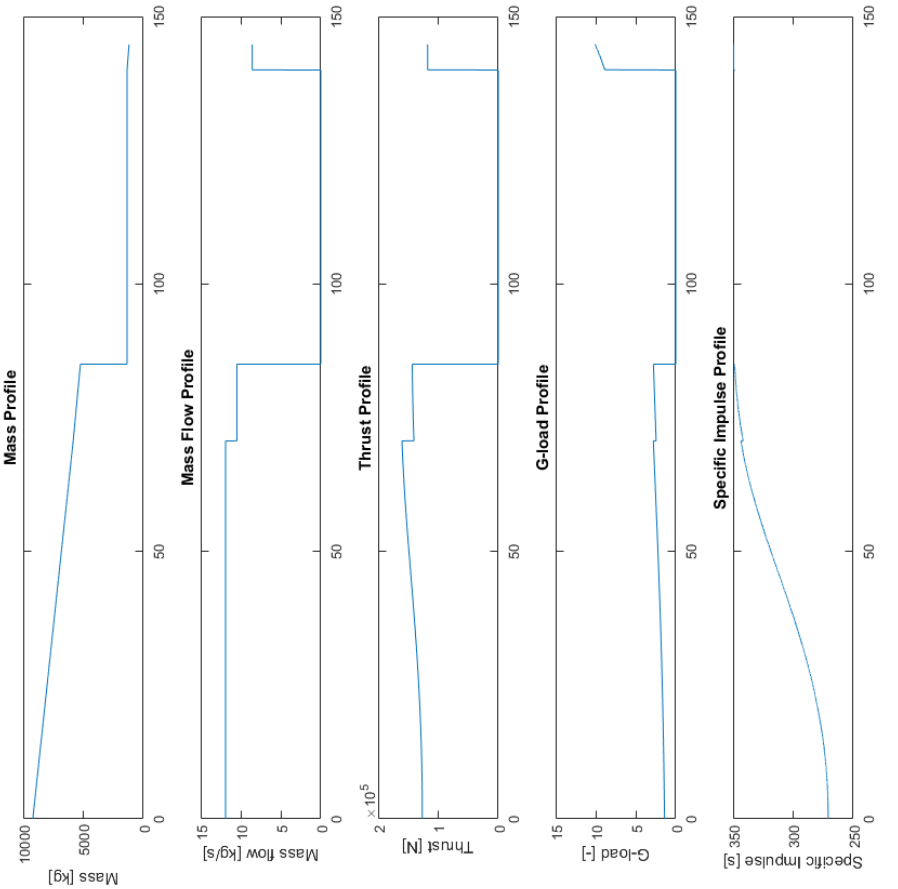

Figure 5.5: Boostback Mass Profiles Simulation

The losses during the boost back manoeuvre are mostly relevant for the drag, and are shown in Figure 5.7. At stage burnout (where gravity loss shows a cut-off) it is clear there is still substantial drag. This is the reason a coast time is needed, allowing the stage to reach greater altitude where drag is low enough to allow for the controlled rotation of the stage needed for the boost back burn.

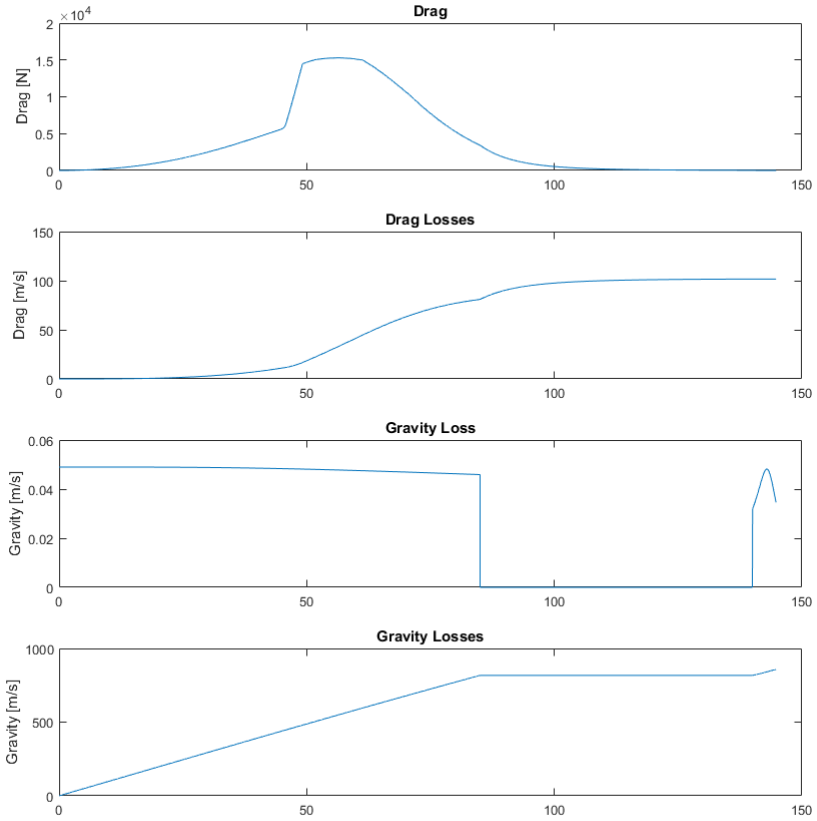

Figure 5.7: Boostback Losses Simulation

5.2. MISSION PROFILE

The complete mission profile of the launch system is displayed in Figure 5.8. The figure shows altitude on the left and velocity on the right, both as a function of time. The figure is illustrative, which means that to depict the mission profile as best as possible, the axes are not to scale. Each step in the profile is elaborated upon with what's physically happening at that stage including the respective altitude, time and velocity. The recovery mission profile is shown in more detail in Figure 5.9.

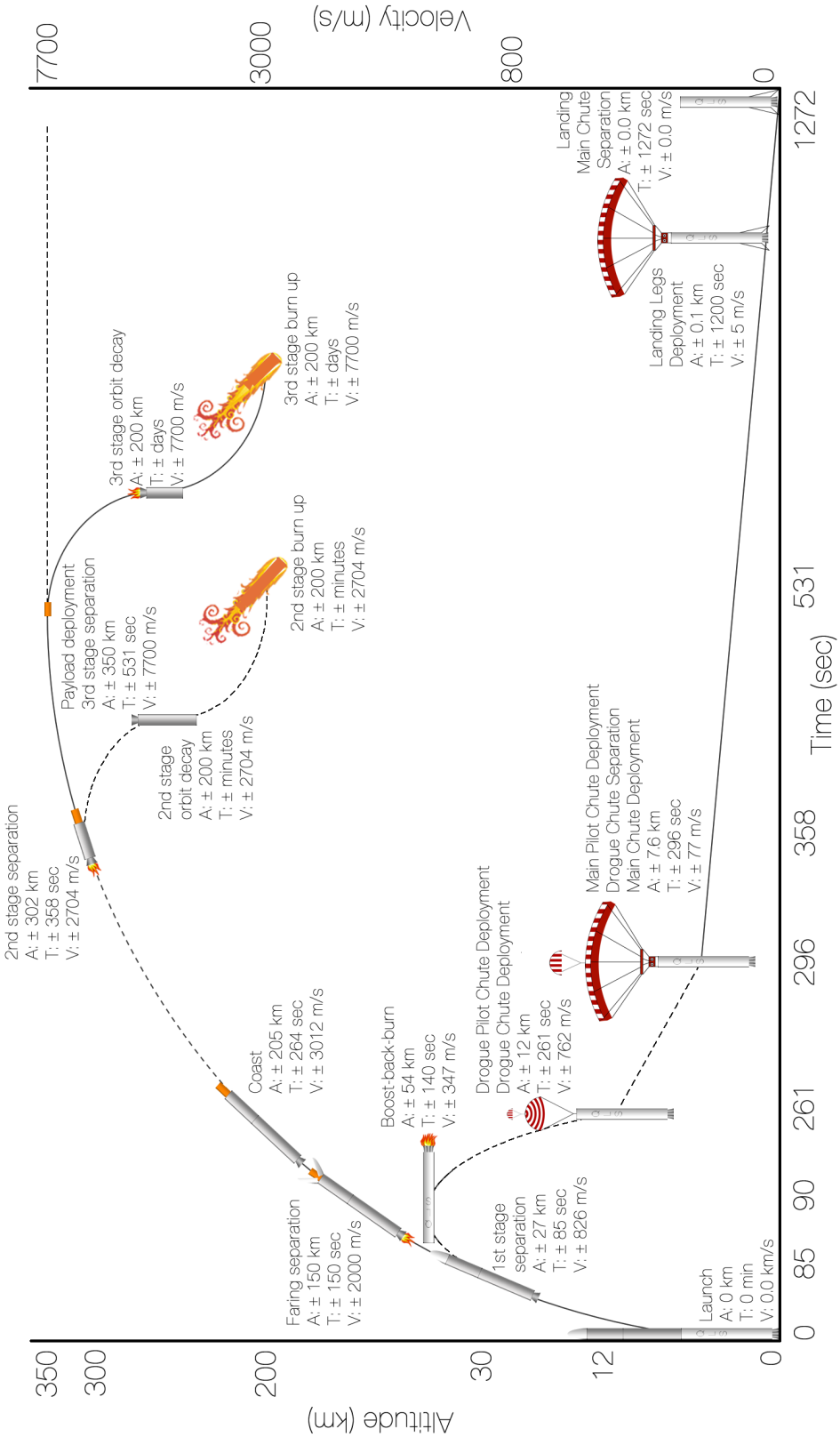

Figure 5.8: Mission Profile of the complete launch system

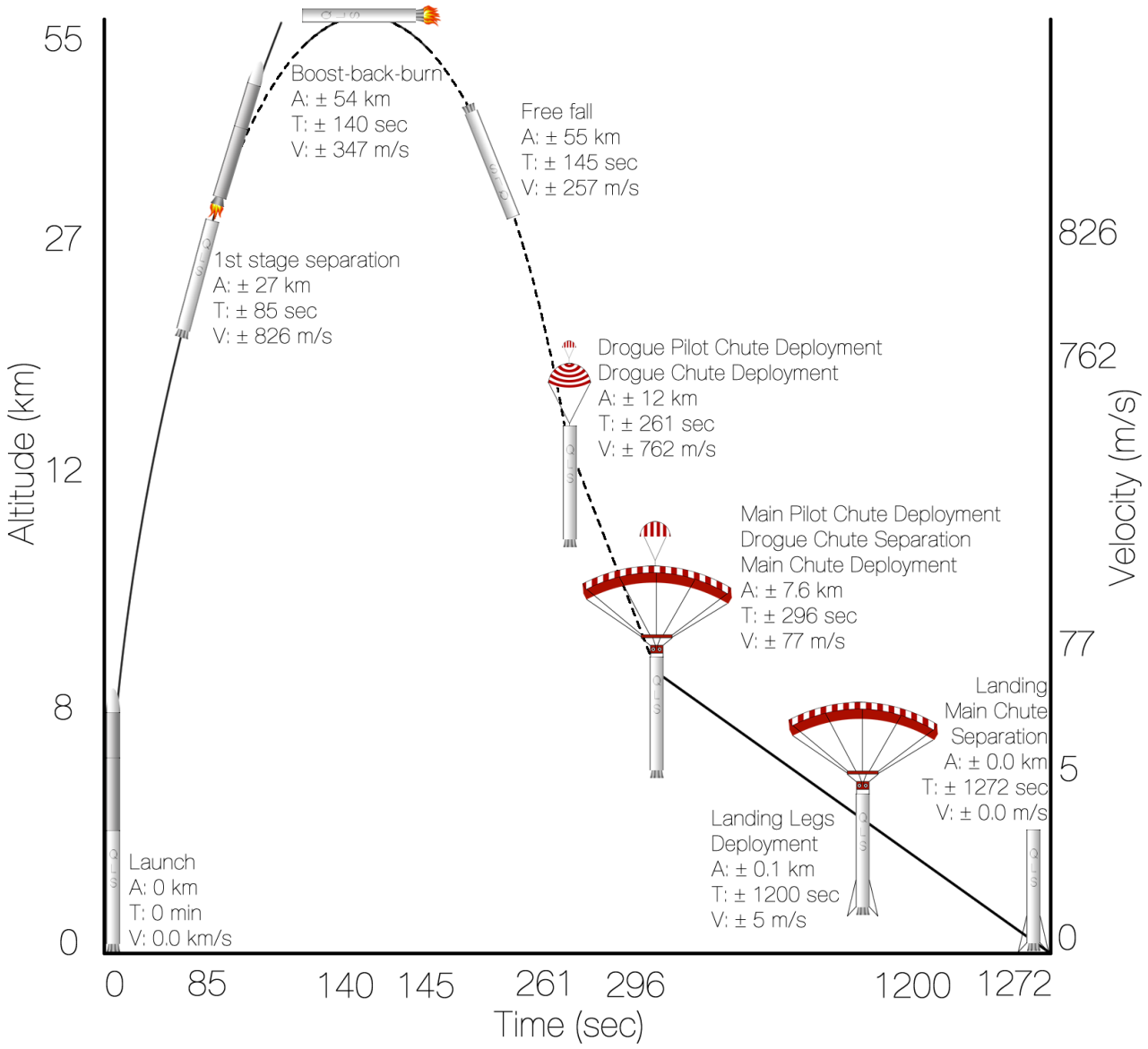

Figure 5.9: Detailed mission profile of the recovery system

5.3. EMISSIONS

Figure 5.10 shows the emissions per 10 km altitude for the full mission (without the boost-back-burn during the recovery). It can be seen that most of the propellant is used during the first stage (ending on 27 km). Between 27 km and 205 km, the second stage is burning fuel. Between 205 km and 302 km, there is no fuel used since that is the coasting stage. The rest of the emissions are due to the third stage.

Figure 5.11 shows the emissions of the first stage alone, including its boost-back-burn for the recovery per 2.5 km altitude. Most of the fuel is used in the first 27 km (during the launch). After 27 km, the engine stops and the first stage's trajectory is determined by its remaining horizontal velocity, vertical velocity and gravity. At 54 km, the engines turn on once more to perform the boost-back-burn. That is the last emission of the first stage.

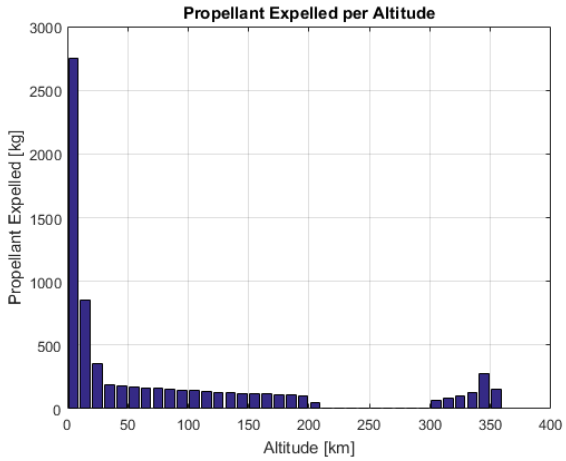

Figure 5.10: Emissions during the lanch (excl. recovery)

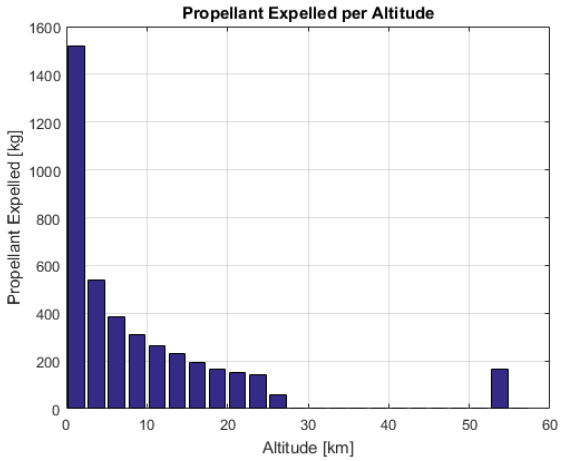

Figure 5.11: Emissions of the first stage (including recovery)

6

SUSTAINABILITY STRATEGY

The following chapter includes the sustainability strategy of the QLS launcher. Sustainability has been one of the main design criteria during the entire design process of the reusable launcher. The focus on sustainability culminates in the recovery subsystem of the first stage. The first stage will be landed by controllable parachutes and retractable landing legs including oil-spring shock absorbers. The requirements for sustainability, as stated in Section 4.4 starting with "QR-SUS-", have been considered throughout the design process of the reusable launcher. These requirements are focused on the reusability of the launcher and using non-toxic and low emission propellants.

The choice of using parachutes to decelerate the stage before landing was done to decrease the use of the propellants. This will not only reduce the amount of propellant required on board of the rocket, but it also provides a sustainable and environmentally friendly solution because no emissions are expelled in the atmosphere. After the first stage separation, the first stage will perform a boost back manoeuvre and propellant is used to cancel out the horizontal velocity of the stage, to enable the landing of the stage, only a few kilometres away from the launch pad. Landing the first stage close to the launch pad will decrease transportation costs and emissions. During landing of the first stage the surrounding environment will not be harmed or polluted, since the propellant system is not used.

The retractable landing legs can be reused multiple times for future launches. The oil in the shock absorbers shall be refilled in case of leakage of the system or at least a check up shall be performed before the next launch. The main pilot parachute and the main parachute can also be reused for future launches. The drogue chute and the drogue pilot chute however, cannot be reused since they are cut off when the vehicle is travelling at a subsonic velocity. In case, the parachutes get damaged during the landing some repairing of the material need to be done, before the next launch. If the chutes are repacked correctly the chutes can be reused indefinitely.

The propellant chosen for all three stages is liquid propellant, with liquid oxygen (LOX) as the oxidiser and liquid methane (LCH4) as the fuel. Liquid methane propellant was chosen mainly for reusability reasons. As it was mentioned in Section 3.2, the LOX/LCH4 is less toxic and a more environmentally friendly option, than a traditional kerosene fuel. The LCH4 does not cause soot or other residues in the rocket engines, which will facilitate the reusability of the propellant tanks and the engines [1].

Space debris will not be an issue for the QLS launcher because the target orbit is at an altitude of 350 km, which is a so-called 'self-cleaning' orbit. This means that the lifetime of the spacecraft will vary between weeks and months, thus not causing space debris.

Testing of the subsystems and their components shall be performed in Europe, for sustainability reasons. The transportation costs and emissions will be reduced if the testing is performed in Europe. Waste of resources and pollution of the environment will be avoided during testing and manufacturing. No toxic substances or no harm shall be released or caused during the testing and manufacturing processes. Innovation for new possibilities to limit waste or pollution shall be encouraged continuously.

To conclude, the QLS launcher provides an innovative and a sustainable solution to launch small payloads into Low Earth Orbit (LEO). The reusability of the first stage will enable the reuse of materials and subsystems. This will not only reduce the required resources for future launches but also significantly reduce cost. Recovering the first stage will also reduce the amount of pollution and waste expelled in the atmosphere and the environment surrounding the launch pad. The use of parachutes will decrease the use of propellant required on board the QLS launcher and the amount of emissions expelled into the atmosphere.

[1] http://www.aerospace.org/crosslinkmag/summer2011/green-propulsion-trends-and-perspectives/, visited on: 15-01-2016

7

PROJECT DEVELOPMENT

The following chapter covers the risk analysis in Section 7.1, operations and logistics in Section 7.2, manufacturing in Section 7.2, assembly and integration plan (MAI) in Section 7.3 and finally reliability, availability, maintainability and safety (RAMS) characteristics in Section 7.4.

7.1. RISK ANALYSIS

The following section gives the risk analysis of the QLS launcher. The risks are linked with the requirements of the launcher. It is important to recognise the risks involved with the mission and analyse the severity and the probability of the risks. The recovery system will introduce some additional risks on the launcher in case it malfunctions, but in general it is a reliable system. The risks are firstly described in Table 7.1 after which a risk map is illustrated in Table 7.2, followed by a risk mitigation description in Table 7.3 and a risk mitigation map in Table 7.4.

Table 7.1: Risk Descriptions

Risk No./ Requirement	Risk	Probability	Consequence	Description
ADCS1/ QR-COM-010, QR-COM-020, QR-COM-030, QR-COM-050	Failure in sending and receiving signals	Moderate	Catastrophic	In case communication is lost or subsystems interfere the launch system becomes uncontrollable. The launcher may de-orbit, which leads to mission termination.
ADCS2/ QR-COM-040	Storability Failure	Moderate	Catastrophic	The communications failure in storability is severe for the ability to successfully communicate with the ground.
ADCS3/ QR-PWR-020, QR-PWR-030, QR-PWR-040	EPS Failure	Moderate	Catastrophic	Power subsystem failure is one of the most occurring causes to mission failure. Most are associated with solar cells and battery charging circuits [51].
ADCS4/ QR-PWR-050	EPS Monitoring Failure	Moderate	Catastrophic	The ability to monitor the EPS features may cause system failure.
ADCS5/ QR-SUS-020	GNC System failure	Unlikely	Catastrophic	The GNC systems fail, potentially causing failed orbit injection, leaving the assigned safety zone or failure to recover reusable items.
ADCS6/ QR-SCN-010, QR-SCN-040, QR-SCN-060	Orbit injection failure	Unlikely	Catastrophic	The system may not be accurate enough to perform a reliable orbit injection.
ST1/ QR-STR-060	Unexpected launch loads	Unlikely	Catastrophic	The maximum expected launch loads are exceeded, because of insufficient modelling/analyses. The risk is that the structure will fail catastrophically in flight.
ST2/ QR-COM-020, QR-COM-030, QR-COM-040, QR-COM-050	Communication blockage	Rare	Major	Communications could be blocked if a part of the structure fails and blocks or even destroys a part of the communication system. Communications can also fail if there is interference with other systems.
ST3/ QR-STR-050	Thermal damage	Unlikely	Major	Thermal damage can occur to both the launch system and the payload. The launch system experiences aerothermal damage if its thermal protection fails. The payload will experience thermal damage, if its thermal protection system fails. This will cause overheating of the payload and ultimately failure.
ST4/ QR-STR-040	Vibrational loads	Likely	Catastrophic	If materials vibrate at their natural frequencies during launch, resonance will occur. This vibrational motion will keep increasing in amplitude, until the structure fails. Furthermore, vibrations from propulsion systems or due to aerodynamic loads can be in the order of several g's, destroying any fragile structure.

OL1/ QR-MIS-120, QR-MIS-130	Insufficient testing facilities	Likely	Major	The availability of testing facilities could cause problems if they are not available at the right period. Insufficiently tested systems may malfunction and cause mission failure.
OL2/ QR-MIS-110	Launch campaign costs	Moderate	Significant	Launch sites may exceed the budget.
OL3/ QR-MIS-110	Development costs	Moderate	Major	The development costs of a new system may be too large due to unforeseen circumstances, which can impact costs or technical performance.
PR1/ QR-PRP-020	Propulsive underperformance	Unlikely	Major	In case of under-performance, the necessary ΔV cannot be achieved. This results in the incapability of reaching the designated orbit thus causing mission failure
PR2/ QR-PRP-030, QR-PRP-060	Propulsion failure	Unlikely	Catastrophic	In case of problems during launch, the payload is not able to be brought into orbit, thus causing mission failure.
PR3/ QR-PRP-010	Propulsion ignition malfunction	Moderate	Minor	If the ignition process malfunctions, the launch system is unable to fulfil its functions. Depending on the type of launch system, reusability is affected.
PR4/ QR-PRP-020, QR-STR-060	Deviating performance due to launch loads	Unlikely	Minor	In case of sloshing of the propellant, unwanted spin and flight trajectories of the launch system can be caused, which leads to mission failure.
SU1/ QR-SUS-010, QR-MIS-090	Environmental hazard	Moderate	Major	The launch system causes damage in any form to the environment. This can be to vegetation, wildlife or humans.
SU2/ QR-MIS-100, QR-SUS-020	Recovery failure	Near certainty	Significant	If the recovery operation fails due to any circumstance, the reusability of the launch system is affected.
SU3/ QR-SUS-030	Orbital debris	Moderate	Insignificant	In case of any failure of the payload in orbit, debris may remain. Debris will not be an issue for the QLS mission because the orbit is at an altitude where the lifetime is from weeks until months tops. However, during the missions it shall not cause damage to other spacecraft in orbit.
REC1/ QR-MIS-100, QR-SUS-020	Parachute deployment failure	Rare	Catastrophic	If the parachutes fail to deploy completely or partially. This will have catastrophic consequences on the recovery system. If the parachute fails to deploy completely, the first stage will crash land uncontrollably, and if the parachutes deploy partially the first stage might land at an ever increasing velocity, which will be too high for the landing legs to support. The structure of the first stage might be damaged due to the increased approach velocity.
REC2/ QR-MIS-100, QR-SUS-020	Parachute controller malfunctions	Moderate	Minor	If the controller of the parachute malfunctions, the first stage will land safely, but the location of the landing will be unpredictable. The landing location will be dominated by the wind speed.
REC3/ QR-MIS-100, QR-SUS-020	Landing Legs fail to deploy	Rare	Catastrophic	This may be caused by a malfunction in the actuators' power supply. If the actuators fail to deploy the landing legs, the first stage will be decelerated by the parachutes but the first stage will land either on the nozzles or on its side. Either way, it will have catastrophic consequences on the recovery system.

After determining the risks in Table 7.1, the risk map is illustrated in Table 7.2. The risks that are not in the green area, thus have a high probability of occurring and a high severity of consequence, of the risk map are mitigated in Table 7.3. Table 7.4 illustrates the risk map of the mitigation strategy defined in Table 7.3.

Table 7.2: Risk Map Launch System

Consequence/ Probability	**Insignificant**	**Minor**	**Significant**	**Major**	**Catastrophic**
Near certainty	-	-	SU2		-
Likely	-		-	OL1	ST4
Moderate	SU3	PR3, REC2	OL2	OL3, SU1	ADCS1, ADCS2, ADCS3, ADCS4
Unlikely	-	PR4		PR1, ST3	ADCS5, ADCS6, PR2, ST1
Rare	-	-	-	ST2	REC1, REC3

Table 7.3: Risk Mitigation

Risk No./ Requirements	**Risk**	**Mitigation Strategy**
ADCS1/ QR-COM-010, QR-COM-030, QR-COM-050	Communications Failure	Interference and malfunction are mitigated by adhering to standards and testing subsystem interfaces at every stage until final assembly.
ADCS2/ QR-COM-040	Communications Storability Failure	The storability of the communications subsystem needs to be tested before launch.
ADCS3/ QR-PWR-020, QR-PWR-030, QR-PWR-040	EPS Failure	The risk on EPS failure is mitigated by creating a proper testing programme. Components and subsystems such as printed circuit boards have to be tested both individually and connected.
ADCS4/ QR-PWR-050	EPS Monitoring Failure	The monitoring system of the EPS has to successfully pass the testing prior to launch.
ADCS5/ QR-SUS-020, QR-MIS-010	GNC System failure	These risks can be mitigated through redundancy and extensive testing. Termination of the ascent phase may be necessary to stay in safety zone.
ADCS6/ QR-SCN-010, QR-SCN-040, QR-SCN-060	Orbit injection failure	This risk is hard to mitigate without having extensive flight testing of the system, and thus will be costly and take long to develop. Commercial-off-the-shelf (COTS) components should be considered. Drop tests can be done to validate subsystem in a 0g environment.
OL1/ QR-MIS-130, QR-MIS-140	Insufficient testing facilities	This risk cannot be reliably mitigated through design or protocol as it relies on external parties. Therefore, testing facilities must be considered as early as possible of the design process. COTS components should be considered.
OL3/ QR-MIS-120	Development costs	Part of the available budget must be allocated to unforeseen costs and COTS components shall be considered.
PR2/ QR-PRP-030, QR-PRP-060	Propulsion failure	Propulsion failure is mitigated by performing an extensive test programme.
PR4/ QR-PRP-020, QR-PRP-060	Propulsion malfunction	This risk is mitigated in the same way as PR2. Next to that, the risk is mitigated even further by providing a proper recovery system to the launch system.
ST1/ QR-STR-060	Unexpected launch loads	This is mitigated by including safety factors.
ST4	Vibrational loads	Safety factors should be included, as well as extensive testing of subsystems.
SU1/ QR-SUS-010, QR-MIS-100	Environmental hazard	This is mitigated by using non-toxic components as much as possible, and pollutants shall be constrained in the launch region. The launch region shall be chosen in accordance with the environment.
SU2/ QR-MIS-100, QR-SUS-020	Recovery failure	In case of recovery failure the waste shall be reduced to a minimum without harming the environment and as many parts shall be recovered as possible.

Table 7.4: Risk Mitigation Map Launch System

Consequence/ Probability	Insignificant	Minor	Significant	Major	Catastrophic
Near certainty	-	-	-		-
Likely		SU2			
Moderate			OL3	OL1, ST4	
Unlikely	-	PR4	SU1	ADCS1, ADCS2, ADCS3, ADCS4	PR2, ST1
Rare	-	-	-	ST2, ADCS5, ADCS6	PR2, ST1

7.2. OPERATIONS AND LOGISTICS

7.2.1. OPERATIONS

The mission is divided into 4 main phases: launcher production, launch preparation, launch, post launch. The different phases are outlined in the Function Flow Diagram (FFD) (see Figure 7.1). It is important to outline the phases to employ a strategy for cost reduction. The strategy is to reduce on engineering staff members, and making them more effective by employing them based on the (sub)system they work on, irrespective of the project phase. This ensures a minimal amount of engineers will be idle as the phases progress. Additionally, the engineers will be more intimate with the behaviour of their (sub)system during the entire mission. This will allow them to more effectively identify how processes relevant to their system can be stream-lined.

LAUNCHER PRODUCTION

The launcher production phase consists of two parallel tracks. The tracks are separated because one track focuses on producing a first stage with as much refurbished components as possible, but the second and third stage are every time produced from scratch. This separation allows for a faster stream-lining (learning effect) of the second and third stage production, as the process is more predictable than the first stage (re)production. This phase ends with flight readiness testing of the stages and delivered the stages to the launch site. The stages are not integrated yet, to reduce costs on the delivery.

LAUNCH PREPARATION

In the launch preparation phase, which happens entirely on the launch site, the entire launcher is assembled horizontally. Horizontal assembly is the fastest and cheapest way of final integration [10]. There is only a payload integration phase, and no testing phase. It is the responsibility of the costumer to extensively test their payload with interfaces provided by QLS. This will save time and costs, but this will be reflected in the price for the costumer. The rocket is then transported to the launch platform, and after all necessary preparations, a final go/no-go decision is made. If the launch must be prematurely aborted for any reason, the propellants must be dumped so the entire system can be recovered in a safe and timely manner. Otherwise, the countdown is started.

LAUNCH

The launch stage starts with ignition of the first stage. The trajectory is controlled, and in case the predicted trajectory poses unacceptable safety risks, the mission is terminated. After first stage separation, recovery is initiated. The function 3.5a is shown in more detail in the FFD, as it comprises an important aspect of our mission. The second and third stage are disposed. The launch phase ends when the payloads are injected into orbit.

POST LAUNCH

The post launch activities start after the mission end. The first stage has been retrieved and it will be thoroughly inspected. If the first stage is not entirely reusable, as much components as possible will be refurbished. The non-reusable parts will be recycled as much as possible. After this the components are securely stored for the next mission. Another vital part of this phase is making sure the entire mission is properly document from begin to end. During the evaluation, opportunities to save costs and time must be identified, and the operations must be improved where possible. The mission ends with a clean-up phase, in which everything must be readied for the next mission.

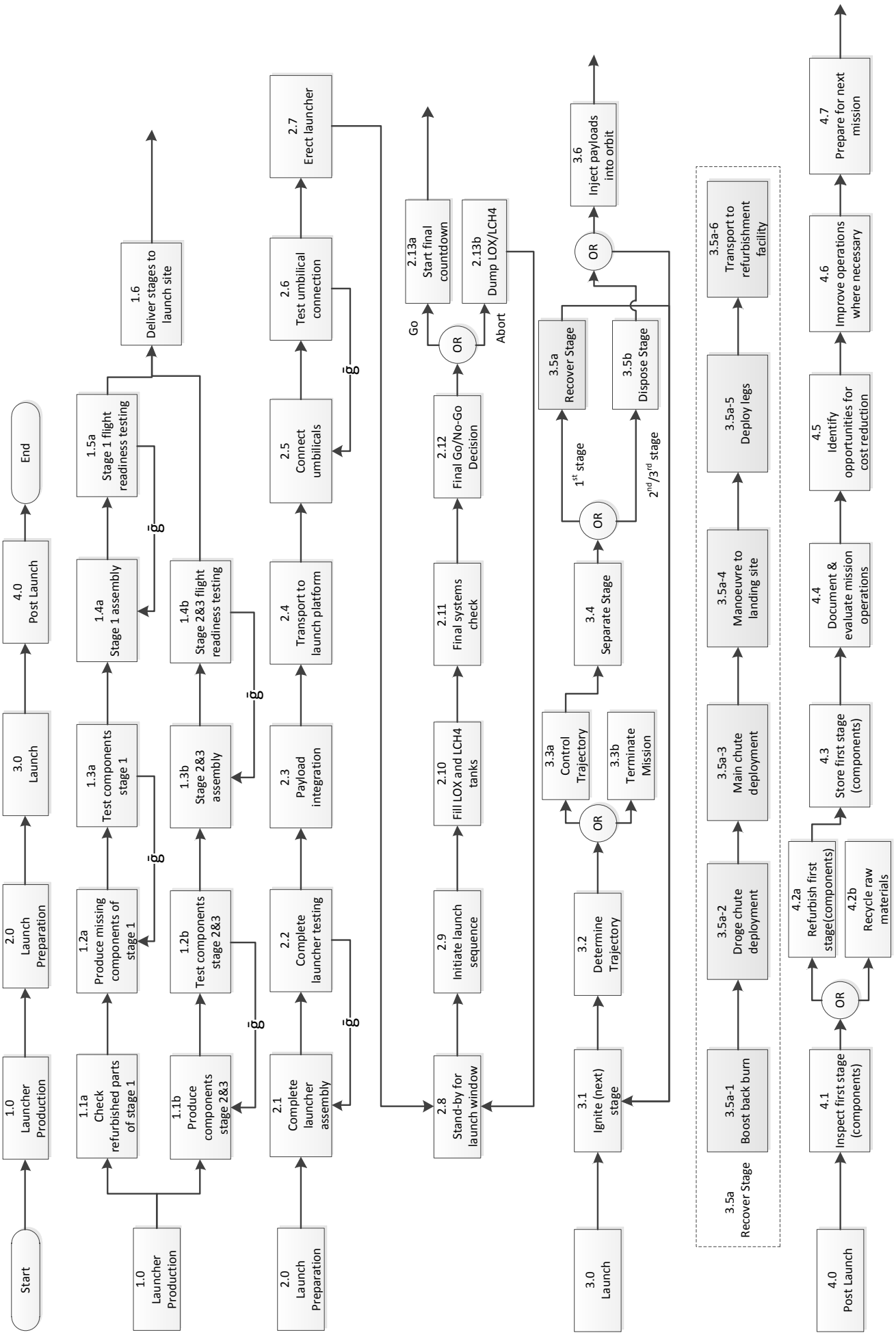

Figure 7.1: Function Flow Diagram of Mission

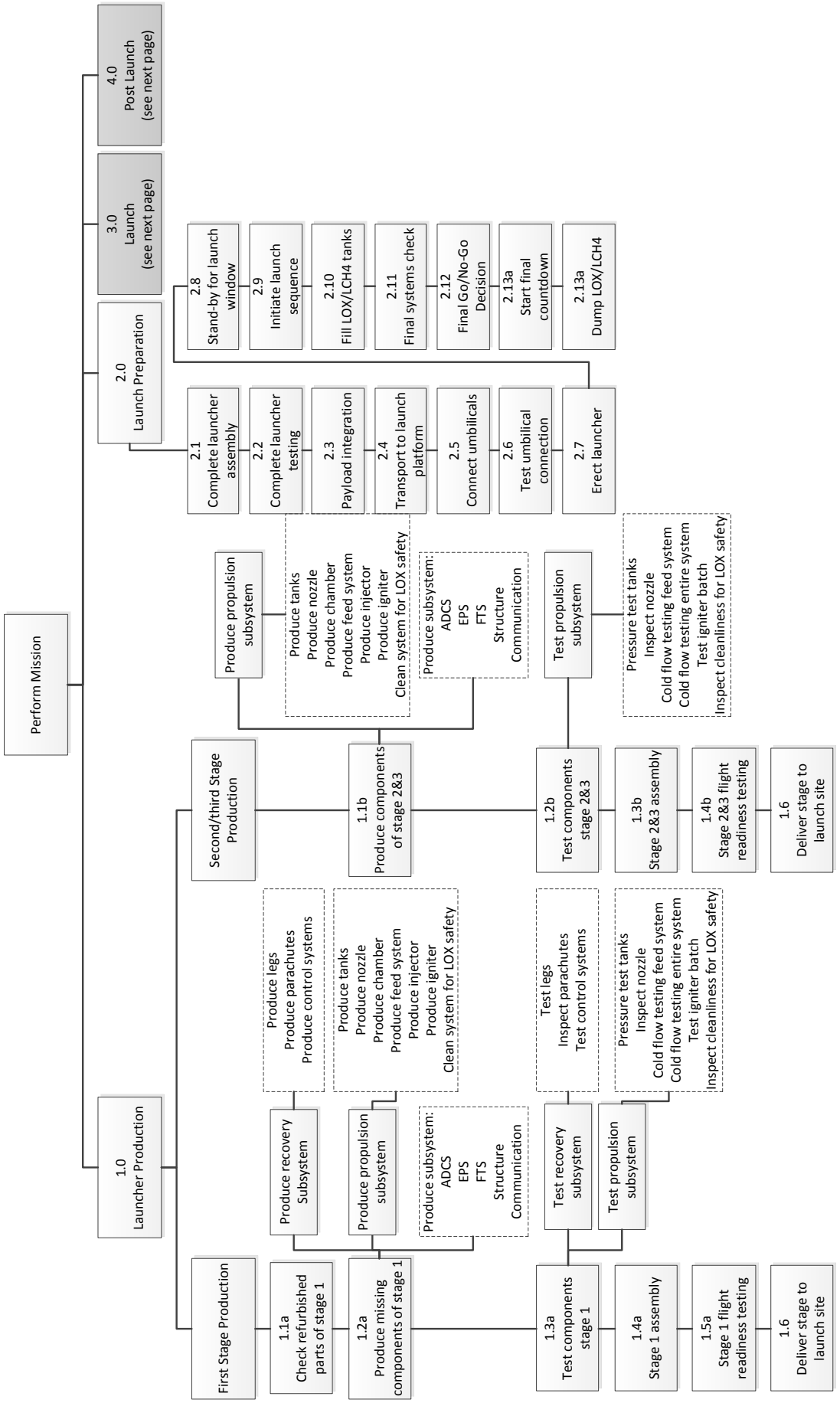

Figure 7.2: Function Breakdown Structure of Mission (part1)

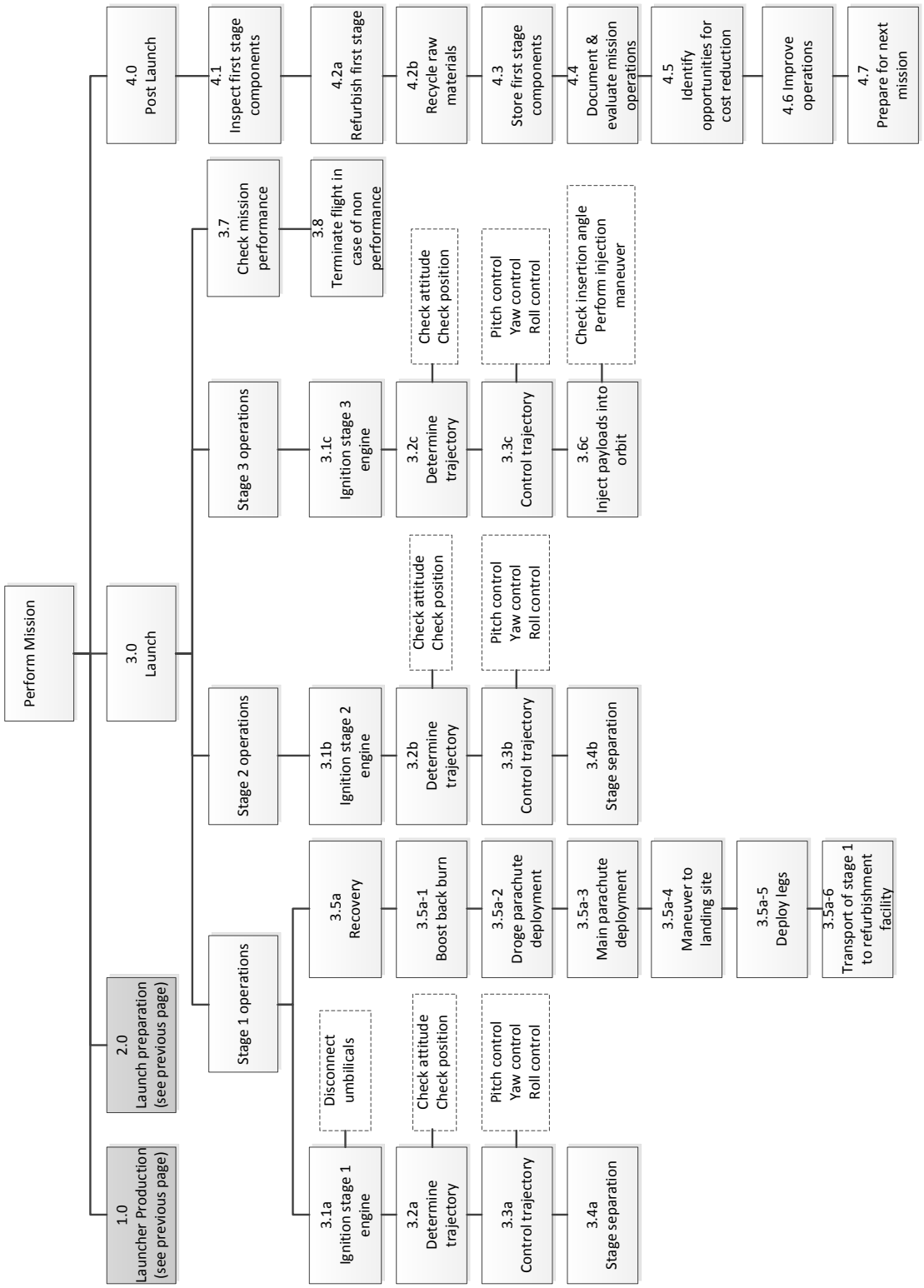

Figure 7.3: Function Breakdown Structure of Mission (part2)

7.2.2. LOGISTICS

For a successful mission many facilities are necessary. These facilities are a non-negligible part of the recurring costs. In order to identify where cost savings can be made, a Logistics Breakdown Structure(LBS) is made with sufficient detail to devise a strategy. Start-up companies have the ability to save costs on logistics, because they do not have to fit into the traditional structure of government subcontractors [10]. By looking at the three main branches, facilities,

transport and supply, the main parameter that can be affected to reduce cost is *location*.

TRANSPORT

Ideally, transportation of components and personnel is minimised to reduce costs in this branch. This is achieved by reducing the amount of locations where operations are performed. It can be expected that the minimum amount of locations is two. This is because one is constrained by the currently existing launch sites. These locations are highly likely to be unavailable for operations other than the final launch preparations. Referring back to the FFD(Figure 7.1), it means that the operations in the launcher production and post launch phases, must be performed in preferably one location. The facilities branch sheds light on how this can be achieved.

FACILITIES

The facilities exist mainly out of the launch site and facilities for production/testing, storage and offices. It is possible to concentrate the last three facilities into one location. The offices of the engineers should be very close to workshops and testing facilities, so they can be intimately involved with their (sub)system during all mission operations. This is also in line with the operations strategy, outlined in Section 7.2.1. The facilities are further reduced by having as much similarity between stage engines as possible. All engines use LOX/LCH4 propellant. The workshop and the testing facilities should for smaller subsystems preferably be in walking distance of each other. And for increasingly large (sub)systems, the workshop and the testing facility should be the same building. In principle, there is nothing against this strategy, other than the availability of certain resources at this single location. This is further investigated in the supply branch. For some testing operations, such as drop tests and parachute tests, it is better to investigate those at existing facilities.

SUPPLY

To what extent the facilities can be concentrated in one location depends on the supply branch. It also provides additional opportunities for cost savings. The feasibility of highly concentrated facilities depends on the size of these facilities. The supply branch reveals where this is possible. The size of the facilities can be reduced by using as much COTS components as possible, as it reduces the equipment and tooling necessary to produce these components, and as well the size of the engineering workforce. The cost of transporting COTS components to workshop and testing facilities, is considered to be marginal. In addition, COTS components greatly reduce development costs [10]. The only remaining issue is that this concentrated location needs an actual location. The other two branches of supply, subcontractors and raw materials, will influence this decision. In certain countries, the needed expertise is simply not available. In addition, the cost of raw materials and subcontractors can greatly vary per country. Also, the constraints posed by politics and regulations, such as ITAR[1], can greatly influence the costs. Often these constraints are Export Restrictions on Dual-Use Goods(items which can be used for both military and civilian purposes). This is another reason why costs can be reduced by having facilities in one location, as Export Restrictions do not apply if facilities are not scattered across countries. The last major consideration for the location is then the “supply” of labour. There are great differences in costs and effectiveness for employees per country [10].

7.2.3. TEST PROGRAM: PROPULSION SUBSYSTEM

Test programs are necessary but also costly, therefore it is of great importance that all done tests are *effective*. In the context of our program a test is considered effective if the components that are not the main focus of the test perform reliably. Thus all produced results mostly concern the components that are the focus of the test. For example: a 30 second hot-burn test is performed. If the test fails because the igniter malfunctions, the test was not effective. The test is effective if the engine is reliably ignited every test. Similarly, the feed system should perform reliably. If the feed system is leaking, the test is considered ineffective, because a lot resources are wasted on testing a smaller component of the entire system. The strategy to achieve this reliability is to thoroughly test smaller components of the systems, before scaling up the scope of the test. For instance, cold-flow tests can be performed on the feed system, and igniters designs can be tested until they are deemed reliable.

In Figure 7.4 the test program is laid out. It shows how smaller components of the system can be tested before further integration. Three types of test return often: leak testing, cleanliness testing and extensive reliability testing. The leak testing is done with an inert substances, such as nitrogen. Physically, (not chemically), nitrogen behaves very similar to oxygen. It allows for cheaper and safer testing of the system. Liquid oxygen or methane leaks pose higher risks with not much added value while leak testing. The leak testing cannot entirely be done with water as the cryogenic temperatures will cause materials to contract, sometimes at different rates. This may expose leaks that cannot be determined at room temperature. Furthermore, some materials may not perform as expected under cryogenic conditions. For instance, polymer seals may become too brittle and stop functioning.

[1] https://www.pmddtc.state.gov/regulations_laws/itar.html, visited on: 18-01-2016

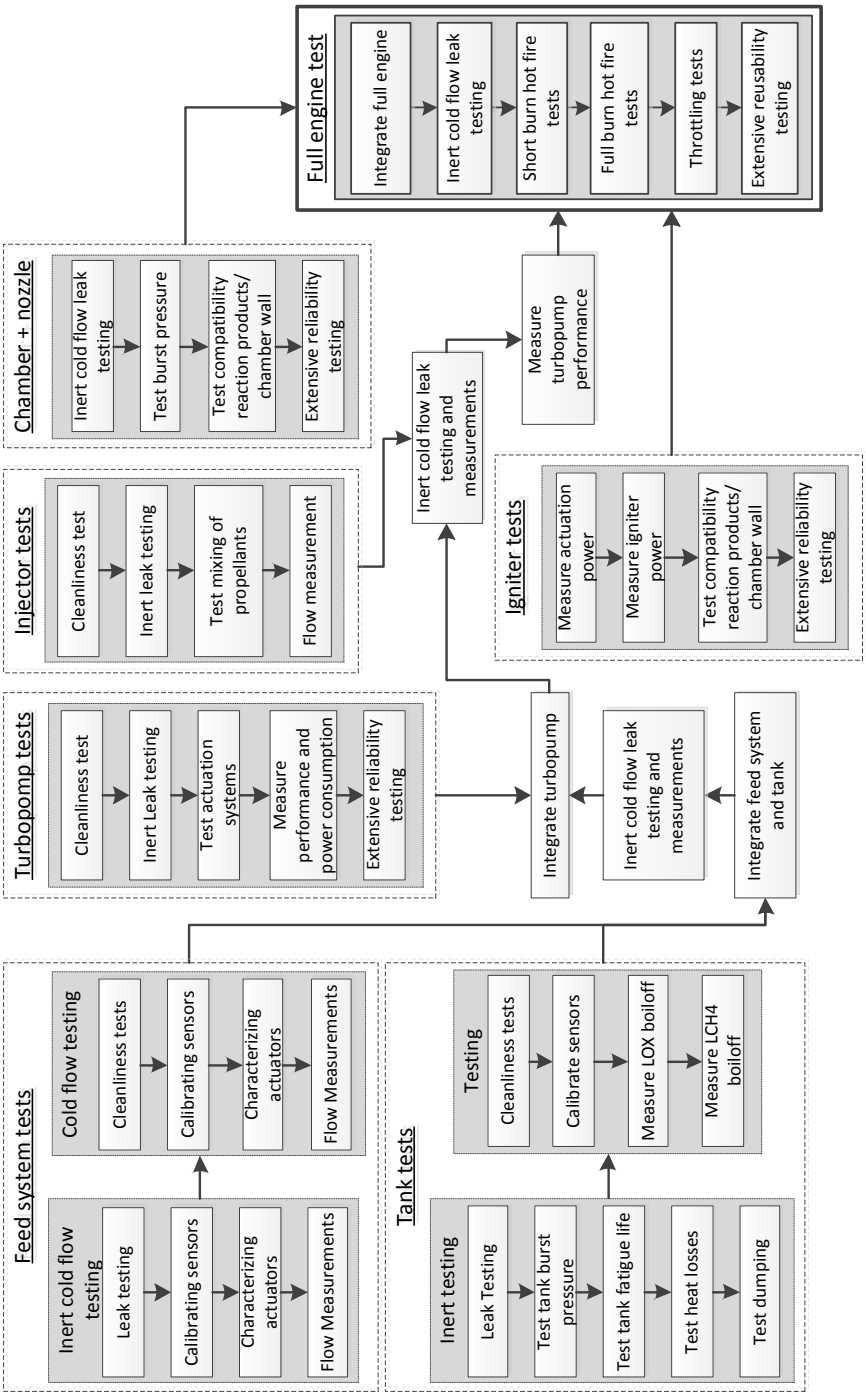

Figure 7.4: Test Program Overview

Cleanliness testing is important because LOX is used as an oxidiser. Tests must be performed to check whether the system can be cleaned properly, and to what standard. The design of the feed system must adhere as much as possible to already well-established standards such as the NASA Safety Standard for Oxygen [52].

The extensive reliability tests are needed on components that need to work every single time for a successful engine burn. The igniter should perform in a predictable manner every test, the turbopump must run reliably for prolonged periods of time, and the chamber must be shown to be reusable time after time. All these tests will determine not only the reliability but often also the reusability of the system.

7.2.4. TEST PROGRAM: SEPARATION SYSTEM

Separation testing includes the separation of the stages and the separation of the fairing. The mechanisms themselves involved are COTS components and therefore do not require small part testing. The final rocket (or a few stages at the time) has to be tested for separation. This can be done at sea level conditions in a large hall in which (parts of) the rocket is set up and cables are attached to the separating parts. When separation takes place, the separating parts will be caught by the cables and nets or soft ground parts to prevent damaging the parts. This does not need a dedicated location. To do better testing for separation without atmosphere (such as fairing separation), a vacuum chamber can be used. The full sized version NASA's Glenn Research centre's[2] vacuum chamber can be used.

7.2.5. TEST PROGRAM: RECOVERY SYSTEM

To test the recovery system there are multiple steps involved, each at increasing in scale. Parachutes that are bought off-the-shelves (such as the drogue chute and pilot chutes) don't require extensive testing as they are proven systems. The proven systems do need to be tested in series with the full recovery system later on. Since the main chute will be designed from scratch, more extensive testing is needed, beginning with small scale windtunnel testing of the parafoil. Testing of the drogue chute and its pilot chute will require small model of the chute in a supersonic windtunnel. Testing of the main pilot chute and the main chute will require the use of a subsonic windtunnel. Due to the size of the main parachute, it will be necessary to create a smaller model. These windtunnel tests will reveal the exact aerodynamic characteristics of the parachutes and will show if and how the parachutes deploy.

The landing legs should be tested to be able to carry the required load. This should be done on a small scale by loading and unloading the hydraulics. And on a large scale by mounting the hydraulics on a mass and dropping the structure a few meters (this drop height should be calculated to be the height needed to have an end velocity equal to the required landing velocity) to see if the hydraulics hold.

After the the parachutes have gone thought the windtunnel tests and the legs have gone through their small drop tests, a final full scale drop test must be preformed. This can be done with a dummy empty first stage (a weight with the right dimensions and center of gravity), which can be dropped from an airplane. This test will reveal if the complete series of parachutes does what it is supposed to do. This will also be an opportunity to test the landing legs system.

To save costs, the tests should all be performed at the same location. This is possible for most cases as institutions (like the TU Delft) offer most of these facilities. The final drop test however, can not be performed everywhere. Within Europe, ESA makes use of Sweden's Esrange Space Center in Kiruna for their parachute tests[3].

7.2.6. TEST PROGRAM: STRUCTURES

The structural testing program is vital to ensure all components can withstand launch loads. Two main load cases are important in the test program: the vibrational loads and the maximum g-loads.

The following tests are performed on test vibrational test benches:

1. **Sine sweep:** Identify resonant frequencies, and structural response to it

2. **Random vibration:** Test performed based on random frequencies. The frequencies could be recorded from motor tests.

3. **Shock testing:** Shock tests can be performed on some test benches. The displacements are not very large, but for smaller less critical systems this test can be a good, cheaper, alternative to drop tests.

Preferably vibrational test benches are part of the facilities to ensure tests can be done often for a lower price.

In addition to vibrational loads all components must withstand acceleration loads. These tests can be done in centrifuges of increasing size. Smaller centrifuges must be available at the facilities so components can be tested extensively. For larger centrifuges, it should be considered to use external testing facilities to reduce costs.

[2] http://www.nasa.gov/image-feature/journey-to-space-in-a-vacuum-chamber, visited on: 18-01-2016
[3] http://www.sscspace.com/launch-services-esrange-space-center, visited on: 18-01-2016

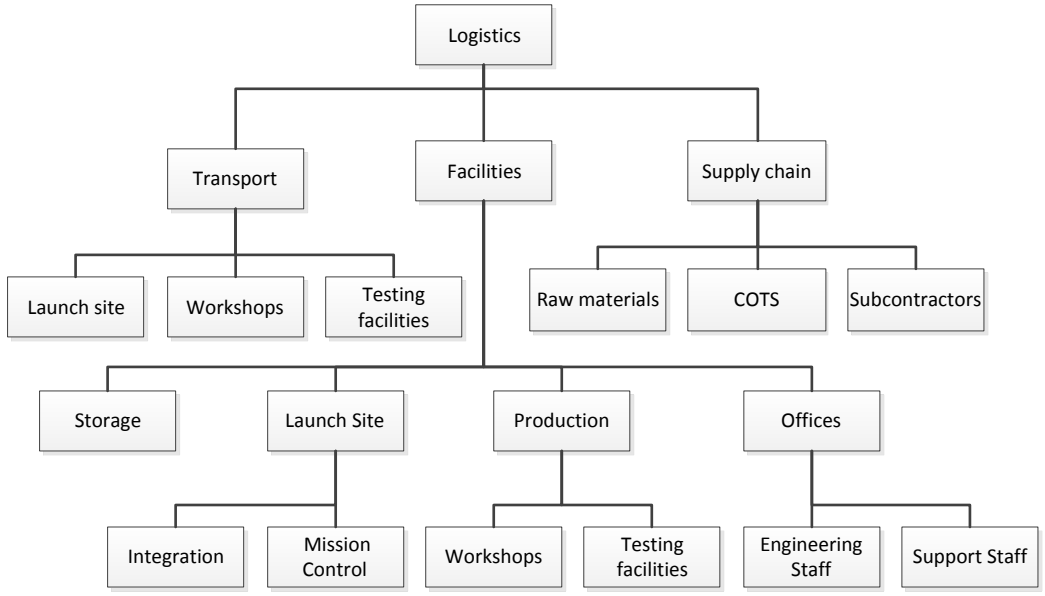

Figure 7.5: Logistics Breakdown Structure

7.3. MANUFACTURING, ASSEMBLY AND INTEGRATION

In this section, the manufacturing, assembly and integration of the system are discussed and incorporated in a production plan. This includes the production of parts that are produced in-house, assembly of the launch system and integration of COTS parts. As QLS is a commercial undertaking, it is beneficial to save on costs by manufacturing as many parts 'in-house' as possible.

As defined in the mission statement, a large focus of QLS is to keep the system cost-effective. Manufacturing is one of the areas where Quantum Space believes significant cost savings can be made. With a projected launch frequency of 5 per year at start and up to 50 per year[53] in the future, series production of parts is expected to take significant use of the learning effect[54] to drive production costs down. Other strategies and techniques QLS shall employ are[53]:

- Advanced low-mass, low-cost materials
- Series production of components
- Use of additive manufacturing ('3D-printing')
- Advanced, reliable COTS technology

The following sections describe the manufacturing, assembly and integration of each subsystem.

Propulsion

The propulsion subsystem benefits most significantly from recent advances in manufacturing technology. 3D-printing of critical engine parts using selective laser melting or electron beam melting has been shown cut production costs by 70% and time by 75%[55]. Components that are already known will be manufactured using 3D-printing are:

- Rocket engine parts:
- Combustion chamber
- Regeneratively cooled nozzle
- Injector
- Turbopump
- Cold gas thruster RCS

The ablative skirts for the second and third stage engines are made from ablative carbon-based materials and made using resin transfer moulding (RTM). As the engines are known to take up most of the resources allocated to production of the system, production of these parts will start early. They will be integrated with the structure only when the entire stage is assembled.

Structures The design of the QLS incorporates integral fuel and oxidiser tanks. Therefore, the first structural part that must be manufactured are the tanks, made of advanced aluminium-lithium alloy. When these are done, they are joined together and the rest of the skin and load-bearing sections are added using stir-friction welding. This process has no need for the filler materials, shielding gasses and costly weld preparation that have to be used in conventional arc welding[56]. The nose-cone is made of CFRP and will be made using (RTM). The payload integration system is COTS, supplied by ISIS Delft[4]. Different stages are kept separated, and the assembly of the stages will happen close to launch in order to keep warehouse logistics as simple as possible.

GNC, FTS and EPS The flight computers, actuators, and sensors of the GNC subsystem, the entire FTS subsystem and the batteries and power management components of the EPS are all COTS products, and will be integrated into the structure after the stage structure and propulsion system are assembled.

Recovery The parachutes and actuators of the first stage recovery subsystem are COTS products. The shock absorbers are machined out of aluminium integrated with the outer structure when the other subsystems have already been integrated. The parachutes and parachute control systems are added last.

The first stage is expected to be reused ten times as mentioned in Section 8.2. Therefore, after manufacturing a number of first-stage cores and perfecting the re-use systems, production focus will shift to the non-reusable stages. A complete production plan for the first launcher can be found in Figure 8.5.

7.4. RAMS

This section discusses the RAMS characteristics of the QLS. Reliability describes the ability of the launch system to perform the specific mission of getting the payload into a 350 km orbit in paragraph 7.4.1. Next to that, availability discusses the ability of the launch system to be kept in a functioning state in paragraph 7.4.2. Afterwards, the maintainability of the launch system is discussed in paragraph 7.4.3. It describes how the launch system can be maintained and repaired. Finally, the safety is addressed in paragraph 7.4.4. It lists the methods that are used in order not to affect the environment, wildlife and humans. Other inspections during the lifetime of the launch system are addressed as well.

7.4.1. RELIABILITY

Reliability engineering consists out of risk management, quality engineering, system safety engineering, design engineering, test and evaluation, maintainability and supportability engineering and cost-effectiveness of the system. Reliability can be defined as $Reliability = 1 - Probability\ of\ failure$ [57]. Despite the few rocket launch accidents, technology has proven that the rocket launch system is a reliable system. The QLS is expected to be highly reliable, after intensive tests and evaluations have been conducted. Examples of these tests can been found in the safety Section 7.4.4.

7.4.2. AVAILABILITY

Availability describes the degree to which the launch system is in the specified operable state at the start of the specified mission. This is related to the point in time at which the mission is initiated. In other words, it addresses the response time of the launch system to a required mission start. First, the launch system is dependent on available resources, such as materials and propellants. These need to be monitored and guided in a proper manner throughout the production process. Next to that, manufacturing multiple parts and components for repairs and sequential launches as described in the MAI Section 7.3, will improve the availability. Upon launch, the weather has a large influence on the availability. As technology keeps on improving, weather forecast does as well and launch windows can be guaranteed with an increasing precision and amount of time prior to launch. QLS strives towards a ten week response time. Nevertheless, this strongly depends on the legal framework of the country of operations, the capacity of the corresponding launch and the resources available.

7.4.3. MAINTAINABILITY

Maintainability involves maintenance planning, supportability engineering and logistic support. It is incorporated in order to perform time efficient processing, preventive and corrective maintenance, rapid fault detection and diagnosis and test and repair validation. In order to so, a maintainability programme is needed to improve operational

[4] http://www.isispace.nl/brochures/ISIS_ISIPOD_Brochure_v.7.11.pdf, visited on: 20-01-2016

availability, optimise logistic support, reduce life cycle costs and provide project management [58] [57]. Next to that, the ease and speed at which maintenance can be carried out is addressed as well. Repairs are to be carried out without affecting still functioning parts. This should be done according to both scheduled and non-scheduled maintenance activities. Hence, future maintenance will become easier and able to cope with changing environments. In order to provide proper maintenance, an outline of the maintenance activities is displayed in Figure 7.6.

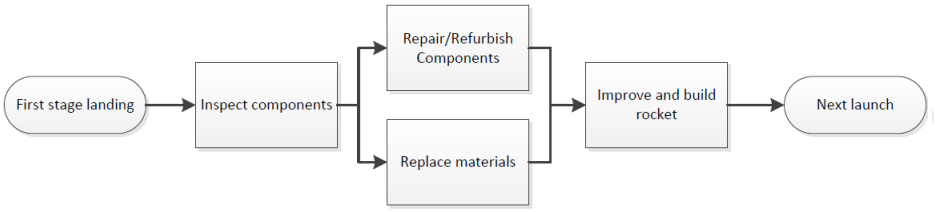

Figure 7.6: Post Launch Maintenance Activities

7.4.4. SAFETY

In order to improve the launch system in terms of safety, multiple tests have to be performed throughout the manufacturing process. This is done in such a way, to reduce risk related to environment, wildlife and human health. Safety also involves the periodic examination by specialists in order to minimise the manufacturing, testing and integration failure risks and to increase the productivity of all the processes. Proper safety management contributes to the minimisation of total cost for the launch system. Safety management is applied in the form of safety measures such as different tests. These can be listed in terms of critical safety functions:

- Chemical component analysis.
- Destructive and non-destructive sample testing.
- Software and computing systems testing, as they are critical to provide safe launch system operations [59] [60].
- Inspection on (sub)components for flaws such as cracks, peeling and loose connections.
- Employee health testing and periodic evaluation; e.g. weekly team meetings and half-year face to face evaluations.
- Geological pollution surveys near the launch site.
- Maintaining safety margins and factor in the design.
- Government related regulations and up date performed certification processes.
- Implementation of standard procedures in order to conduct activities in an efficient and correct manner. The productivity increases with both experience of the employees and the quality of manuals and instructions.
- Implementation of general safety measures and control in the whole construction process. This involves a safe working environment, with the necessary safety measures such as emergency exits, fire extinguishers and safety inspections.

Furthermore, redundant (sub)systems are implemented the launch system, in order to ensure the safety. One example is the flight termination system, which has its own battery and circuitry, such that it can always be used. Next to that, the structural components have been designed with proper safety factors, both for the reusable and expandable parts.

8

BUSINESS PLAN

8.1. MARKET ANALYSIS

In this chapter, first the market for nano- and microsatellite launchers will be discussed in Section 8.1. Next to the current market, the future market will be discussed, and recent developments like reusable launch vehicles in Section 8.1. Furthermore, the market opportunities for the QLS will be treated.

MARKET TRENDS

In this section the market trends are analysed and predicted. Firstly the current market is sketched and from this it follows why the QLS is needed. After that, the market in the near future is analysed (approximately until 5 years from now) and then the distant future market (more than 5 years from now) is predicted.

CURRENT MARKET

Currently, most of the nano- and microsatellites are launched into the space by piggybacking with other missions in order to save costs [61]. The main disadvantage of this method is, that the payload is dependent on the launch window of the rocket, and it is restricted in orbit altitude and inclination of this launch to get the payload into orbit. To get into another orbit, it needs orbit transformation [62]. Currently, there are no dedicated launch options for satellites with masses up to 50 kg [63].

NEAR FUTURE MARKET

In the satellite development a recent trend can be found, that satellites are becoming much smaller for mass reduction. Because of this mass reduction, satellite launches will become cheaper, which will make satellite launches affordable for commercial companies and universities. This growth can become even bigger, when cheaper and more flexible launch opportunities will become available [61]. Next to that, technology development will increase the capabilities of small satellites, which increases the possibilities of space missions [1].

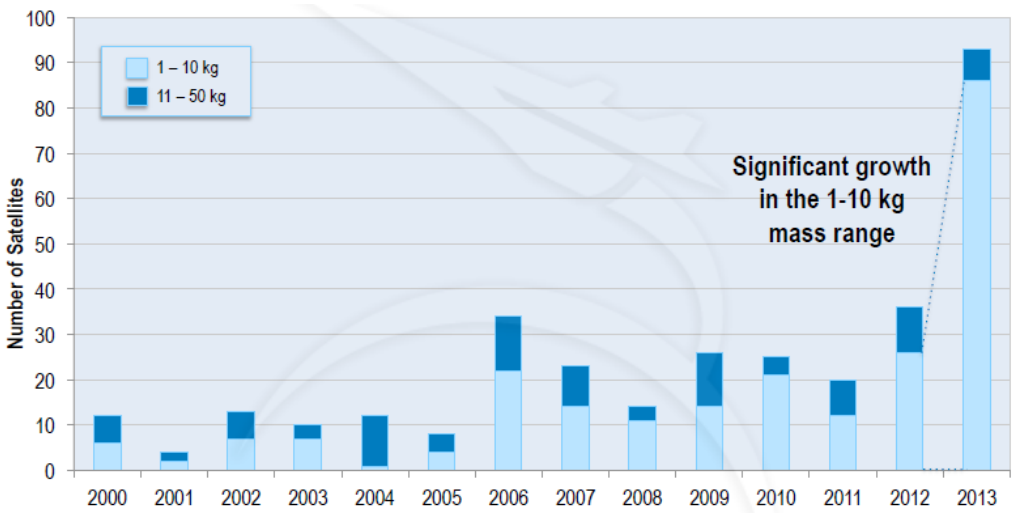

Figure 8.1: Number of nano- and microsatellite launches [64]

In Figure 8.1, the number of satellite launches in the range of 1 to 50 kg can be seen. From this figure, it can be

[1] http://www.newtonlaunchsystems.com/Modules/Activities/MarketFeasibility.aspx, visited on 13-11-2015

concluded that the amount of nano-and microsatellite launches is increasing, especially in the last few years in the range of 1 to 10 kg. According to SpaceWorks, there was a market growth for nano- and microsatellites of 37.2 % between 2009 and 2013 [64].

They expect a growth of 23.8% per year until 2020. CubeSats of 1U (10x10x10 cm with a mass of 1 kg) are used very often. However, 25% of the future nanosatellites will be around 6 kg (3U CubeSats) [64]. The only threat to this growth is the current low availability of launch systems for small satellites [65]. Next to that, a trend can be found that most of the nanosatellites will have an orbit between 600 and 850 km. However, these altitudes are most likely more due to the launch vehicle availability, than their functional applications, such as technology demonstration/experimentation, telecommunications, and earth observation [63].

DISTANT FUTURE MARKET

The QLS should be profitable on a long term basis. It should be designed for the current and short term market, but should also anticipate on the future satellite market, in terms of more than 5-10 years after the first launch. In this section several possible future market scenarios are predicted.

The first possible scenario is that there will nothing change in the current market. CubeSats will stay in the range of 1-2 kg (1U CubeSat) and 6 kg (3U CubeSat). This is also the expected market for the coming years, see Section 8.1.

The second scenario relates to the fact that electrical components become smaller every year. This means that there is a large possibility that micro satellites will become smaller as well. Predictions expect satellites in the range of hundred grams (picosatellites) in the next years and several companies are already developing them [2]. If this happens, there are two possibilities. Firstly, small satellites are common but are not launched in huge amounts every year. Secondly they are common *and* are launched in huge amounts every year. These two possibilities imply different market needs and business possibilities, and are elaborated below.

If satellites are in the order of 100 grams and the QLS brings payloads of 60 kg in orbit, 600 satellites are needed to reach the maximum payload and thus to be profitable. If the satellites become smaller, but market does not catch on and the yearly amount of picosats launched is in the order of 100-200 then the QLS will likely not be profitable. Because then it has to launch either less than the 60 kg payload and ask more money per kg or it has to wait 3 years for one launch. This is against the wishes of the customers as they want to launch quickly.

The second option is that when the picosatellites become cheap, due to smaller launch masses and more possible launch vehicles, it will become more popular. Then universities, high schools, hobbyists and other people can launch their own satellites into space for several hundred Euros. The annual amount of satellites launched would reach several thousands and the QLS can inject these satellites with hundreds at the same time. The QLS will then launch frequently and can become a big market player and provide access to space for everyone.

The possible future trends are sketched above, but there is a big uncertainty in the future trends, so the QLS should choose an option that supports a sustainable business plan for the long term. It is also possible to aim for several trends and develop a system that can handle both trends.

SHARE IN MARKET

The QLS aim on bringing payloads to an orbit of 350 km. Since this is a self-cleaning orbit, satellites will burn up in the atmosphere within in weeks to months, the greatest potential market will be the market for technology demonstration satellites. These satellites don't need a long orbital lifetime, since the demonstration will not take a very long time and within a year the technology will be most likely already outdated. This orbit choice also eliminates the concerns about space debris of CubeSats and is thus a sustainable solution.

Looking at Section 8.1, it is clear that there are no launch systems available for (clusters of) nanosatellites yet. The QLS can attract customers who want an affordable, dedicated launcher to place payloads in an orbit up to 350 km in a desired inclination.

For the coming years, it is expected that satellites become smaller. Next to that, customers want their satellites in space as soon as possible. For the QLS it would be of high importance that it can be launched quickly on demand of the client. To be flexible in launch dates, the launch vehicle should be able to launch different payload masses. It should be easy to adapt so it can launch different payload sizes together.

TARGET COST

To be competitive, the launch price should not be higher than the price of the launch systems mentioned in 8.1 and a piggyback launch. The average price for the future launch systems will be around $38.000 per kg (excluding the far

[2] http://news.discovery.com/space/private-spaceflight/tiny-thumbsats-aim-to-bring-space-to-all-151026.htm, visited on: 24-11-2015

more expensive Pegasus). So this price has to be aim for to be a competitive player in the market. The selling points of the QLS will be that it has the possibility to choose its own inclination and can be launched at any time which suits the customers. The customers might be willing to pay a bit more for the launch, due to added flexibility and independency.

POTENTIAL CUSTOMERS

Potential customers for the QLS will be universities, research and commercial institutes and the military, who wants to launch pico-and nanosatellites into an orbit up to 350 km altitude, to demonstrate their technology.

The Delft University of Technology is the first potential client. It has its own satellite program, called the Delfi Program. This program contains the development and operation of CubeSats [3]. However, since the development costs of the QLS will likely be too high for the Delft University alone, other clients should be found, who want to co-invest in the development of the launch system. Furthermore, if more launches are conducted and more satellites are launched together, the costs per launch per satellite can be reduced.

COMPETITORS

Commercial companies started developing launch systems for small satellites, including nano- and microsatellites. These companies planned their first flights in the coming years and thus can also become competitors of the QLS. Below are some examples.

- Virigin galactic is developing the *LauncherOne*, which is a rocket that will be air launched via a carrier aircraft. It can carry a payload of 200 kg and it will cost less than $10 million [4].
- Firefly Space Systems Inc. has the *Firefly α*. This rocket is ground launched, and will be able to bring a 200 kg payload to an altitude of 500 km. They promise a cost of $8 million per launch [5].
- Rocket Lab USA makes the *Electron*, a rocket that will be capable of bringing a 150 kg payload into an orbit of 500 km. The price of a launch will be $4.9 million [6].
- XCOR is developing the *LYNX*, a space aircraft, which is foremost used for space tourism. The LYNX can fly up to an altitude of 100 km, from which it could bring small satellites further into space. The price for launching payloads is not known. The price for a ticket will be between $100.000 and $150.000 [7].
- GenerationOrbit is developing the *GoLauncher 2*. This is an air launched rocket, which is capable of bringing payloads up to 45 kg into altitudes up to 740 km, for a price of $2.5 Million [8].
- Interorbital Systems is developing *Neptune N-series launch vehicles*, which can be customised for each mission by varying the number of common propulsion modules and stages. Payloads varies from a minimum of 30 kg up to 1000 kg. The cost varies from $4.000 to $12.500 per kilogram to a LEO of 310 km.
- On the ISS, NanoRacks has installed a launch system for CubeSats. These CubeSats are transported to the ISS with cargo load, after which they are launched into space with the *CubeSat Deployer*, which makes use of a spring. Currently, PlanetLabs is making use of this device to place their CubeSats in orbit.

One of the few available launch systems for small satellites up to now is the *Pegasus*. This is an air launched rocket, which is capable of bringing satellites up to 400 kg into Low Earth Orbit. The price of a launch is $55 Million [9] [10]. In Table 8.1, the price per kg of payload for these launch systems is shown.

[3] http://www.delfispace.nl/, visited on: 16-11-2015
[4] http://www.virgingalactic.com/satellite-launch/, visited on: 13-11-2015
[5] http://www.fireflyspace.com/vehicles/firefly-a, visited on: 13-11-2015
[6] http://www.rocketlabusa.com/, visited on: 13-11-015
[7] http://aerospace.xcor.com/reusable-launch-vehicles/lynx-spacecraft/, visited on: 13-11-2015
[8] `http://www.generationorbit.com/golauncher2.html`, visited on: 18 November 2015
[9] https://www.orbitalatk.com/flight-systems/space-launch-vehicles/pegasus/, visited on: 16-11-2015
[10] http://innerspace.net/current-launch-vehicles/pegasus-launch-cost-soars-to-55-million/, visited on: 16-11-2015

Table 8.1: Prices per kg payload for various launch vehicles

Launch Vehicle	Payload Mass [kg]	Orbit altitude [km]	Price/kg [$]
LauncherOne	200	Not known yet	50.000
FireFly	200	500	40.000
Electron	150	500	32.666
GoLauncher 2	45	740	55.000
Neptune N-series	30 - 1000	310	12.500
Mean			**38.000**

REUSABLE VEHICLES

Currently, a few companies are experimenting with reusable vehicles to become cheaper. Some examples are listed below. These are not operational yet, they are all still in the development phase, except for the *Falcon 9*. SpaceX succeeded to recover the first stage landing it vertically on land in December 2015.

- Airbus Space and Defence is developing *Adeline*. The main stage of the rocket, with avionics and motor will fly back to Earth and land horizontally [11].
- SpaceX is developing *Falcon 9*. The main stage of the rocket lands vertically back on Earth [12].
- Blue Origin's *Orbital Launch Vehicle*. The vehicle, which is intended for manned flight, will land with a parachute, whereas the main stage will land vertically with rocket boosters [13].
- Reaction Engines is developing *Skylon*. This is an aircraft that can go to space, which uses SABRE engines. These engines are firstly used as aircraft engines, and when leaving the atmosphere they "transform" into rocket engines [14].
- Swiss Space Systems is developing *SOAR*, a re-entry vehicle which will be air launched, and can bring small satellites into orbit [15].

FINAL RECOMMENDATION ON BUSINESS PLAN

To conclude, the main objective of the QLS should be to launch small payloads to an orbit of 350 km. This orbit is ideal for small satellites as the lifetime is long enough to demonstrate new technology, and it is also a self-cleaning orbit. This means that the space debris problem is solved. Later, when small satellites become even cheaper, actual operational missions can also be placed in this orbit. When the operational payload falls back to Earth it is cheap and easy to replace it by a new (updated) version of the same satellite. Not many launchers can launch to this orbit yet, so the QLS should respond to this.

Customers prefer to launch as soon as possible after they reserve a launch slot. The QLS should respond to this need to obtain a strong competitive position among other launch providers. That is why it is important that different payload sizes can be launched, so the client has not to wait until other clients have registered until the required amount of payload is reached. Next to that, operations and logistics should be kept as simple as possible, so a quick launch could be guaranteed.

Furthermore, the market needs may change in the future and QLS should capitalise on this to stay profitable on a long term basis. It is advisable to consider a design that is able to launch either smaller and bigger payloads, in the range of 10 to 60 kg, while still making profit.

The vision here at Quantum is that once the QLS can place payloads into orbit of 350 km for a competitive price and the trend in miniaturisation of satellites continues, it can work in favour of the sales volume: it becomes cheap to place nano- and picosats in space so everyone can and will do it. Then the demand on launches increases dramatically and the QLS can launch more frequently and make more gross revenue. This results in affordable access to space for everyone.

[11] https://airbusdefenceandspace.com/reuse-launchers/, visited on: 13-11-2015
[12] http://www.spacex.com/falcon9, visited on: 13-11-2015
[13] https://www.blueorigin.com/technology, visited on: 13-11-2015
[14] http://www.reactionengines.co.uk/space_skylon.html, visited on: 13-11-2015
[15] http://www.space.com/20449-swiss-private-rocket-plane-2017.html, visited on: 13-11-2015

8.2. COST ANALYSIS

The cost per launch will be divided in two different segments; production costs and operational costs.

Production Costs
The production costs consists of the costs for all the subsystems, which can be found in table 8.2. The propulsion, structure and recovery subsystem will be produced by the company itself. The costs for the other subsystems, which are bought of the shelf, were based on the price mentioned by the supplier. If these were not given, estimations were made according to similar products. Since the first stage will be recovered, the production costs for this stage can be saved for the next launchers. These are the structure costs and engine costs and the recovery system. The parts of the ADCS, EPS and RCS which are in the first stage can also be used again.

The main costs for production consists of the propulsion subsystem. The engine production cost can be calculated with Equation 8.2, based on the TransCost Model [10]. In this equation the costs for the whole propulsion system is included. The cost reduction factor (f_4) can be calculated with Equation 8.1, where p is the learning factor (assumed at 0.8). The commercial cost reduction factor f_{11} is assumed at 0.5, based on [66] and [10]. Next to that, the productivity factor f_8 is assumed at 0.86, assumed it will be build in Europe [10]. The automatic fabrication reduction factor f_{10} is added, because 3D printing technology will be used which will give a reduction factor of 0.5, since almost all touch labour costs, which are in total 30 % of total production costs [10], can be removed, and the automatic fabrication factor of the TransCost Model is applied, which gives a value of 0.7. Myr is the cost for one manyear, which has a value of $320,000 according to the Transcost Model. However, it says that this value could be much lower for start up companies [10], so a value of $130,000 is used.

The production costs for building the structure, can be calculated with Equation 8.3. Here the automatic fabrication factor will be 0.7 according to [10], since 3D printing technology can not be used to build the whole structure. The other factors remain the same.

The recovery system consists of a parachute. The price estimation for the parachute is based on the fact that building a human parachute costs $2,000 [16]. The recovery parachute is thirteen times as big, so the costs will be around $30,000.

$$f_4 = N^{\frac{ln(p)}{ln(2)}} \tag{8.1}$$

$$C_{engine} = 1.2 \cdot M^{0.535} \cdot f_4 \cdot f_8 \cdot f_{10} \cdot f_{11} \cdot Myr \tag{8.2}$$

$$C_{stage} = 1.265 \cdot {M_{dry}}^{0.59} \cdot f_4 \cdot f_8 \cdot f_{10} \cdot f_{11} \cdot Myr \tag{8.3}$$

Table 8.2: Production costs

Subsystem	**Costs [$]**
Engine stage 1	501360
Engine stage 2	127760
Engine stage 3	84310
RCS stage 1	10000
RCS stage 3	10000
Structure stage 1	1034300
Structure stage 2	521350
Structure stage 3	368320
ADCS	23000
Recovery	30000
EPS	7500
Communication	3000
FTS	5000
Production costs first production	2725900
Saved by recovery	1588910
Production costs next launcher	**1295881**

Operational costs
The operational costs consist of the ground and flight operations, propellants and the recovery of the system. An overview of these costs is given in Table 8.3. These costs are much influenced by the number of launches N and launch rate L, which are assumed to be 10 and 5, respectively. It is assumed that higher values for this give a to large

[16] http://www.nationalparachute.com/page8.html, visited on: 15-11-2016

reduction factor f4. The pre-launch ground operations can be calculated with Equation 8.4. This segment consists of the assembly of the rocket on the launch pad and testing of the systems [10]. New factors in this equations are f_v and f_c, which are factors for the vehicle type and the assembly and integration mode. f_v is fixed at 0.7 for reusable launch vehicles, f_c is 0.7 for a rocket which will be assembled horizontally, after which it will be lifted vertically. The propellant costs are also included in the operational costs. These costs can change a lot over a long period of time. However, as can been seen, propellant is not a huge cost factor and will have almost no influence on the total costs.

$$C_{ops} = 8 \cdot \frac{MGTOW}{1000}^{0.67} \cdot L^{-0.9} \cdot N^{0.7} \cdot f_v \cdot f_c \cdot f_4 \cdot f_8 \cdot f_{11} \cdot Myr \tag{8.4}$$

Furthermore, the launch, flight and mission operation costs are considered. This phase consists of mission planning and preparation, launch and ascent flight control until payload separation and control of the re-entry of the first stage. It can be calculated with Equation 8.5. In this equation, Q_N is a complexity factor, which is the sum of complexity of each stage, given a complexity factor of 1.0 for the first stage (because of reusability) and 0.4 for the second and third stage.

$$C_M = 20 \cdot Q_N \cdot L^{-0.65} \cdot f_4 \cdot f_8 \cdot Myr \tag{8.5}$$

Finally, the recovery costs are considered. These costs consist of the recovery of the first stage. This can be calculated with Equation 8.6. Here M is the mass to recover. These costs are low as expected, since only a mass of around 700 kg has to be recovered. Next to these costs for transportation back to the launch pad, maintenance and refurbishment costs has to be taken into account for the first stage. A budget of $215,000 is reserved for this, since it is assumed not every flight components have to be changed.

$$C_{Rec} = \frac{1.5}{L(7L^{0.7} + M^{0.83})} \cdot f_8 \cdot f_{11} \tag{8.6}$$

Table 8.3: Operational costs

Pre-launch ground operations	$ 234140
Propellant costs	$ 9200
Mission operation costs	$ 673730
Recovery and maintenance costs	$ 215000

COST DISCUSSION

In Table 8.4 an overview of the costs per launch is given. It is assumed that the first stage can be used at least ten times before it has to be replaced. This will give a production cost reduction of around $1.5 million.

This cost model is only used as a overview of the project costs, and in a further phase of the design the exact costs can be calculated based on material and man hours needed. Next to that, bought of the shelf subsystems could differ in price than is stated. However, these costs will not influence the total price per launch very much, because they cover only a slightly part of the costs. Man hours needed, during production and operations, will have the most influence on the total costs. For example, increasing the manyear costs from $130000 to $150000, will increase the costs per launch by 15 %. Reducing the Also the number of total launches have a big impact on the price per launch, increasing the number of launches can further decrease the costs per launch. This is mainly due to the series production reduction factor. In Figure 8.2 this factor shown for the number of flights. As can been seen, this value will also largely depend on the learning factor p. However, there will be a maximum for this, and to be safe a value of 0.4764 is chosen.

Table 8.4: Cost per launch

Production Costs	$ 1295881
Operational costs	$ 1132070
Cost first launch	$ 3857970
Cost next launch	$ 2427951
Mean costs per launch	**$ 2570953**
Price per kg payload	**$ 42850**

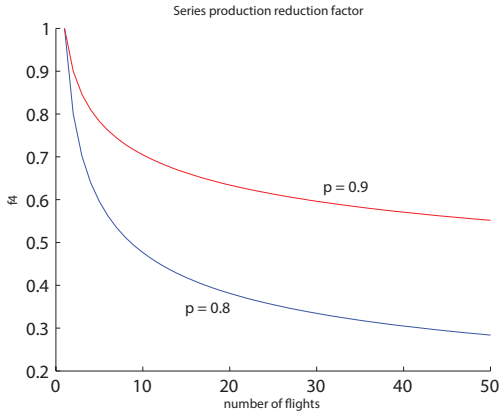

Figure 8.2: Series production reduction factor

8.3. SPACE LAW OBEDIENCE AND CERTIFICATION

In order to guide all space related activities in an organised manner, according to the United Nations Space Treaties [67], the Dutch government has established the law for space activities. The purpose of this law is to regulate the space activities that belong to Dutch jurisdiction. Next to that, procedures tracing the establishment and registration of space objects is identified. The Dutch government holds the responsibility for the damage that is caused by space objects, which are operationally controlled on a daily basis from within the Netherlands.

In order to conduct space activities, QLS has to provide an application for a permit to the Dutch government. This permit will allow to either launch, control and/or maintain space systems from within the Netherlands. The permit request will be submitted for approval to the Dutch Telecom Agency, who will perform the authorisation process. They will take a look to the finances, the insurances and the techniques involved in the space related activities. A report will be made which discusses the safety and feasibility of the proposed space system, with which approval can then be granted. [68] [69]. On January 15th, 2015, the Dutch space law has been expanded in order to conduct permits for unguided satellites [70]. This is beneficial for the Netherlands, who is one of most prominent market players on the are of developing and building unguided satellites and components as well as distributing to third parties. On an academical level Delft University of Technology stimulates the development of technology by means of educative programs in the area of unguided satellites. They are being developed and build by students, in cooperation with the Dutch aerospace industry.

8.4. POST-DSE ACTIVITIES

Now that the conceptual design phase during the DSE has been completed, the next phases of the project mission should be considered. These are shown in Figure 8.3. In the next phase, the preliminary design phase, the different subsystems have to be designed in more detail, after which they have to be verified. In the detailed design phase, all these subsystems have to be integrated with each other. After this integrated design is made, it has to be verified and validated. This will be iterated until an optimal final design is generated. Once this design is made, the production and testing phase starts. After assembly of every subsystem and the system as a whole, testing occurs. In case of errors or failures, the seriousness of these problems have to be assessed. In most cases re-assembly is performed, but in case the (sub)system will not perform as expected, that particular (sub)system will have to go back to the design phase. When all the test results are satisfactory, the production phase is finalised and the system is ready for launch. The first launch is scheduled in the year 2021. The time schedule for the different phases is shown in the Gantt chart, in Figure 8.4 and 8.5. In this chart it can be seen that the different subsystems will be designed, assembled and tested in parallel, where the complex subsystems (propulsion in particular) are scheduled to take more time. During the detailed design, the complete system design task runs throughout the whole phase because the different subsystems have to be integrated into the whole system, which is an iterative process.

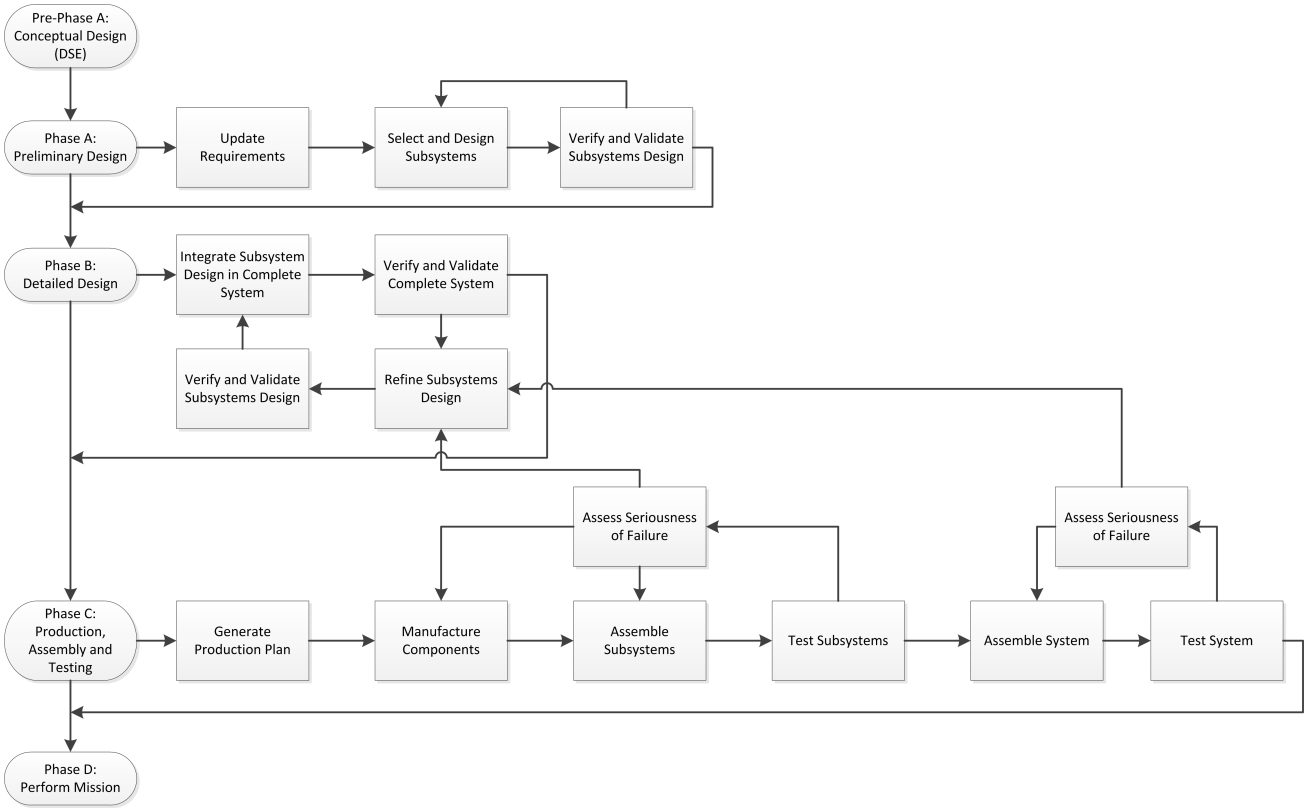

Figure 8.3: Project Logic Flow Diagram

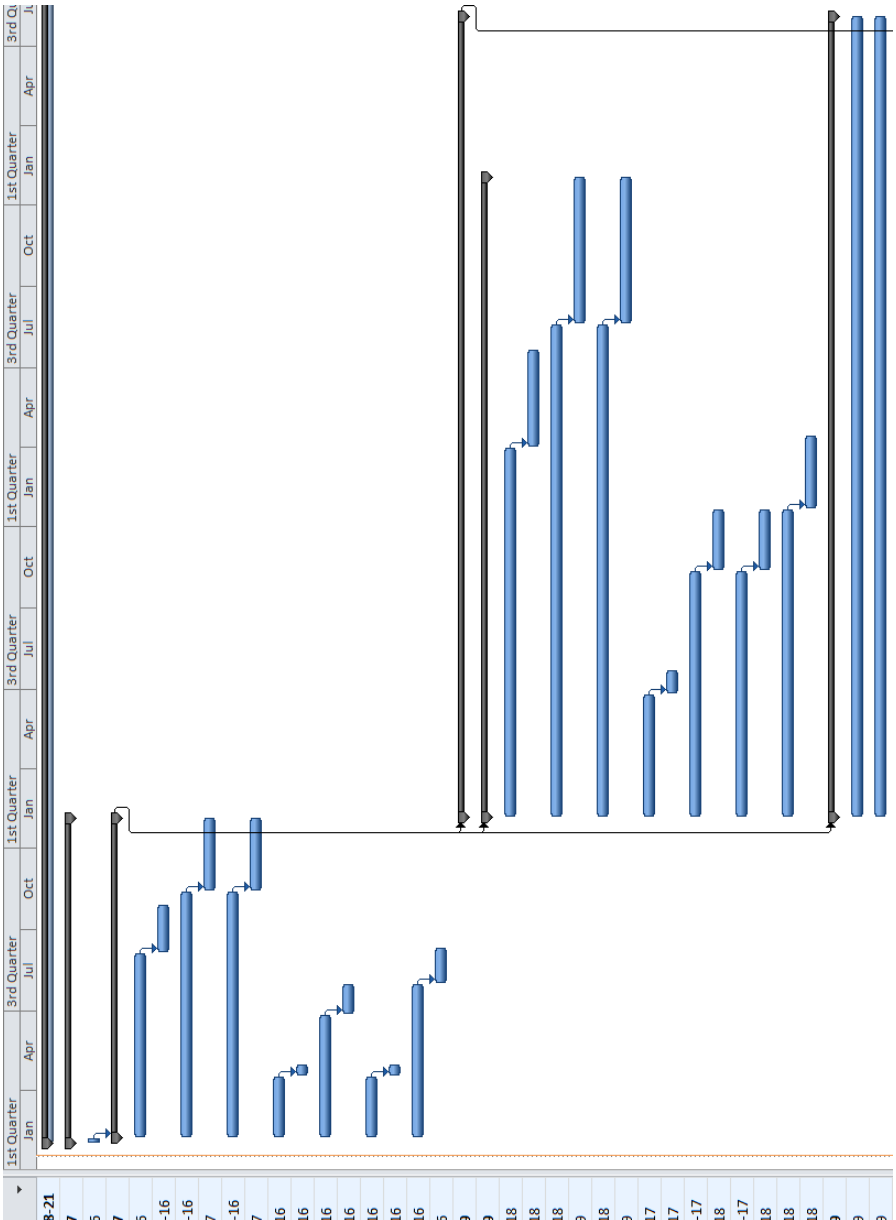

38	**Phase D: Production, Assembly and Testing**	**535 days**	**Mon 5-8-19**	**Fri 20-8-21**	
39	Generate Production Plan	4 wks	Mon 5-8-19	Fri 30-8-19	
40	**Subsystems Production**	**340 days**	**Mon 2-9-19**	**Fri 18-12-20**	
41	**ADCS Production**	**110 days**	**Mon 2-9-19**	**Fri 31-1-20**	
42	Manufacture ADCS Components	1 wk	Mon 2-9-19	Fri 6-9-19	
43	Assemble ADCS	1 wk	Mon 9-9-19	Fri 13-9-19	
44	Test ADCS	20 wks	Mon 16-9-19	Fri 31-1-20	
45	**Propulsion Subsystem Production**	**340 days**	**Mon 2-9-19**	**Fri 18-12-20**	
46	Manufacture Propulsion Subsystem Components	5 wks	Mon 2-9-19	Fri 4-10-19	
47	Assemble Propulsion Subsystem	8 wks	Mon 7-10-19	Fri 29-11-19	
48	Test Propulsion Subsystem	55 wks	Mon 2-12-19	Fri 18-12-20	
49	**Structures Subsystem Production**	**250 days**	**Mon 2-9-19**	**Fri 14-8-20**	
50	Manufacture Structures Subsystem Components	10 wks	Mon 2-9-19	Fri 8-11-19	
51	Assemble Structures Subsystem	20 wks	Mon 11-11-19	Fri 27-3-20	
52	Test Structures Subsystem	20 wks	Mon 30-3-20	Fri 14-8-20	
53	**FTS Production**	**180 days**	**Mon 2-9-19**	**Fri 8-5-20**	
54	Manufacture FTS Components	1 wk	Mon 2-9-19	Fri 6-9-19	
55	Assemble FTS	10 wks	Mon 9-9-19	Fri 15-11-19	
56	Test FTS	25 wks	Mon 18-11-19	Fri 8-5-20	
57	**EPS Production**	**65 days**	**Mon 2-9-19**	**Fri 29-11-19**	
58	Manufacture EPS Components	1 wk	Mon 2-9-19	Fri 6-9-19	
59	Assemble EPS	4 wks	Mon 9-9-19	Fri 4-10-19	
60	Test EPS	8 wks	Mon 7-10-19	Fri 29-11-19	
61	**Communication Subsystem Production**	**55 days**	**Mon 2-9-19**	**Fri 15-11-19**	
62	Manufacture Communication Subsystem Components	1 wk	Mon 2-9-19	Fri 6-9-19	
63	Assemble Communication Subsystem	2 wks	Mon 9-9-19	Fri 20-9-19	
64	Test Communication Subsytem	8 wks	Mon 23-9-19	Fri 15-11-19	
65	**Recovery Subsystem Production**	**275 days**	**Mon 2-9-19**	**Fri 18-9-20**	
66	Manufacture Recovery Subsystem Components	5 wks	Mon 2-9-19	Fri 4-10-19	
67	Assemble Recovery Subsystem	10 wks	Mon 7-10-19	Fri 13-12-19	
68	Test Recovery Subsystem	40 wks	Mon 16-12-19	Fri 18-9-20	
69	**Complete System Production**	**175 days**	**Mon 21-12-20**	**Fri 20-8-21**	
70	Assemble Complete System	15 wks	Mon 21-12-20	Fri 2-4-21	
71	Test Complete System	20 wks	Mon 5-4-21	Fri 20-8-21	
72	**Phase E: Launch**	**1 day**	**Mon 23-8-21**	**Mon 23-8-21**	

Figure 8.5: Project Gantt Chart - Phases D and E

9

Conclusion and Recommendations

9.1. Conclusion

The main task of this report was to come up with an affordable, sustainable and reusable rocket design which can bring payloads up to 60 kg into 350 km LEO for less than $50,000 per kg.. For this purpose, an assisted aircraft launch system, a reusable ground launched rocket and a railgun system were considered. In the trade-off before the mid term review half way throughout the project, the reusable ground launched rocket was selected for the final detailed design, which has the lowest costs and copes best with the specified payload.

The way to achieve the design was an iterative design process together with a systems engineering approach. Many iterations were made and to optimise the design with respect to lift off mass. In order to have both a sustainable and reusable rocket, the clean propellants LOX and LCH4 are used. This combustion process leaves a very low amount of soot and other residues in the engine. The 18 m high, 1 m wide and 9202 kg heavy rocket consists out of three stages, from which the third stage has an adaptive payload bay. Several payload configurations can be fitted, such as multiple nano-satellites, pico-satellites and small micro-satellites. The rocket flies to the designated 350 km LEO, at which the payload will be injected into a self-cleaning space debris orbit.

The first stage will be fully recovered. This is done using a boost back manoeuvre in order to direct the first stage towards the landing zone within 1 km from the launch site. At 12 km altitude the 13 m^2 drogue chute deploys in order to decrease the terminal velocity of 762 m/s and reach the safe subsonic velocity of 77 m/s, at which the main ram air 507 m^2 parafoil unfolds. This parafoil is being controlled by two servo motors, in order to make accurate landings up to 20m. The landing is assisted by three deployed oil-spring shock absorbing landing legs to reduce the landing speed from 5 m/s to a full stop without damaging any systems.

Production costs are reduced by making use of automatic fabrication, such as 3D printing for several engine parts (turbo pumps, nozzles). Next to that, using similar propellant tanks, engines and nozzles in different stages will make fabrication more affordable. The operational costs are reduced by placing all the facilities needed at one place. The minimum amount of facilities needed is two; production/testing facility and the launch site. When this all is realised, the price per kg payload will be $42850.

9.2. Recommendations

Further improvements can be added into the TST. First, it would be to better simulate the control losses of the launcher. The contribution of disturbance forces can also be modelled to allow for a more accurate representation of the trajectory and losses. The non-spherical Earth assumption can also be taken out to include earth rotation and J2 effects. Finally the TST can be expanded into a three dimensional analysis to show the possible inclination changes and variation. For the propulsion it is recommended to implement changing gas properties for the throttling calculations. The other calculations are deemed to be of sufficient enough quality. The actual designs of the engines can however be improved significantly, now it only gives estimations on the mass. This is a time consuming process, so sufficient resources should be made available for this.

Further vibrational analysis should be done using finite element methods. This would give more accurate damping coefficients and natural frequency. The same holds for structures, a finite element analysis should be done in order to analyse the parts of the launcher which carry low stresses, since these could have a lower thickness, which means the total structural mass could be lower. Next to that, The EPS can be further expanded upon in the next detailed design phase of the design process. This can include more detailed mass and power estimations to include in the iteration process. Exact load profiles can also be analysed to further refine the EPS load and regulation requirements and possibly reduce total EPS mass. The Quantum launch system is expected to be able to launch from a wide range of launch sites, as long as the propellants LOX and LCH4 are available. Nevertheless, it can be recommended to select the most optimal launch sites, taking logistics and availability into account.

An important note is that all starting point inputs for the design of the main parafoil parachute came from reference parachutes. Those inputs determine every design parameter of the chutes. For the pilot chutes and drogue chute (which can be off-the-shelve chutes) those data will be quite accurate. The main parafoil chute will need extensive experimenting and testing to get more accurate inputs. During testing it might be discovered, that the final size and mass of the parachute may therefore differ.

Finally, to cut on the cost, it should be investigated whether existing (off-the-shelf) engines may be adopted, since engines are the most complex parts of the system.

REFERENCES

[1] B. Zandbergen, *AE4-S01 Thermal Rocket Propulsion, Lecture Notes* (Delft University of Technology, 2012).

[2] H. Burkhardt, M. Sippel, A. Herbertz, and J. Klevanski, *Comparative study of kerosene and methane propellant engines for reusable liquid booster stages,* ICLT, DLR (2002).

[3] R. A. Braeunig, *Rocket & Space Technology* (Braeunig, 2015).

[4] J. Cornelisse, *Rocket Propulsion and Spacecraft Dynamics* (Pitman, 1979).

[5] A. Urbano and F. Nasuti, *The influence of liquefied natural gas composition on its behavior as a coolant,* EUCASS (2013).

[6] A. H. Holger Burkhardt, Martin Sippel and J. Klevanski, *Comparative Study of Kerosene and Methane Propellant Engines for Reusable Liquid Booster Stages*, Tech. Rep. (DLR, 2002).

[7] G. P. Sutton and O. Biblarz, *Rocket Propulsion Elements* (Wiley Intersience, 2001).

[8] K. H. H., *Handbook of Astronautical Engineering* (McGraw-Hill Book Company, New York, 1961).

[9] S. Harper, *Bipropellant Rocket Engines* (Aerojet Rockeydyne, Redmond, 2009).

[10] D. E. Koelle, *Handbook of Cost Engineering and Design of Space Transportation Systems* (TCS - TransCostSystems, 2013).

[11] A. Ponomarenko, *Rocket Propulsion Analysis Tool* (Kharkov Aviation Institute - KhAI, USSR, 2008).

[12] A. Cervone, *Power and Propulsion, Lecture Notes* (Delft University of Technology, 2012).

[13] J. R. Hulka, *Scaling of Performance in Liquid Propellant Rocket Engine Combustion Devices*, Tech. Rep. (NASA Technical Reports Server, Jacobs Engineering ESTS Group, Huntsville, 2009).

[14] A. Joshi, *Lithium Aluminium Alloys - The New Generation Aerospace Alloys*, Tech. Rep. (Mechanical Engineering Department-Indian Institute of Technology-Bombay, 2015).

[15] M. D. Klem, *Liquid Oxygen/Liquid Methane Propulsion and Cryogenic Advanced Development*, Tech. Rep. (NASA Glenn Research Center, Cleveland, Ohio, USA, 2015).

[16] e. a. P.Baiocco, G.Ramusat, *Marshall Space Flight Center,* NASA (2015).

[17] M. Pessin, J. Butler, and J. S. Sparks, *Thermal Protection Systems* (Engineering Innovations, 2005).

[18] B. Zandbergen, *Aerospace Design & Systems Engineering Elements I, Part: Launcher Design and Sizing*, Delft University of Technology (2015).

[19] P. Ritter, *Optimization and Design for Heavy Lift Launch Vehicles*, Tech. Rep. (University of Tennessee, Knoxville, 2012).

[20] G. Crowell, *The Descriptive Geometry of Nose Cones*, Tech. Rep. (University of Sao Paulo, 1996).

[21] R. D. Breuker, *Lecture notes,* AE2106:Vibrations (2014).

[22] N. Granick and J. E. Stern, *Material Damping of Aluminum by a Resonant-Dwell Technique*, Tech. Rep. (NASA Goddard Space Flight Center, Greenbelt, Md., 1965).

[23] C. de Visser and R. van Paassen, *Course summary,* AE2235-I:Aerospace Systems and Control Theory (2015).

[24] e. a. P.Baiocco, G.Ramusat, *Aerodynamic predictions, comparisons, and validations using missile datcom (97) and aeroprediction 98 (ap98),* Journal of Spacecraft and Rockets **42, No. 2**, 257 (2005).

[25] G. Navistar, *Global Positioning System Standard Positioning Service Performance Standard*, Tech. Rep. (U.S. Department of Defence, 2008).

[26] M. Naeije and E. Mooij, *Ae4870a rocket motion: Air launch to orbit,* Lecture slides (2015).

[27] J. R. Wertz and W. J. Larson, *Space Mission Analysis and Design*, 3rd ed. (Microcosm, 1999).

[28] A. Cervone, *Spacecraft telecommunications, lecture 10,* AE 2111-II Aerospace Design and Systems Engineering Elements Lecture Slides (2013).

[29] A. Cervone, private communication (January 2016).

[30] B. Zandbergen, *Aerospace Design & Systems Engineering Elements I, Part: Spacecraft (bus) Design and Sizing*, Delft University of Technology (2013).

[31] A. Cervone, *Spacecraft telecommunications, lecture 09,* AE 2111-II Aerospace Design and Systems Engineering Elements Lecture Slides (2013).

[32] P. Fortescue, G. Swinerd, and J. Stark, *Spacecraft Systems Engineering* (John Wiley & Sons, Ltd, 2011).

[33] E. Smit (T-Minus Engineering), private communication (January 2016).

[34] T. Knacke, *Parachute Recovery Systems Design Manual* (Para Publishing, 1992).

[35] J. Lingard, *Precision Aerial Delivery Seminar Ram Air parachute Design*, Tech. Rep. (Martin-Baker Aircraft Co. Ltd., 1995).

[36] Y. Li and H. Lin, *Theoretical Investigation of Gliding Parachute Trajectory With Deadband and Non-Proportional Automatic Homing Control*, Tech. Rep. (Chinese Academy of Space Technology, 1991).

[37] e. a. Cindie Giummarra1, Bruce Thomas, *New Aluminum Lithium Alloys For Aerospace Applications*, Tech. Rep. (Bombardier Aerospace, 2007).

[38] N. S. Currey, *Aircraft Landing Gear Design Principles and Practices* (American Institute of Aeronautics and Astronautics, 1988).

[39] FAA, *Expected casualty calculations for commercial space launch and reentry missions,* (2000).

[40] FAA, *Title 14 code of federal regulations (cfr),* (2016).

[41] ITT Industries, *Non-traditional flight safety systems & integrated vehicle health management systems,* (2003).

[42] R. C. Council, *Enhanced flight termination system study,* (2002).

[43] D. Tow and D. Arce, *Enhanced flight termination system flight demonstration and results,* (2007).

[44] R. C. Council, *Flight termination receiver catalog,* (1993).

[45] R. C. Council, *Irig standard 313-01: Test standards for flight termination receivers/decoders,* (2001).

[46] R. C. Council, *Irig standards for uhf command systems,* (1985).

[47] E. Mooij and Z. Papp, *Simulation, verification and validation,* Lecture Notes (2015).

[48] M. Naeije, *Project Guide DSE - Affordable and Sustainable University Launch System*, Delft University of Technology (2015).

[49] J. Hartsfield, *NASA X-38 Team Flies Largest Parafoil Parachute in History*, Tech. Rep. (Johnson Space Center, 2000).

[50] A. Cervone, *Verification & validation for spacecraft propulsion,* AE 3211-I Systems Engineering and Aerospace Design Lecture Slides (2015).

[51] H. Hecht and M. Hecht, *Reliability prediction for spacecraft,* National Technical Information Service - RADC-TR-85-229 (December 1985).

[52] NASA, *Safety Standard for Oxygen and Oxygen Systems*, Tech. Rep. (NASA, 1996).

[53] A. e. a. Van Kleef, *Innovative Small Launcher*, Tech. Rep. (Reinventing Space Conference, 2015).

[54] J. Sinke, *Lecture Notes Production of Aerospace Systems, AE3211-II,* Delft University of Technology (2015).

[55] M. K. Steitz, D.E. and E. Dick, *Industry Test Additively Manufactured Rocket Engine Injector*, Tech. Rep. (NASA, 2015).

[56] C. H. Shitong Wei and J. Chen, *Study of friction stir welding of 01420 aluminum–lithium alloy,* Material Science and Engineering **452-453**, 170 (2007).

[57] M. S. Fayssal, R. Stutts, and S. Broussard, *Reliability and Maintainability Role in Designing for Safety and Affordability* (NASA, 2013).

[58] E. Gill, *Aerospace Design & Systems Engineering Elements I, Lecture Notes* (Delft University of Technology, 2012).

[59] D. P. Murray and T. L. Hardy, *Developing safety-critical software requirements for commercial reusable launch vehicles,* FAA, Washington (2011).

[60] B. O'Connor, *NASA Software Safety Guidebook, NASA Technical Standard*, nasa-gb-8719.13 ed. (NASA, 2004).

[61] A. van Kleef and B. Oving, *Affordable Launch Opportunities for Small Satellites*, Tech. Rep. (Nederlands Lucht- en Ruimtevaartcentrum, 2012).

[62] J.-J. Miau and R. Holdaway, *Reducing the Cost of Spacecraft Ground Systems and Operations* (Springer Science & Business Media, 2000).

[63] D. DePasquale, A. Charania, H. Kanayama, and S. Matsuda Matsuda, *Analysis of the Earth-to-Orbit Launch Market for Nano and Microsatellites*, Tech. Rep. (American Institute of Aernoautics and Astronautics, 2010).

[64] E. Buchen and D. DePasquale, *Nano / microsatellite market assessment,* SpaceWorks Enterprises (2014).

[65] N. Crisp, K. Smith, and P. Hollingsworth, *Small Satellite Launch to LEO: a Review of Current and Future Launch Systems*, Tech. Rep. (The University of Manchester, 2014).

[66] D. Gibson, *Commercial Space Tourism: Impediments to Industrial Development and Strategic Communication Solutions* (Bentham Books, 2012).

[67] United Nations, *United Nations Treaties and Principles on Outer Space* (United Nations, New York, 2002).

[68] P. Haanappel, *The Law and Policy of Air Space and Outer Space* (Kluwer Law International, 2003).

[69] I. Diederiks-Verschoor and V. Kopal, *An Introduction to Space Law*, 3rd ed. (Wolters Kluwer, 2008).

[70] N.L. Government, *Dutch Bulletin of Acts and Decrees*, 18th ed. (Government Gazette, 2015).

A

Group Organisation

This appendix lists the group members in Table A.2. Next to that, the personal contribution of each team member to this midterm report is given in Table A.1. For the remaining chapters, the writing has been mostly performed by the names indicated. Next to that, contributors performing assistance are indicated.

Table A.1: Task Division

Chapter		Member(s) Responsible
Preface		Y
Summary		J, B
1.	Introduction	L, J
2.	Project Overview	L, A
3.1	Flight Dynamics	P, G
3.2	Propulsion Subsystem	A, S, Th
3.3	Structures	A, M, Th, S, Y
3.4	Aerodynamics	J, G, Y
3.5	ADCS	L, J, B
3.6	Electrical Power Subsystem	G
3.7	Communication Subsystem	L, B
3.8	Recovery Subsystem	M, To, Y
3.9	FTS Subsystem	A
3.10	Payload Integration	S
3.11	Design Process	S, P, G
3.12	Layout	T, Th
4.1	Verification and Validation	Y, S, L, A, P, J
4.2	Compliance Checks	S, J, Y, A
4.3	Sensitivity Analysis	P, G
5	Performance Analysis	To, P
6	Sustainable Strategy	M
7.1	Risk Analysis	M, Th
7.2	Operations & Logistics	J, To
7.3	MAI	B
7.4	RAMS	Th
8.1	Market Analysis	S, L
8.2	Cost Analysis	L
8.3	Space Law Obedience and Certification	Th
8.4	Post-DSE Activities	L, A
9.1	Conclusion	Th, L

Table A.2: Team Members' Initials

Member	Initials
Tom Becx	To
Alessandro Gianolio	A
Bart Helder	B
Thomas van't Klooster	Th
Stijn Koehler	S
Michelle Koivisto	M
Lars van der Linden	L
Gary Phua	G
Jorgis Theodoulou	J
Peter Wiegman	P
Yama Shewan	Y

B

List of Contacts

Table B.1 displays a list of both internal and external contacts that were contacted in order to give assistance to several different fields of engineering applied to the project.

Table B.1: List of Internal and External Contacts

Name	From	Field
A. Bonnema	ISIS BV	Launch logistics
A. Calvi	ESA	Structures
A. Cervone	TU Delft	Propulsion
A. Gianolio	ESA	Space Systems
A. Ho	ISIS BV	CAD Modelling
A. van Kleef	NLR	Space Systems
A. de Windt	TU Delft	Missle DATCOM
B. Orving	NLR	Small Space Systems
B. Zandbergen	TU Delft	Rocket Propulsion
C. Kassapoglou	TU Delft	Structures
C. Stavrinidis	ESA	Mechanics
C. Verhoeven	TU Delft	Micro Electronics
E. Colizzi	ESA	Space Systems
E. Gill	TU Delft	Space Systems
E. Mooij	TU Delft	Re-entry systems
E. Smit	T-Minus Engineering	Electronics
F. van 't Klooster	ESA	Space laws and certification
G. Gatti	ESA	Communications
J. Guarino	University of Sevilla	Shock absorbers
F. Schrijer	TU Delft	Aerodynamics
J. Schneiders	TU Delft	Aerodynamics
J. Carvajal Godinez	TU Delft	Space Systems
K. van 't Klooster	ESA	Communications
L. Scolamiero	ESA	Mechanics
L. Stagnaro	ESA	Electronics
M.M. Abdalla	TU Delft	Vibrations
M. Bolhuis	ISIS BV	Launch logistics
M. Falcone	ESA	Space Systems
R. De Breuker	TU Delft	Vibrations
R. Pischel	ESA	International Relations
T. Tirolien	ESA	Cryogenics
W. Simons	TU Delft	Astrodynamics
Q. Zhang	TU Delft	Missile DATCOM